DESIGN OF A CONTACT TYPE ACOUSTIC SENSOR FOR THE NONINVASIVE DIAGNOSIS OF CARDIOVASCULAR OBSTRUCTIONS

A THESIS SUBMITTED TO
THE GRADUATE SCHOOL OF NATURAL AND APPLIED SCIENCES
OF
MIDDLE EAST TECHNICAL UNIVERSITY

BY

ÇAĞLAR YAZGAN BALÇIK

IN PARTIAL FULFILLMENT OF THE REQUIREMENTS
FOR
THE DEGREE OF MASTER OF SCIENCE
IN
MECHANICAL ENGINEERING

DECEMBER 2022

Approval of the thesis:

DESIGN OF A CONTACT TYPE ACOUSTIC SENSOR FOR THE NONINVASIVE DIAGNOSIS OF CARDIOVASCULAR OBSTRUCTIONS THESIS TITLE

submitted by **ÇAĞLAR YAZGAN BALÇIK** in partial fulfillment of the requirements for the degree of **Master of Science** i**n Mechanical Engineering, Middle East Technical University** by,

Prof. Dr. Halil Kalıpçılar
Dean, Graduate School of **Natural and Applied Sciences** _____

Prof. Dr. Mehmet Ali Sahir Arıkan
Head of the Department, **Mechanical Engineering** _____

Prof. Dr. Yiğit Yazıcıoğlu
Supervisor, **Mechanical Engineering Dept., METU** _____

Examining Committee Members:

Prof. Dr. Cüneyt SERT
Mechanical Engineering Dept., METU _____

Prof. Dr. Yiğit Yazıcıoğlu
Mechanical Engineering Dept., METU _____

Prof. Dr. Mehmet ÇALIŞKAN
Mechanical Engineering Dept., METU _____

Assoc. Prof. Dr. Bülent ÖZER
Mechanical Engineering Dept., METU _____

Assist. Prof. Dr. Hüseyin Enes SALMAN
Mechanical Engineering Dept., TOBB ETU _____

Date: 12.12.2022

I hereby declare that all information in this document has been obtained and presented in accordance with academic rules and ethical conduct. I also declare that, as required by these rules and conduct, I have fully cited and referenced all material and results that are not original to this work.

Name Last name : Çağlar Yazgan Balçık

Signature :

ABSTRACT

DESIGN OF A CONTACT TYPE ACOUSTIC SENSOR FOR THE NONINVASIVE DIAGNOSIS OF CARDIOVASCULAR OBSTRUCTIONS

Balçık, Çağlar Yazgan
Master of Science, Mechanical Engineering
Supervisor : Prof. Dr. Yiğit Yazıcıoğlu

December 2022, 115 pages

The idea of determining arterial occlusions by non-invasive methods is a subject that has been studied for many years. Current diagnostic methods are mostly invasive, potentially risky and costly. There are studies in the literature that concentrate on the turbulent flow occurring in the arteries as a result of arterial occlusions. This results in acoustic pressure exciting the internal artery wall. In this study, a contact-type acoustic sensor design was carried out with based on the existing studies in the literature and a prototype was produced. The contact-type acoustic sensor that has been designed and prototyped has a receiving sensitivity of –126 dBV (ref 1 Pa) and a 5-dB beamwidth of 70 degrees. In addition, the prototype produced is a structure that can be used as a contact-type acoustic sensor with a fixed response up to 2000 Hz. In addition, an experimental setup modeling arterial occlusion was produced to validate the design. Measurements were made with the prototype sensor at occlusion rates of 99%, 90% and 70%, at blood flow rates of 10 mL/sn and 20 mL/sn. The results have been found to be relevant to the findings available in the past studies. The effect of turbulent flow in the arteries has been found to be between 100 Hz and 600 Hz and dominant around 300 Hz. The threshold to detect the occlusion in the artery by using acoustic methods has been determined to be 70% which is in agreement with the existing literature.

Keywords: Acoustic diagnosis, contact sensor development, atherosclerosis

ÖZ

KARDİYOVASKÜLER DAMAR TIKANIKLIKLARINDA GİRİŞİMSEL OLMAYAN YÖNTEMLERLE TANI KOYMAK İÇİN TEMASLI AKUSTİK SENSOR TASARIMI

Balçık, Çağlar Yazgan
Yüksek Lisans, Makina Mühendisliği
Tez Yöneticisi: Prof. Dr. Yiğit Yazıcıoğlu

Aralık 2022, 115 sayfa

Damar tıkanıklıklarının tahribatsız yöntemlerle belirlenmesi fikri uzun yıllardır üzerinde çalışılan bir konudur. Mevcut teşhis yöntemleri çoğunlukla girişimsel, potansiyel olarak riskli ve maliyetlidir. Bu dezavantajlar, tahribatsız teşhis çalışmaları için önemli motivasyonlardır. Literatürde arter tıkanıklıkları sonucu damarlarda meydana gelen türbülanslı akış üzerine yoğunlaşan çalışmalar mevcuttur. Bu akış, iç arter duvarında akustik basınç oluşturur. Bu çalışmada literatürdeki mevcut çalışmalardan yola çıkılarak kontakt tip akustik sensör tasarımı gerçekleştirilmiş ve bir prototip üretilmiştir. Tasarlanmış ve prototipi yapılmış akustik sensör –126 dBV (ref 1 Pa) alış hassasiyetine ve 70 derecelik 5 dB-hüzme genişliğine sahiptir. Ek olarak, tasarımı doğrulamak için arteriyel tıkanıklığı modelleyen bir deney düzeneği üretilmiştir. Prototip sensör ile %99 , %90 ve %70 tıkanıklık oranlarında, 10 mL/sn ve 20 mL/sn kan akış hızlarında ölçümler yapılmıştır. Sonuçların geçmiş çalışmalarda mevcut olan bulgularla ilintili olduğu tespit edilmiştir. Arterlerdeki türbülanslı akımın etkisinin 100 Hz ile 600 Hz arasında olduğu ve 300 Hz civarında da baskın olduğu saptanmıştır. Akustik yöntemlerle arterdeki tıkanıklığın saptanma eşiği mevcut literatürle uyumlu olarak %70 olarak belirlenmiştir.

Anahtar Kelimeler: Akustik teşhis, kontak mikrofon geliştirme, ateroskleroz

To My Family…

ACKNOWLEDGMENTS

The author wishes to express his deepest gratitude to his supervisor Prof. Dr. Yiğit Yazıcıoğlu for their guidance, advice, criticism, encouragement, and insight throughout the research.

The author would also like to thank Assoc. Dr. Hüseyin Enes SALMAN for his suggestions and comments.

The technical assistance of Mr. Ahmet Levent Avşar, Mr. Ekrem Şahin, Mr Ufuk Yiğit, Mr. Ali Aydoğmuş, Mr. Ertuğ Olgun, and Ms. Gamze Önüker are gratefully acknowledged.

The author would like to thank Mr. Metin Şengül for his support and encouragement.

The author would also like to thank Mr. Güray Aybar for his close support in all matters throughout this thesis study.

The author would also like to thank his precious wife, who he knows is always there for him with her sensitive support and endless patience, and her parents, brother, and friends who are always there.

Finally, thanks to all my managers at Meteksan Savunma Inc., for supporting this study through granting access to the facility and invaluable know-how.

TABLE OF CONTENTS

LIST OF TABLES

TABLES

LIST OF FIGURES

FIGURES

LIST OF ABBREVIATIONS

ABBREVIATIONS

RVS: Receiving Voltage Sensitivity

DI: Directivity Index

PML: Perfectly Match Layer

BPF: Background Pressure Field

IWD: Inner Water Domain

CHAPTER 1

INTRODUCTION

1.1 Statement of the problem

Hypercholesterolemia, arteriosclerosis, hypertension, diabetes, and obesity are serious health issues partly due to lifestyle decisions. These problems can cause the arterial wall to thicken and the mechanical structure of the arteries to deteriorate. The thickening of the arterial wall by building plaque layers, especially of fatty substances such as cholesterol, causes a reduction in the blood flow area. Plaques on the inner wall of the artery can break off and progress in pieces. These pieces are called thrombi. These thrombus fragments can cause atherosclerosis at a point where the blood vessel narrows. The accumulation of lipids, cholesterol, and other substances in and on the artery walls is known as atherosclerosis. Atherosclerosis can occur in all vessels, but it is primarily seen in the arteries that feed the organs.[1]

The onset of arterial occlusion is at an early age. It is inclined to increase with age, with symptoms difficult to observe. Generally, patients continue their lives without any problems in the beginning of the disease. However, as the disease progresses, symptoms begin to appear. Arterial occlusion shows different symptoms according to the vessel in which it develops. Symptoms such as chest pain, pain in the left arm, and numbness occur in cardiovascular disease (CAD), known as coronary artery disease. Coronary artery disease, which is mostly encountered in the elderly, is the most common cause of death in the world among patients over twenty [2]. Peripheral Arterial Occlusive Disease (PAOD) is the name of the vascular occlusion disease observed in the arm and leg arteries. The presence of PAOD disease can also be seen as a sign of the presence of other atherosclerosis diseases. Diagnosis of this disease obliges the control of other vascular occlusion diseases [3].

Loss of strength in the arms and legs, numbness, and speech problems are seen in the blockage of the carotid arteries (CVA) [4]. Changes in lifestyle such as a healthy diet, general improvements in weight loss, cessation of smoking and other bad habits, and regular exercise are recommended as the primary treatment. If the lifestyle is not changed, drug therapy and surgical intervention become necessary and the artery occlusion is removed with various methods.

Atherosclerosis may result in sudden death and function loss. In the current world, treatment and diagnosis techniques are improving every day, yet sustainable healthy living habits are dwindling. The most significant causes of atherosclerosis disorders are the consumption of fast food due to time restrictions in modern business life, excessive stress, lack of routine health measures. Atherosclerosis affects about 13 million people in the United States [5].

Coronary angiography is the most popular diagnostic method for coronary artery disease. In the coronary angiography method, a liquid called “radio-opaque contrast agent” is injected into the coronary arteries that feed into the heart layers. With the help of X-ray imaging of this opaque substance, the rate of intravascular occlusion gets revealed. In today's technology, coronary angiography is a gold standard diagnosis method for viewing the occlusion status of the arteries. However, coronary angiography is also invasive, expensive, requires hospitalization, and involves some risks for the patients [6, 7].

The Electron Beam Computer Tomography (ebCT) method is another alternative, which is preferred in vascular occlusion diseases other than CAD. A substance called “radio-opaque contrast agent” is given to the patient's artery and is monitored. In this method, the patient is exposed to a significant amount of radiation In addition, this method requires significant financial investments (such as the provision of necessary devices for the diagnosis method) and an advanced workforce (the need for trained and experienced technicians in the application of this method) [6, 7].

Stress Electro-Cardiology (ECG) is a relatively old method. ECG constitutes a moderate risk level but is costly. The diagnostic success of the ECG method relies on the stability and experience of the personnel. It has been observed that statistically, it gives low specificity and sensitivity values, especially in studies conducted on women [6, 7].

Ankle Brachial Index (ABI) is another non-invasive method that can be used in peripheral arteries. In this method, blood pressure is measured in the arteries of the arms and legs during the systole phase using Doppler instruments.

Looking for occlusions in the peripheral arteries to make inferences about coronary arteries is also a suitable method. Since the accumulation of fat in the body is likely to occur at every point of the body, PAOD patients carry a risk of at least 20% CAD [8].

1.2 Literature review

Many studies in the literature focus on vascular sound. First, Burns [9] investigated periodic sounds coming from deep inside the heart. In this study, it was reminded that the flow regime could be determined depending on the Reynolds number, and inferences were made about the vascular sound. It has been stated that turbulent flow caused by stenosis may constitute an acoustic source.

Subsequently, Lees and Dewey [10] introduced the word "phono-angiography", assuming that vascular occlusion can be diagnosed using a non-invasive method. In this study, acoustic measurements were made on two individuals aged 54 and 65, who were both diagnosed with atherosclerosis. Measurements were made from the stenosis area and from the left femoral, left carotid, right femoral and right carotid arteries. The patients were given the supine position and measured using a piezoelectric-based acoustic sensor. The results came out to be similar to the outputs of Bakewell et al. [11].

There are also other non-invasive studies. Blanks et al. [12] introduced a new approach to detecting shear waves in the chest cavity caused by stenosis. In this study, he created and used an experimental chest cavity model. The viscoelastic mathematical model has been verified with the experimental data of the phantom material [12].

Azimpour et al. [13] presented a study on non-invasive acoustic detection. In this study, individuals between the ages of 18 and 89 that applied to the clinic with the suspicion of vascular occlusion that can cause chest pain or heart attack were selected. Acoustic measurements were made using the 3M Littman electronic stethoscope Model 4000, while the patients were laid in the supine position. A total of 156 patients underwent a "catheter-based coronary angiography" procedure after acoustic measurements. According to the results, a detection success of 50% was achieved at a severity rate of 95%.

Winter et al. [14] stated that heart sounds and noise in the coronary artery may vary with respect to coronary diseases. The study aims to confirm the accuracy of the portable acoustic device used for diagnostics. In the study, among 1675 people with coronary artery diseases, patients with highly severe symptoms were excluded, and tests were performed. Patients were classified by scoring as per an algorithm. The outputs of the proposed acoustic diagnostics method were compared with that of the classical method. The results suggest that the new non-invasive method can as well be used as an auxiliary clinical tool [15][16][17].

Lowe [18] produced a physical model to establish a relationship between the upper arm and aortic pressure in his study. Two parameters were examined in the time axis, aortic pressure was modeled using supra-systolic upper arm pressure waveforms. A high degree of correlation (>90%) was found between the two pressure values.

In another study, Campo [19] showed that the mechanical structure of arteries contains important clues for many vascular diseases [20][21]. Arterial stiffness value has great importance in informing cardiovascular risks [22]. First, the pulse

wave velocity was measured via laser Doppler vibrometry, which is a non-contact and non-invasive measurement method. Afterward, stiffness parameters were obtained by using pulse wave velocity values of arteries (especially carotid, branchial, and coronary arteries). According to the results, measuring arterial stiffness with this non-invasive method has been found to be a potential clinical diagnostic method.

Campo and Dirckx [23] reached stiffness values by measuring pulse wave velocity.

Wang et al. [24] conducted studies on non-invasively diagnosing stenosis by using acoustic data acquired from the coronary vascular region with the help of a microphone. The resonant frequencies of the arteries are not excited in the normal flow regime [25]. However, acoustic traces of arteries can be detected due to the resonance frequencies of arteries that were excited by the flow-induced turbulence. In light of this information, high-frequency isolated diastole sounds in coronary vascular structures with stenosis were detected by advanced signal processing methods [26][27].

There are experimental studies on the non-invasive diagnosis of stenosis. The flow dynamics that occur after stenosis are the main focal points of the studies. On the other hand, Borisyuk et al. [28] conducted an in-vitro experiment to reveal the change in the flow regime in the arteries. The effect of the flow regime on the creation of an acoustic field was investigated. Disk-shaped parts are placed inside the cylindrical channel with different flow areas. In this way, theacoustic field that occurs due to congestion has been characterised. An overall increase in the noise power spectrum was noticed and additional signals at new frequencies have emerged. This new acoustic power characteristic is the vortex formation characteristic that occurs after stenosis. These acoustic power values are fourth-order proportional to the severity of the obstruction and the Reynolds Number.

Figure 1.1 shows flow regions in the cylindrical channel with an obstruction. The flow was investigated by dividing the channel into 5 different sections. The first section is the flow in the laminar regime where the critical Reynolds Number is not

exceeded. In the second one, there is a reduction in the cross-sectional area of the flow due to the obstruction and in accordance with that, a subsequent increase in the flow velocity. In the third section, stenosis has finished and flow separation has started (i.e., the critical Reynolds Number limit has been exceeded). Recirculating flow is observed on the walls of the arteries, which causes the flow to take place in the turbulent regime in this section. The highest acoustic signal (the highest vascular sound) occurs here. In the fourth section, the flow is directed toward the arterial wall again. Where the channel is long enough, flow stabilization is expected to occur in the final and fifth sections.

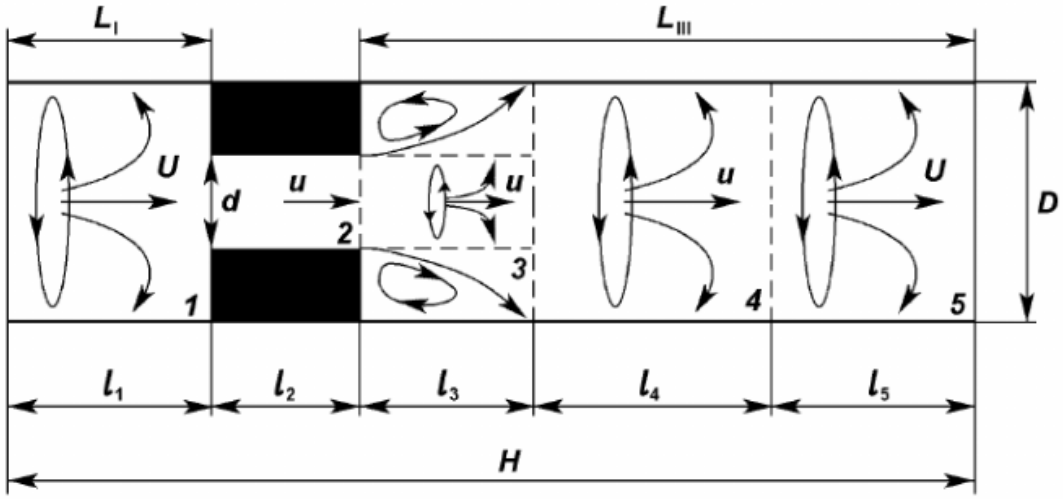

Figure 1.1 Flow regions in the cylindrical channel with an obstruction [28]

Yazicioglu et al. [29] both theoretically and experimentally studied the vibration of the tube having thin walls, which is made of viscoelastic material. The vibration of the tube caused by flow was studied taking into account the internal flow and viscoelastic tissue-like tube material as coupled. Vibration and pressure measurements were made using a catheter-type pressure transducer and Laser Vibrometry (LDV) in experiments where a gravity force was created between two reservoirs.

Tobin and Chang et al. [30] studied the variation of acoustic pressures in the vessel wall according to x/D in the case of occlusion. Occlusions are axially in a

symmetrical and cylindrical structure. In the experiments, a constant flow was provided into a latex rubber tube and measurements were taken. Different degrees of stenosis severity were studied. The frequency spectrum and amplitude of the pressure were compared, and a strong correlation was observed. Also, the spectral density function was obtained by introducing new dimensionless variables (At the peak point).

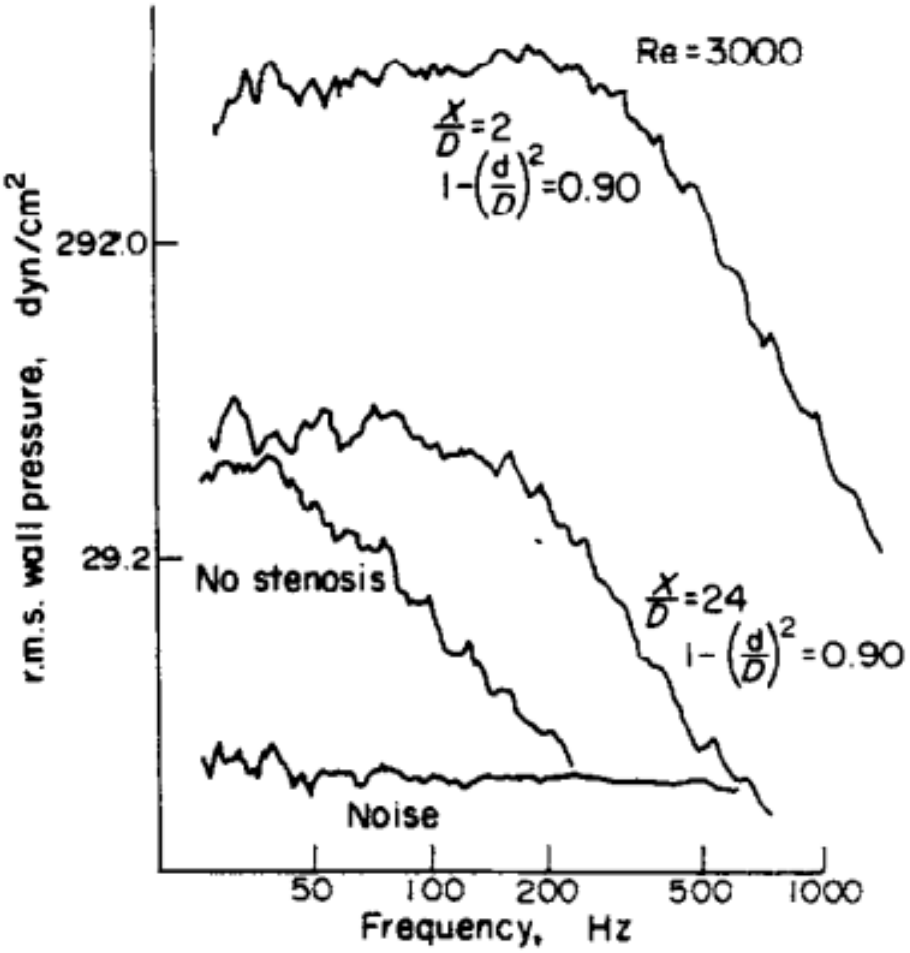

Figure 1.2 The wall pressure spectra (with respect to different x/D) [30]

Salman et al. [31] modeled a narrowed flow in a thin cylindrical model using ADINA as the modeling tool. As a result of the analysis, the recirculation region was observed at the contraction output, and it was determined that the vibrations spread overa band of several hundred Hz. It was observed that fluctuating modeled

artery wall pressure increased at the exit of stenosis. The resulting numeric solutions were compared with the related studies in the literature. As a result of the comparison, it was stated that the study provided similar outputs with the experimental studies in the literature [29] in terms of general spectral behavior and increase in pressure fluctuations with increasing stenosis severity.

Salman and Yazicioglu et al. [32] studied computational analysis for stenosis in peripheral arteries. They stated that atherosclerosis affects the entire cardiovascular system and the presence of vascular occlusion in the peripheral arteries, which is a part of the cardiovascular system, can also be seen as an indicator of the presence of occlusion in vital organs. Computer Tomography-based tissue structure and idealized tissue structure were modeled for thigh, upper arm, neck arteries, and tissues around the arteries. The pressures at the arteries' wall from the stenosis outlet to 100 mm were calculated with computational analyzes using these models. In cases of stenosis greater than 70% severity, an increase in vibration response amplitudes, especially around 250 Hz was observed.

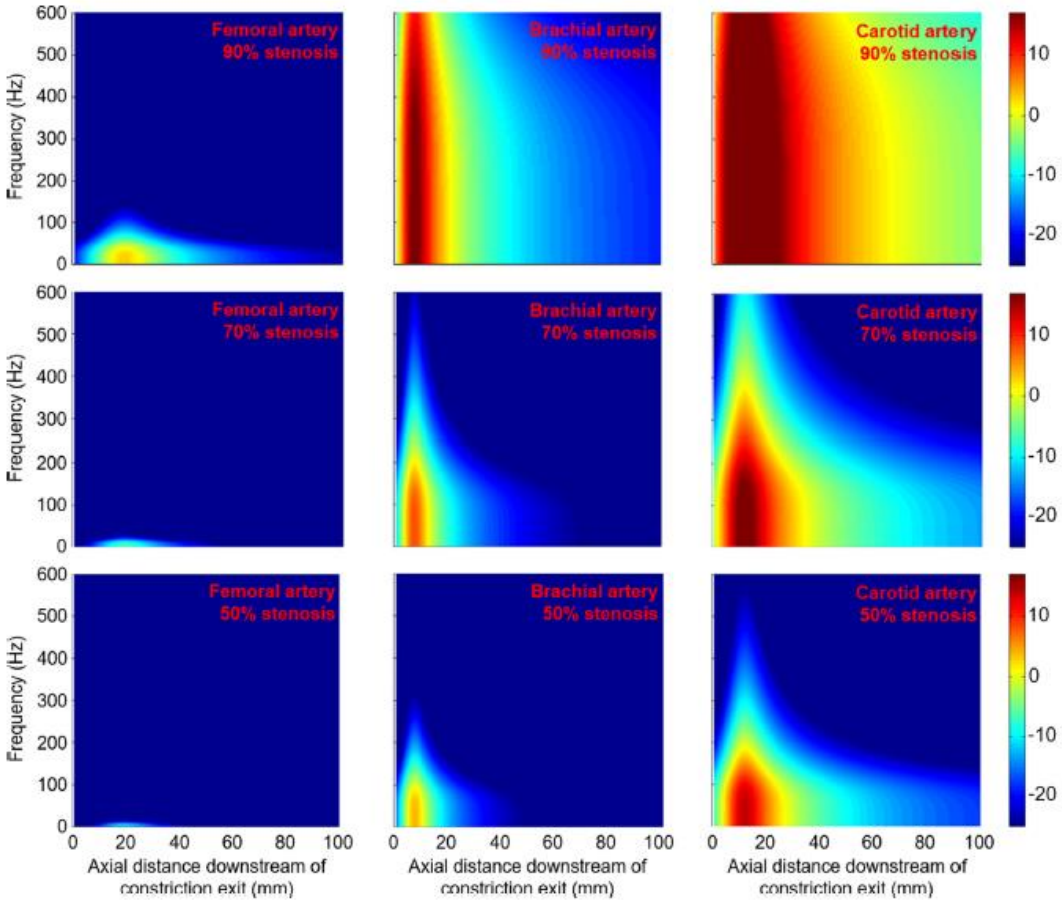

Figure 1.3 Acoustic pressure (dB reference: 1 Pa) fields as a function of axial position and frequency. Pressure fields are obtained at peak blood flow rates for 50, 70, and 90% stenosis in the femoral, brachial, and common carotid arteries.[32]

Semmlow and Ketaki et al. [33] described the importance of early and non-invasive diagnosis in CAD disease. They also summarized the signal processing algorithms requirements for the non-invasive diagnosis of CAD.

Veramrien et al. [33] studied the load applied to the skin by the phonocardiography microphones whilst measuring. The first step of these experimental studies was to identify the coupling characteristic of the phonocardiography microphone and the skin. In the experiments, an ultra-light microphone as well as a microphone with a higher mass were placed on the skin. The average vibration amplitudes were recorded, and the differences between the two recordings were summarized.

Lukkarinen et al. [35] developed and used a recording system to analyze heart sounds. The recording system used in the study involves the use of an electronic stethoscope headphone and a computer capable of processing acoustic signals [36]. Based on the recordings taken between the frequencies 20 Hz and 22 kHz, it has been decided that the system is qualified to detect heart valve disorders in children.

Padmanabhan et al. [37] tried to design a transducer that complies with phonocardiography requirements. High sensitivity and low noise were aimed during the design phase. The transducer, which uses a 125 mV/g accelerometer as its sensor, is of the accelerometer type, weighing 5g. The transducer has an operating frequency band between 200 Hz and 800 Hz. The design was given shape according to the fact that the measurement efficiency at high frequencies decreases at heavy loads [38] [39]. Design verification was achieved by comparing the transducer using 4 different measurement methods.

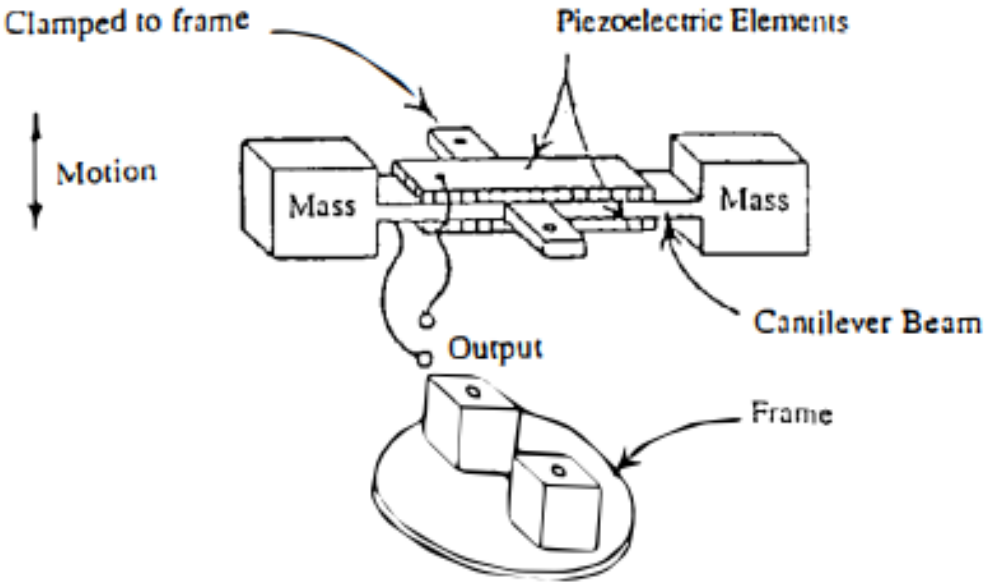

Figure 1.4 Bender Type Padmanabhan's accelerometer.[37]

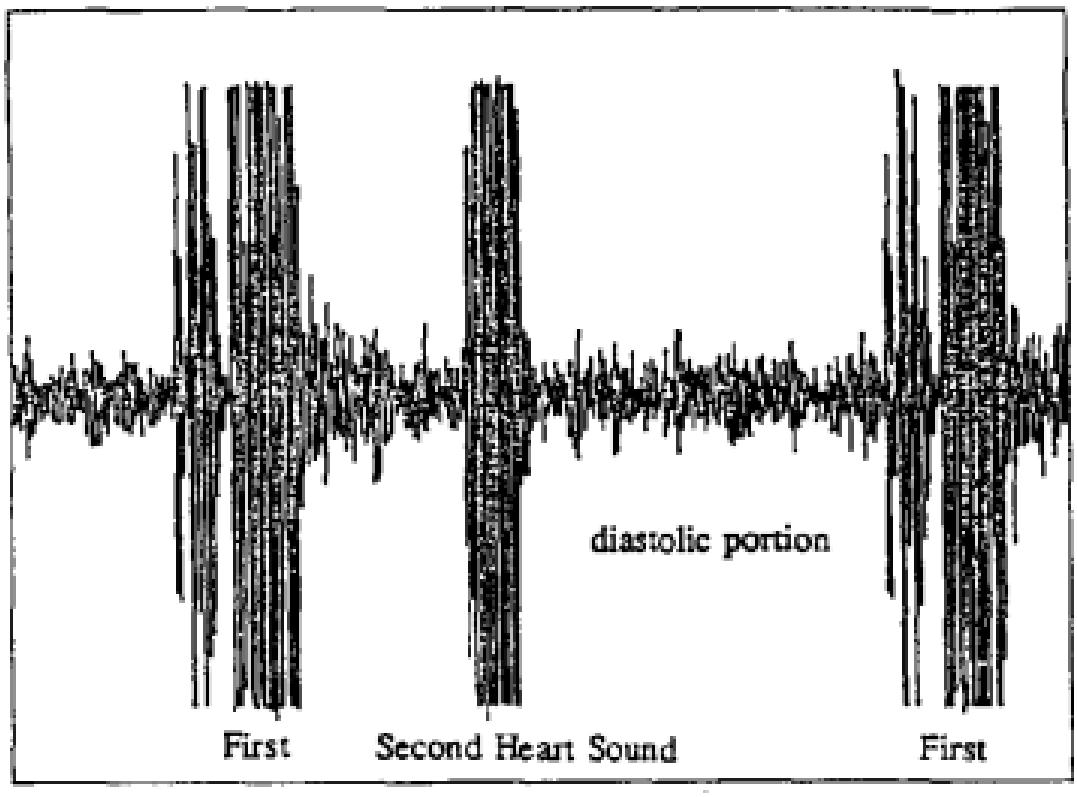

Figure 1.5 Heart sound obtained with Padmanabhan's accelerometer.[37]

Asada studies a designed a new digital stethoscope for CAD diagnosis. [40]

U.S. Army Research Lab., Murrill et al. [41] studied a sensor in order to understand the state of the soldier. This sensor is an impedance-matching type of sensor that detects cardiovascular movements. The hydrophone tip is filled with an acoustic gel material. This design makes it possible to record cardiovascular movements. However, it is also open to airborne noise from the environment.

According to Kroli et al. [42] designed a measuring device that records low-frequency heart sounds. It is a device that measures by touching the patient's chest and the left side of the body. The flexible diaphragm inside the device measures the noise caused by heart sounds. In front of the diaphragm, a specific liquid that contains no air bubbles is placed. This liquid acts as a transmitter of the acoustic signal. Figure 1.6

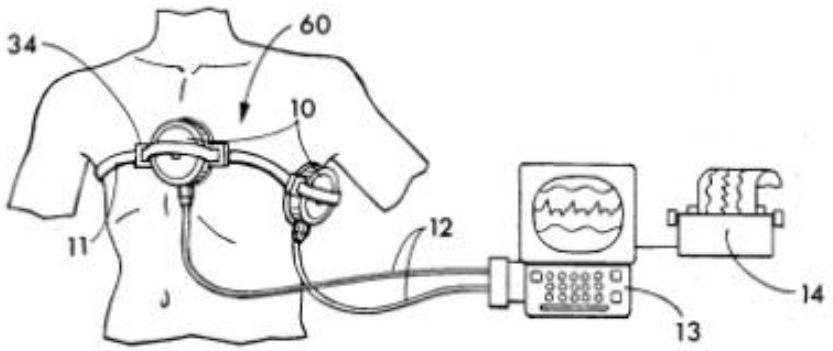

FIG. 1

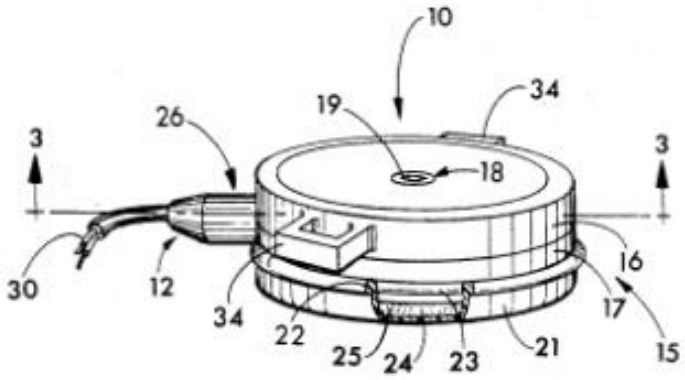

FIG. 2

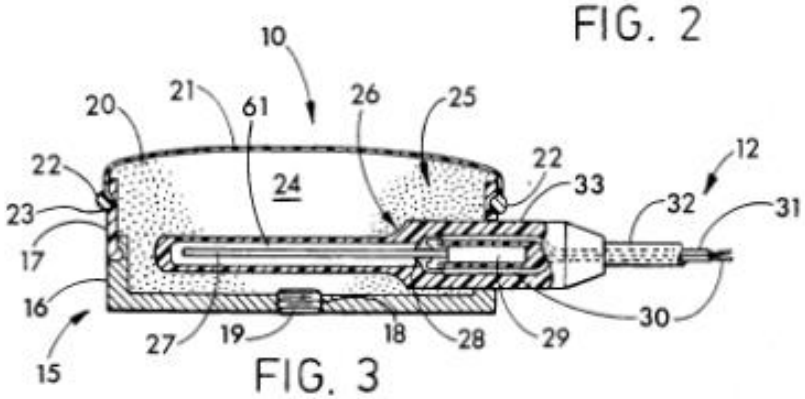

FIG. 3

Figure 1.6 Kroli measuring device [42]

Schwartz et al. [43] presented another impedance-matching transducer design. The lossless transmission of the signal was aimed, where the entire signal path has been formed using materials of similar impedance characteristics [44][45][46], Figure 1.8. The transducer was designed to operate between 1 Hz and 1 kHz. In the study,

the new design was compared with two microphones that were available on the market. The sketch of the design can be seen in Figure 1.8.

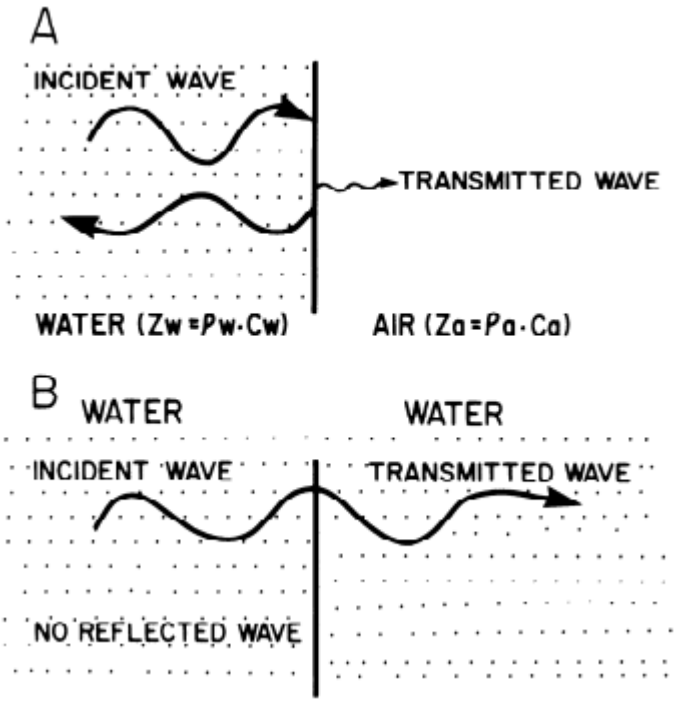

Figure 1.7 Path of the acoustic signal [43]

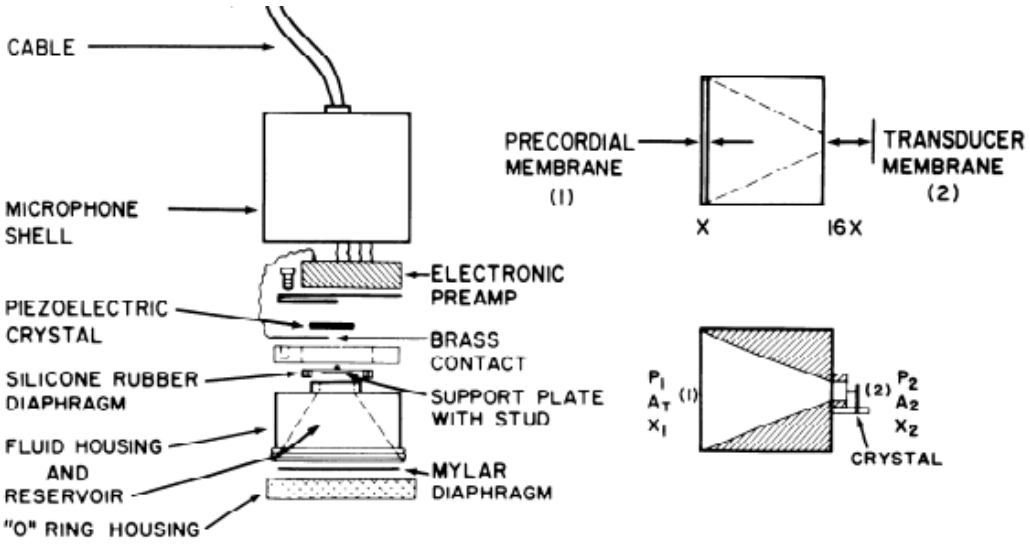

Figure 1.8 The sketch of the transduser[43]

Courteville et al. [48] presented a high-sensitivity muscle-vibration sensor that has been re-designed for clinical use. The muscle vibration at the frequency band of between 1 Hz and 30 Hz has been used and modeled to improve the measurement technique [49][50][51]. The acoustic impedance matching model was then used for the sensor design. The designed sketch of the sensor can be seen in Figure 1.9.

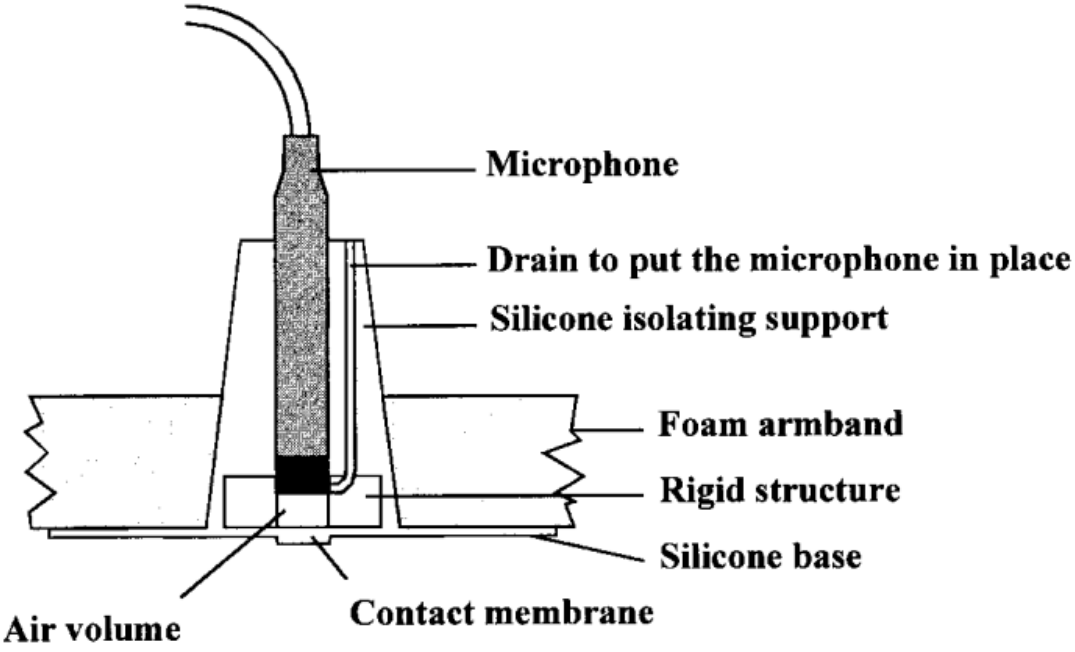

Figure 1.9 The sketch of the sensor[48]

1.3 Motivation and objective

In the literature, there are many studies on the acoustic effects of vascular occlusion and the diagnosis of vascular occlusion by acoustic methods. Most of these studies reveal the effects of acoustic sources caused by intravascular occlusion. In practice, sensors that are developed to measure vascular occlusion are limited in number. The main motivation of this study is to develop and conceptually prove the design of a sensor that can non-invasively diagnose vascular occlusion by making use of the developments in the material science and design tools.

With this motivation, the sensor designs and studies that could be of inspiration and thus input to this new sensor design were reviewed, the design parameters were determined and a sensor design was made using materials used and available in the industry. A prototype was produced shortly after. An experimental setup physically close to the intravascular structure was designed and an artificial obstruction was created.

The aim of the study was to design, model and prototype a sensor, and by using it measure the turbulent flow that occurs in the arteries in the case of vascular occlusion, and see whether the designed sensor is able to detect occlusions within the artery. Another objective was to question whether non-invasive acoustic measurements and vascular occlusion diagnosis studies are indeed feasible.

COMSOL, a commercial finite element analysis software was used for the modeling of the sensor during the design phases. With the help of this tool, the sensitivity and directivity values of the sensor were obtained and compared with the studies in the literature.

1.4 Thesis Outline

The thesis work consists of a total of 4 main chapters. In the first of these, Chapter 1 Introduction, the problem that was the source of the study as revealed, and previous studies on the subject are briefly mentioned. In Chapter 2 Sensor Design, the design criteria, design stages, and selection of materials used are explained in detail. In Chapter 3 Experimental Studies, the experimental studies made for design verification are covered. Finally, in Chapter 4, all the results are evaluated and future studies are mentioned.

CHAPTER 2

SENSOR DESIGN

In any design, the structure of the sensor and the acoustic signal to be measured must be evaluated in conjunction to achieve a sensor that can successfully detect vascular occlusion non-invasively. As stated in many studies given in the literature review (Chapter 1), the turbulence regime of the blood flow caused by atherosclerosis can be considered as an acoustic source.

2.1 Design parameters

2.1.1 Signal-to-Noise ratio

The most important parameter to detect the signals for a sensor is the signal-to-noise ratio. Sensors can detect signals at points where the signal can be distinguished from noise. Increasing the signal level and lowering the noise level increases the detection capacity.

From that aspect, fully understanding the parameters of the signal to be measured is essential for a proper design. First of all, a source inspection should be done. In other words, determining the strength of the signal at the source is the first step of the design process. Then, the level of the acoustic signal and from which direction the sensor is expected to receive these signals should be decided (i.e., the desired directivity of the sensor).

2.1.1.1 Acoustic signal

Salman et al. [52] modeled the blood flow in the vessel and tested the model with experimental studies. In the study, an artery was modeled by passing a latex tube

through the phantom material and an artificial occlusion was created. A flow with a Reynolds number of 1750 was provided with the help of an elevated supply tank. The turbulence caused by artificial occlusion created a vibration on the surface of the phantom material, and this effect was measured with a single-point non-contacting Laser Doppler Vibrometer IVS-300, Polytech, Auburn, MA (sensitivity is 125 mm/s/V).[52]

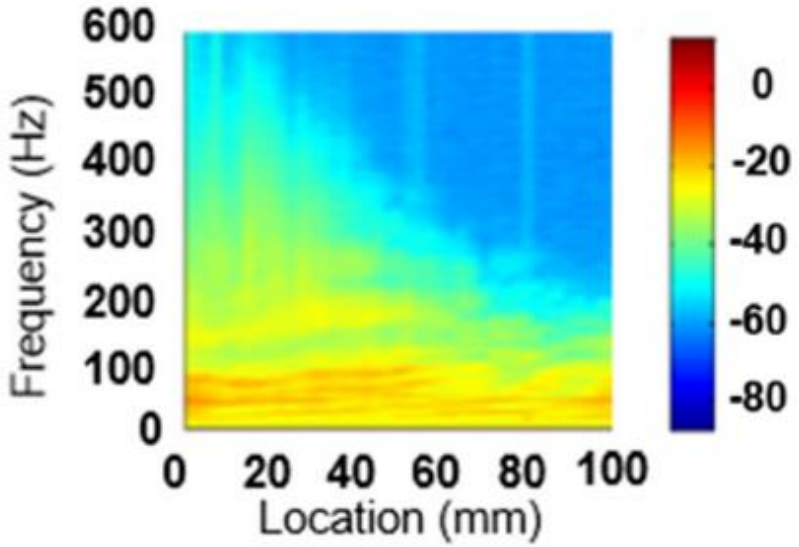

Figure 2.1 Empirical result for radial velocity (dB Reference 1 Mm/S) On Phantom. [52]

Yazicioğlu et al. [29] revealed the relationship between wall pressure and frequency by using the empirical equation (Eqn. 2.1). Acoustic pressure amplitudes have been modeled with the help of experimental outputs of Tobin and Chang [30].

In Figure 2.2 and Figure 2.3, pressure values are given respectively for Reynolds number 1000 and Reynolds number 1750. The stenosis levels are 90% and the measurements have been made between DC (0 Hz) and 600 Hz. The pressure values were between 15 dB and -20 dB. (dB Reference 1 Pa). It can be claimed that the pressure reaches its highest value at a distance of 0 to 30 mm after the constriction exit.

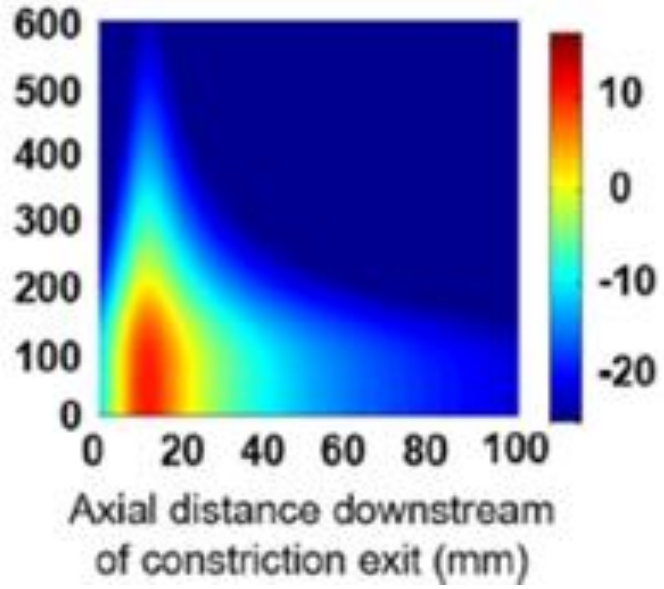

Figure 2.2 Acoustic pressure (db Reference 1 Pa)- 90% stenosis Reynolds Number: 1000 [52]

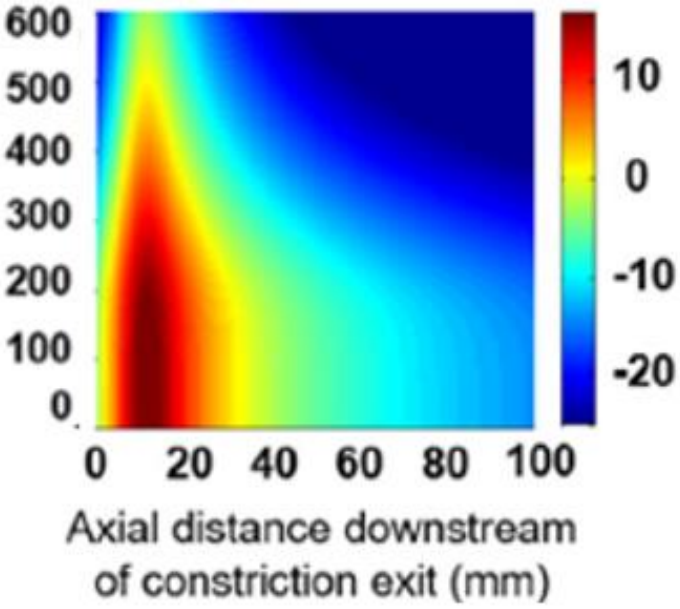

Figure 2.3 Acoustic pressure (dB Reference 1 Pa) for 90 % stenosis, Reynolds Number: 1750 [52]

$$P[x] = 1.82F_{n1}[x/D]\rho U^{3/2}\frac{D^{5/2}}{d^2}\left(\frac{1}{1+20\left(\frac{fd^2}{UD}\right)^{5.3}}\right)^{1/2} \quad \text{Eqn. 2.1}$$

Salman et al and Yazicioğlu et al. [32] calculated the pressure of the femoral, branchial and carotid arteries for cases of 90%, 70% and 50% stenosis. The lumen diameters of the arteries are around 10 mm, 4 mm and 6.4 mm, respectively [53][54][55]. According to the peak flow rates, the peak value Reynolds numbers are 750, 1300 and 3840 for the arteries respectively for femoral branchial and carotid arteries.

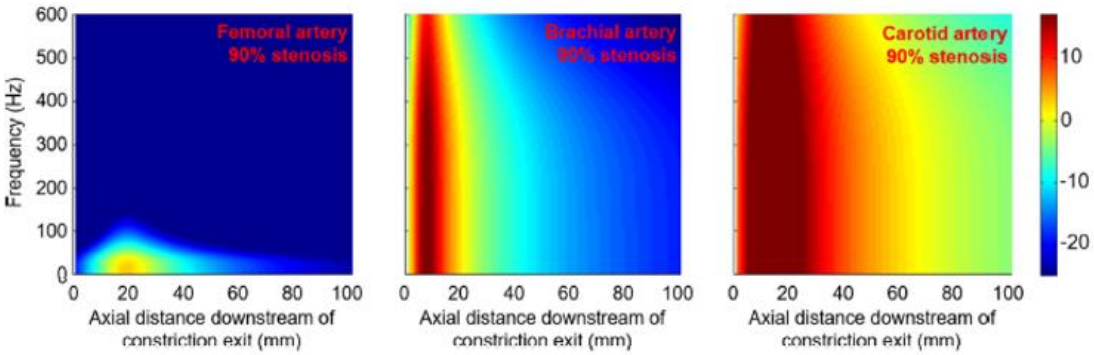

Figure 2.4 Acoustic pressure (dB reference: 1 Pa) fields as a function of axial position and frequency. Pressure fields are obtained at peak blood flow rates for 90% stenosis in the femoral, brachial, and common carotid arteries. [32]

As seen in Figure 1.3 and Figure 2.4, the turbulence in the blood flow creates a pressure value between 20 dB and -20 dB from the point where the obstruction exit to 30 mm. With dB ref: 1 Pa information, it corresponds to 20 dB 10 Pa and -20 dB 0.1 Pa. Salman and Yazicioglu et al. [32] and [52] concluded that stenosis effects are dominant around 300 Hz. In Figure 1.3 arteries with 70% stenosis have a pressure value between -5 dB and +15 dB. The generated signal at the wall of arteries corresponds to 15 dB → 5.62 Pa and -5 dB → 0.56 Pa with ref:1 Pa. The sensor must be carefully designed and tailored in accordance with these signal parameters so that it will be able to receive and extract the acoustic data.

2.1.1.2 System Noise

While considering the first of the design parameters, i.e., signal-to-noise ratio, the second half of the SNR is the noise.

There are two main sources of noise for the sensor system. Noise originating from electronic components (electronic/thermal noise), and acoustic ambient noise received by the sensor's sensing elements. It is vital to carry out a specific design as a whole that aims to minimize the electronic noise of the electronic circuitry that will acquire the data, the electronic noise of the passive sensing elements of the sensor, and the acoustic noise originating from the environment that the sensor receives and transmits to the electronic circuits as electrical signals.

Recall that once the acoustic signal has been digitized by the acquisition system, the signals are processed with signal processing software. The detection and extraction of the data from the signals where the levels of the signals are below the ambient noise level, require enhanced software, algorithms, and signal processing power. Moreover, if the electronic noise floor is higher in power/amplitude than the signal, it is impossible to retrieve the signal out of the electronic noise, and the signal is never received.

Extremely small acoustic pressures caused by the stenosis-induced turbulence on the sensor are converted into electrical signals. A data acquisition system is presented with an interface after digitizing the electrical signals flowing through the sensor. All electronic components that take place in the data acquisition system as well as the sensor systems, in which the electrical signals are evaluated, have internal electronic noise. It is necessary to choose the front-end electronics circuitry to have the lowest input noise floor characteristics. Otherwise, even if the sensing elements inside the sensor convert the acoustic signal created by the stenosis-induced turbulence into analog signals of high amplitudes, they will still carry the risk of getting lost in the internal electronic noise within the system.

The total noise floor of the sensor system and data acquisition system used in this study is -130 dBV (Vref: 1V). This noise level is declared under the assumption

that it is constant across the entire frequency band. The noise level within the entire frequency band is shown in Figure 2.5. In Chapter 2.3, the technical features of all system components, and the selection criteria will be explained in detail.

$$20 \log_{10}(\frac{V}{Vref}) \qquad \text{Eqn. 2.2}$$

Eqn. 2.2 is the formula for the noise level. According to the Eqn. 2.2 the min voltage that can be read is 0.30 µV.

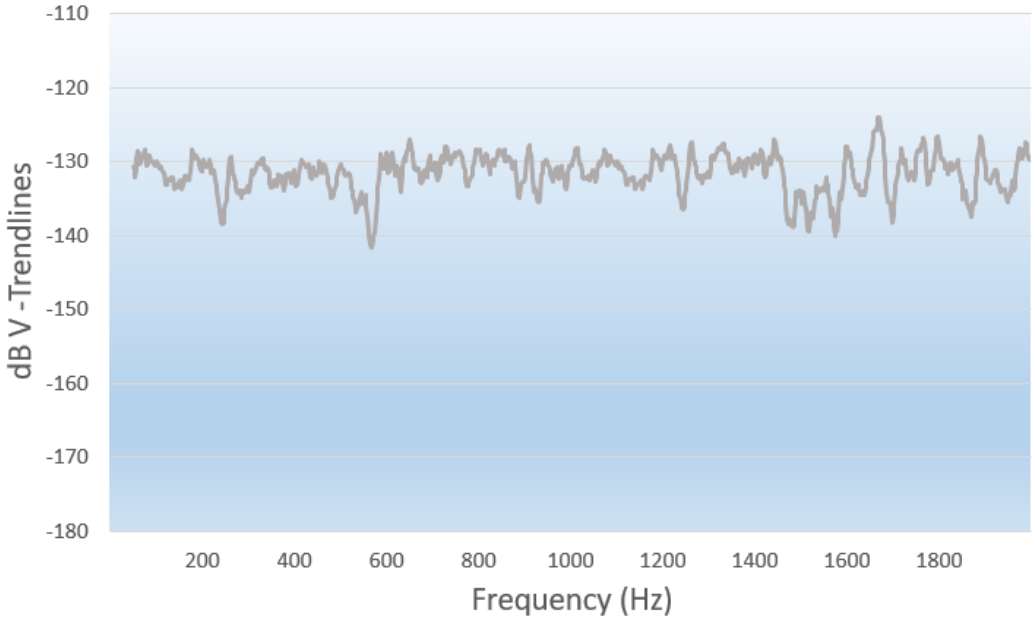

Figure 2.5 Internal electronic noise of the system

Another parameter of the total noise of the system is acoustic noises caused by environmental factors. The power supply that feeds the system, the computer, the air conditioner, and any other sounds in the measurement environment are the main sources of acoustic noises that affected the measurements. To mitigate the effects of this, an acoustically isolated environment was provided, and relevant experiments were carried out there.

2.1.2 Receiving Voltage Sensitivity (RVS)

RVS (Receiving Voltage Sensitivity) defines how much electrical potential in terms of Voltage is produced by the sensor per unit pressure. In short, it is a term that describes the sensitivity of the sensor to acoustic pressure. Sensitivity is an application-dependent definition and does not have a universally common definition among all processes. On the contrary, it is the evaluation of the output produced by the device according to a pre-determined certain reference point. This reference point is a pressure point for hydrophones or microphones where pressure is the input. For air, as in the case of microphones, the reference pressure is generally 20 µPa whereas for the solid materials and water is 1 µPa [57] [58] [59]. 20 µPa an 1 µPa reference points are the human ear hearing threshold of around 1 kHz. In other words, the hearing limit of the human ear is assumed to be 0 dB. Some examples of airborne sound levels in water and air are given in Table 2.1.

On the other hand, changing the selected reference point according to the condition of the measured source might lead to clearer expressions. For example, Salman and Yazicioglu et al. [32] and [52] reference acoustic pressure assumed to be 1 Pa. All graphics are around this reference value. Some examples of airborne sound pressure levels are also given in Table 2.1 [58] [59].

Table 2.1 Some examples of airborne sound levels [58] [59]

Typical sound in air/ ***marine mammal sound***	**Water standard (dB re 1 μPa)**	**Air standard (dB re 20 μPa SPL)**
Threshold of human hearing (1,000 Hz)	[26]	0
Very quiet living room	[66]	40
Seal threshold underwater (1,000 Hz)	80	[54]
Normal speech (1 meter)	[86]	60
Beluga threshold (1,000 Hz)	100	[74]
Lion's roar (10 meters)	[116]	90
Jet airliner (10 meters)	[130]	104
Fin whale call (100 meters)	140	[114]
Human threshold of pain (at ear drum)	[166]	140
Some military artillery	[186]	160
Beluga echolocation call (1 meter)	220	[194]

Sensitivity value is especially important for the classification of the sensor. Another point of use is the selection of sensor parts (sensing structures-ceramics). A general formulation of the sensitivity at any frequency is given in Eqn 2.3. The RVS definition can be changed according to the application. In many acoustic sensor applications, the reference pressure point may change. For example, in underwater acoustic applications, this point is 1 m away from the sensor. For contact acoustic sensors, it makes sense to refer to the sensor surface.

$$20\,log_{10}\left(\frac{Voltage\ on\ Sensor}{Pressure\ on\ Sensor}\right) \qquad \text{Eqn. 2.3}$$

The sensitivity of all microphones and hydrophones varies with respect to the operational frequency. In general, sensitivity values at 1000 Hz are used to indicate the sensitivity of the devices with a single value. For example, for air microphones, the reference point is the 1000 Hz sine signal at a source pressure level of 94 dB (SPL), i.e., 1 Pascal (Pa) pressure.

In this study, due to the necessity of the application, the frequency band of 50 Hz-1000 Hz has been examined. Compared to the frequency bands of microphones in the market, this band might be regarded as narrow, however, the sensitivity of the entire band has been calculated with a resolution of 0.25 Hz.

The output voltage of the microphones and hydrophones is captured, evaluated, and monitored by a data acquisition system. The analog signal from the sensor is digitized and sorted according to a reference. This value returns the sensitivity value in dBV. The selected Vref value is usually 1V. The formula of analog to digital can be seen in Eqn. 2.4. In Chapter 2.3 the acquisition system used in this study will be explained in detail.

$$20\log_{10}\left(\frac{Voltage\ on\ Sensor}{Vref}\right) \qquad \text{Eqn. 2.4}$$

The RVS graphic of the TC-4032 model of the Low Noise Sea-State Zero Hydrophone series produced by TELEDYNE RESON is given in Figure 2.6 [60].

According to the value in the graph, the Receiving Sensitivity value of the sensor is -170dB re 1V/ µPa (-164 dB with differential output).

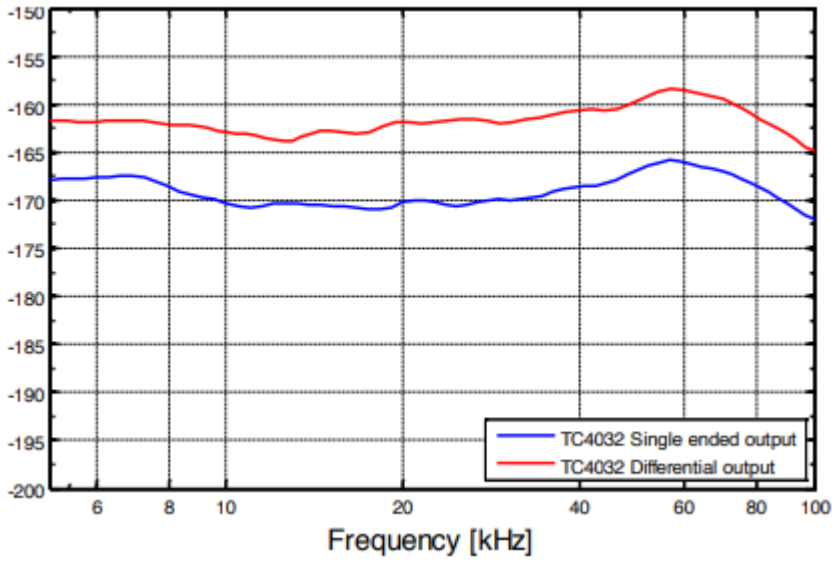

Figure 2.6 Receiving sensitivity of TC 4032 [dB re 1V/µPa @ 1m][60]

2.1.3 Polar pattern

The polar pattern is the representation of the directivity of the sensor – the ability to pick up signals from different directions. Acoustic signals are vector quantities and can radiate from a single point, a surface, or a volume. The direction from which the acoustic signal of interest comes can be crucial depending on the application.

In acoustic contact microphones made for the detection of vascular occlusion, it is critical to receive the signal from the right point in terms of diagnosis. Because turbulent flow that occurs due to the changes in the blood flow regime creates acoustic signals at small amplitudes. There are many sources of acoustic signals of comparable amplitudes within the human body. Considering this, the sensor has two important design criteria in terms of directivity in sense:

- The sensor must be sensitive enough to sense acoustic signals caused by vascular occlusion.
- It must differentiate the signals of interest from the ambient noise and sounds originating from non-vascular organs.

In order to meet these two criteria at the same time, the directional sensitivity of the sensor must be precisely tuned. It should also be "deaf" to the noise coming from the environment, whilst being "all-ears" to the point of interest.

The polar pattern of a microphone is judged by the directivity index parameter. The directivity index can be defined as the ratio of the reception sensitivity of the microphone at a given axis to the average reception sensitivity. Different definitions can be made, but usually, the reference receiving value is taken as SPL averaged over all angles. DI formula can be seen in Eqn. 2.4. [61]

$$D((\theta, \phi) = \mathrm{Lp}(\theta, \phi) - \mathrm{Lpavg}\,(\theta, \phi) \qquad \text{Eqn. 2.4}$$

Where:

- D (θ, ϕ): Directivity index of a given direction
- Lp (θ, ϕ): RVS (Receiving Voltage Sensitivity) for a direction
- Lp_{avg} (θ, ϕ) = RVS (Receiving Voltage Sensitivity) averaged over all angles
- (θ, ϕ) = A direction indicator

As the RVS (Receiving Voltage Sensitivity) varies with the frequency, so does the directivity index. It is usually displayed over polar plots.

In this study, the requirements of the polar pattern of the sensor and the design decisions made to achieve the desired DI level will be explained in detail in Chapter 2.3.

The DI plots of the TC-4032 model of the Low Noise Sea-State Zero Hydrophone series produced by TELEDYNE RESON are given Figure 2.7[60]. According to

the value in the graph, the sensor at 100 kHz can be considered omnidirectional since the RVS fluctuations are within a small band, such as ±1.5dB.

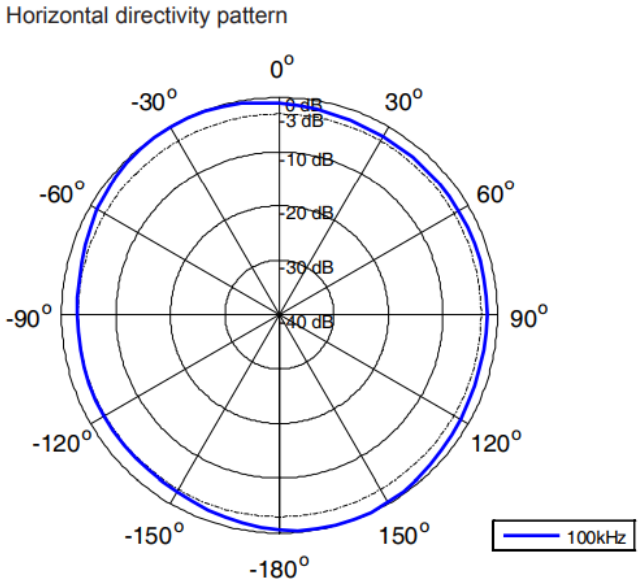

Figure 2.7 Horizontal DI pattern of TC 4032 [60]

2.2 Sensor types

There are 2 types of acoustic sensors types for the detection of vascular occlusion.

- Minimum load sensing element type design
- Type impedance matching type design

Next chapters will discuss these two types of designs in more detail.

2.2.1 Minimum load sensing element type

Acoustic wave, which is formed in the arteries and propagate to the skin surface, is delivered to the sensing elements via a tissue medium. The sensor surface creates a load on the skin surface while in contact. At high frequencies, microphones are particularly sensitive to this loading effect. With the increase in the mass of the sensor, the mechanical loading of the sensor on the surface will increase, which

damps the signals above 500 Hz. Since the signals of interest are damped, the sensitivity of the sensor has to be much higher [33] to overcome this effect.

The minimum load sensing element type design is aimed to capture the acoustic wave without any mechanical loading. The medium to be placed between the skin surface and the sensor's sensing elements is considered a compressible substance. Mostly, this compressible medium is "air". Acoustic signals emanating from the skin surface reach the sensing elements through the air. In other words, the sensor does not touch the surface, so does not constitute any physical thus electrical load. In this design, the surface is not suppressed, so the signal loss is avoided.

Two important points should be considered when using this type of design. If an air-coupled design is preferred, the sensor becomes sensitive to ambient noise since ambient noise from the outside is also carried by air. In this case, it is necessary to consider the conditions of use. Either the environment should be suitable for the use of the sensor, i.e., the environment should have low ambient noise, or this fact should be considered an input to the sensor design. Conventional stethoscopes with condenser microphones are generally designed with air-coupled medium [62]. The size of the medium to transfer the acoustic signal, the coupling chamber, varies according to the frequency range to be measured. It can be adjusted, and instead of air-coupled designs, different media can be also used [33].

The second important issue is the propagation and reflection losses, while the acoustic signal propagates through many layers with different acoustic impedance values. Schwartz et al. [43] visualized the progression of the acoustic wave in Figure 1.7.

Due to these two major disadvantages, the minimum load sensing element type design is not the preferred solution for detecting very small signals. There are predominant acoustic signals occurring in the cardiac and other arteries like Korotkoff Sounds [63]. Changes in the flow regime due to atherosclerosis creates weaker acoustic signals compared to Korotkoff sounds, and these signals are quite challenging to perceive using a sensor of this type.

2.2.2 Impedance matching type design

Turbulence-induced acoustic signals reach the skin surface by passing through many tissue layers from the arterial wall. The acoustic signal to be captured also takes a path from the skin surface until it reaches the sensor elements inside the sensor. In order for the radiated energy of the acoustic signal to be transmitted to the sensing elements with high efficiency throughout this entire path, the acoustic impedance of the layers through which the signal passes must be close to each other. For this reason, with the impedance matching type design, maximum energy can be drawn from the source. As a first step in the design, the materials used on the sensor surface should have nearly the same acoustic impedance value as the skin surface where the acoustic signal comes from.

When viewed at the cellular scale, the human body is mostly made up of water. Accordingly, it is not difficult to estimate that the acoustic impedance of the human body is close to water. Szabo et al. [64] calculated the acoustic impedances of tissues in the human body. In light of this information, it may be appropriate to use water or a material with similar impedances as the contact material of the sensor.

Acoustic impedance and density are directly proportional values. The density of the material to be used in the sensor and to make contact with the skin surface should be close to water. In this case, signals coming from the sensor surface at high frequencies cannot be detected due to the damping effect [33] mentioned in chapter 2.2.1.

Salman, Sert, and Yazicioglu et al. [31], Salman and Yazicioglu et al. [32] and et al. [52], Padmanabhan et al. [37], and Schwartz et al. [43] showed that the acoustic signals originating from turbulence were mostly below 800 Hz and the major effect was around 350 Hz.

In this study, for the sensor design method, considering the application area and the signal frequency band to be measured, "Impedance matching type design" was

preferred, where relatively weak acoustic signals can be received and low frequencies can be measured efficiently.

	Density	Speed of Sound	Impedance (MRayl)
	ρ (kg/m³)	c (m/s)	Z (10^6 kg/m²/s)
Air (25°C)	1.16	344	0.0004
Water (22°C)	998	1482	1.48
Blood	1060	1584	1.68
Skeletal muscle	1041	1580	1.65
Liver	1050	1578	1.64
Kidney	1050	1560	1.64
Fat	928	1430	1.33
Bone	1600	3360	5.69

Figure 2.8 Acoustic impedances of air, water, and tissues [64]

2.3 Sensor design

The first step in the sensor design process is to decide on the type of acoustic sensor. In Chapter 2.2, it was explained that the Impedance matching type design is suitable for the non-invasive detection of arterial occlusion by acoustic methods. In the next stage, the geometric boundaries of the sensor will be determined in accordance with the application environment. Then, the type and number of sensors to be used will be determined and the sensor will be designed.

Salman and Yazicioglu et al. [32] studied the acoustic pressure fields (Axial Position and Frequency) for 50%, 70%, and 90% stenosis and for femoral and brachial common carotid arteries. In Figure 1.3, the axial position downstream of the stenosis can be seen clearly. The turbulence effects continue up to 100 mm in the most extreme condition. At low occlusion rates, there are stenosis effects that persist up to 60 mm.

On the other hand, the value of the femoral arteries' diameters is 10 mm, and in the carotid arteries, around 6.4 mm [32].

It might be beneficial to also take into account the wavelengths of the shear waves at these frequencies while deciding on the sensor dimensions, however the effective deciding factor was assumed to be the sizes of the human body parts. Considering the average neck, leg, and rib cage size of the human body and the length at which turbulence effects persist, a design decision was made to have the sensor dimensions around 50 mm.

2.3.1 Type of ceramics

Piezoelectric ceramics are planned to be used as the passive sensing element within the sensors. For more sensitive detection, it is appropriate to use a single crystal or textured ceramics that give high RVS (Receiving Voltage Sensitivity) values. However, conventional piezoceramics are mostly the first option since these types of ceramics are not available to supply and their costs are very expensive.

Piezoelectric ceramics are produced in two different types:

- Hard piezoelectric ceramics
- Soft piezoelectric ceramics

Hard piezoelectric materials are stable against environmental conditions such as stress, temperature, humidity, and electric field. They are generally used in acoustic applications where energy is required to be sent over long distances and are generally used within narrow frequency bands around the resonant frequency. They are mostly used to generate and transmit an acoustic signal within that narrow operational band, not to measure acoustic signals at or near the resonant frequency [66].

Soft piezoelectric materials are used for sensing acoustic signals. The coupling factors, dielectric constant, and high permittivity coefficients are high. The fact

level of these coefficients is an indication of the sensing capacity of the sensor [66][67].

Considering all this information and due to its availability in the material supply process, PZT5A1 piezoelectric material, which is a Navy II-type piezoelectric material, was chosen in this study. In Figure 2.9, Morgan Technical Ceramics Material Catalogue is given. The key features of PZT5A1 piezoelectric materials are highlighted. The difference in voltage strain, dielectric component, and associated mechanical coupling coefficients is compared to hard PZT values as seen below.

Material		Units	PZT401	PZT402	PZT5A1	PZT5A3	PZT802	PZT807
Designation			Hard PZT	Hard PZT	Soft PZT	Soft PZT	Hard PZT	Hard PZT
Navy Type			I	I	II	II	III	III
EN 50324-1			100	100	200	200	100	100
Thermal Properties								
Curie Temperature	T_c	°C	330	325	370	350	300	300
Max Operating Temperature	T_{max}	°C	165	160	185	175	150	150
Mechanical Properties								
Density	ρ	kg/m³	7600	7720	7750	7910	7500	7650
Poisson's ratio	σ	-	0.31	0.31		0.31		
Compliances	S^E_{33}	x 10^{-12} m²/N	15.60	15.57	17.20	17.69	13.50	15.65
	S^E_{11}	x 10^{-12} m²/N	12.70	12.30	16.70	14.73	11.50	10.90
	S^D_{33}	x 10^{-12} m²/N	7.76	7.94	9.40	8.77		8.20
	S^D_{11}	x 10^{-12} m²/N	11.10	10.89	15.00	12.79	10.10	9.90
	Y^E_{33}	x 10^{10} N/m²	6.41	6.42	5.81	5.65	7.41	6.39
	Y^E_{11}	x 10^{10} N/m²	7.87	8.19	5.99	6.80	8.70	9.17
	Y^D_{33}	x 10^{10} N/m²	12.89	12.59	10.64	11.40		12.20
	Y^D_{11}	x 10^{10} N/m²	9.01	9.18	6.67	7.83	9.90	10.10
Electrical Properties								
Dielectric Constant	K^T_{33}	-	1395	1320	1800	1936	1150	1105
	K^T_{11}	-		1303		1616	1290	1190
Dielectric Loss	tan δ	-	0.20%	0.22%	2.00%	1.35%	0.30%	0.16%
Coercive Field	E_c	kV/mm		1.50		1.44		
Piezoelectric Properties								
Coupling Factors	k_p	-	0.58	0.56	0.62	0.62	0.54	0.55
	k_{31}	-	0.35	0.33	0.34	0.36	0.30	0.29
	k_{33}	-	0.67	0.70	0.67	0.71	0.64	0.69
	k_t	-		0.42	0.45	0.35		0.47
	k_{15}	-	0.70	0.71	0.69	0.69	0.55	
Charge or Strain Constants	d_{33}	pC/N or pm/V	315	307	409	425	250	260
	d_{31}	pC/N or pm/V	132	125	176	183	97	93
	d_{15}	pC/N or pm/V	511	495		585	300	294
Voltage or Stress Constants	g_{33}	x 10^{-3} V m/N	26.8	26.3	25.7	24.8	24.6	25.1
	g_{31}	x 10^{-3} V m/N	12.0	10.7	11.0	10.6	10.9	10.1
	g_{15}	x 10^{-3} V m/N		38.0		36.2	28.9	28.8
Frequency Constants	N_p	Hz-m	2190	2235	2000	2012	2285	2320
	N_1	Hz-m	1636	1650	1370	1400	1700	
	N_{3t}	Hz-m		2000	1940	1880	2070	2030
	N_5	Hz-m	1800	1944	1465	1750		
Mechancial Quality Factor	Q_m	-	600	575	60	90	1000	1200

Figure 2.9 Morgan technical ceramics material catalogue [67]

PZT5A1 can be defined as the most widely used piezoelectric material in sensor applications. It is frequently preferred in the space industry, medical industry, and defense industry products. The fact that it is produced and used in large quantities also provides a cost advantage over other types of ceramics.[68][69]

The type of piezoelectric materials that will be used as well as the material itself are important for the success of the design.

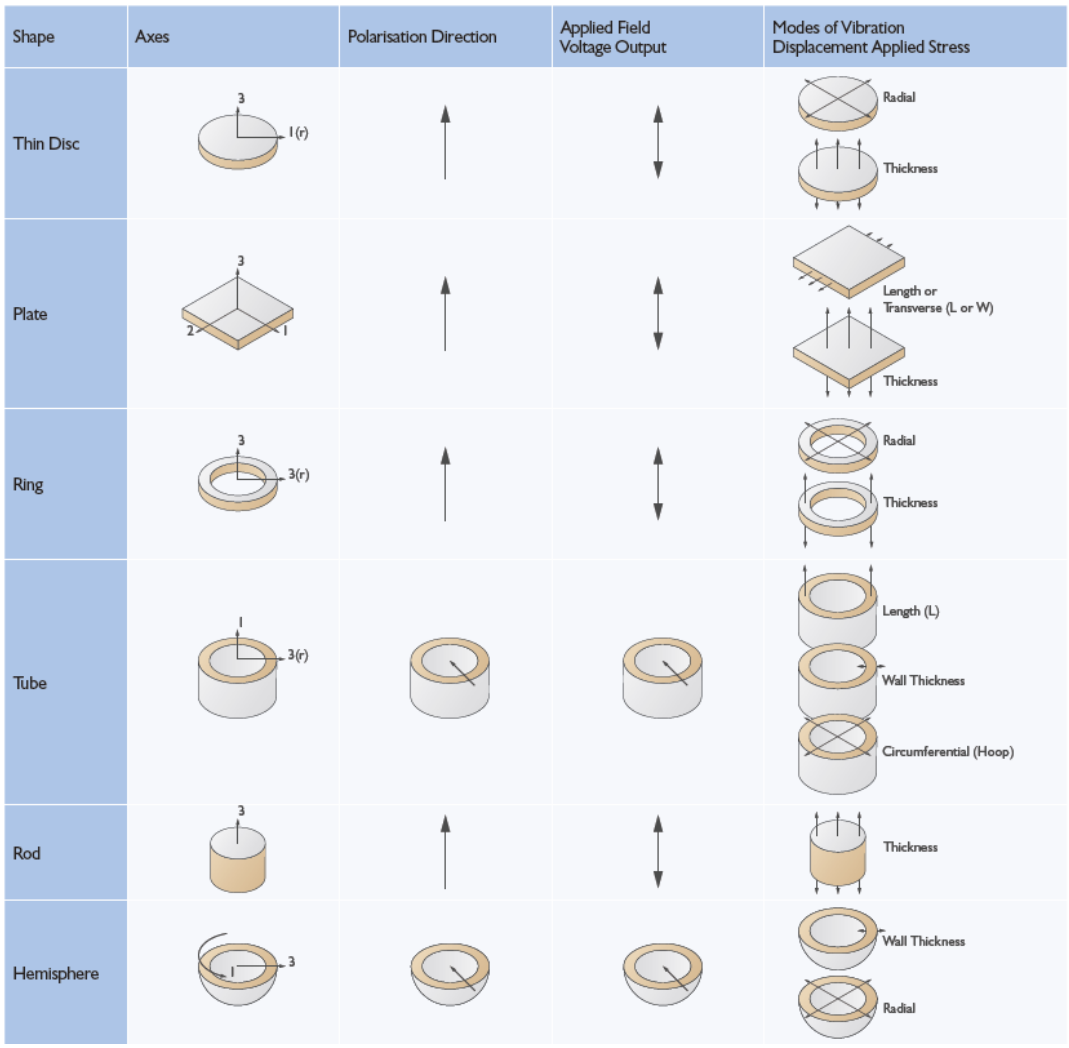

Figure 2.10 Morgan ceramics pzt product catalogue [67]

The general design logic is to create a ceramic cluster that will give maximum electrical output for a limited surface area (the decision the sensor area is at the limit of 100 mm was taken in Chapter 2.3). Available piezo ceramics can be seen in Figure 2.10 Morgan ceramics pzt product catalogue [67]. These ceramic designs and the preferences of the polarization directions are the most used ones. A comparison of all models of the ceramic products under similar conditions was made and the ceramic that will be used in the design was determined.

The voltage values that emerged by applying 1 Pa pressure on 5 types of ceramic materials (plate type piezo ceramic was not included in the analysis, due to the fact that itis in an asymmetrical shape and as such, not suitable for application) in Figure

2.10 were compared. Choosing the ceramics can also be done according to the static voltage values found in the catalogs published by the manufacturers (Morgan Ceramics PZT Product Catalogue [67]).

In the finite element method analysis of piezoceramics via the COMSOL 6.0 tool, the polarization directions are defined as shown in Morgan Ceramics PZT Product Catalogue [67]. Immediately afterward, the relevant ceramic surfaces are defined as “ground” and “terminal” according to this polarization direction. The voltage generated on the “terminal” surfaces was calculated with a cumulative average operator “aveop” and plotted according to frequency.

Disc-type piezoceramic mesh structure and polarization direction are shown in Figure 2.11. A pressure of 1 Pa was applied to all surfaces of the piezo disc polarized in the Z-axis direction. Since the aim was to select the piezoceramic parts to use, the analysis was carried out under ideal conditions without introducing the application conditions as inputs to the analysis.

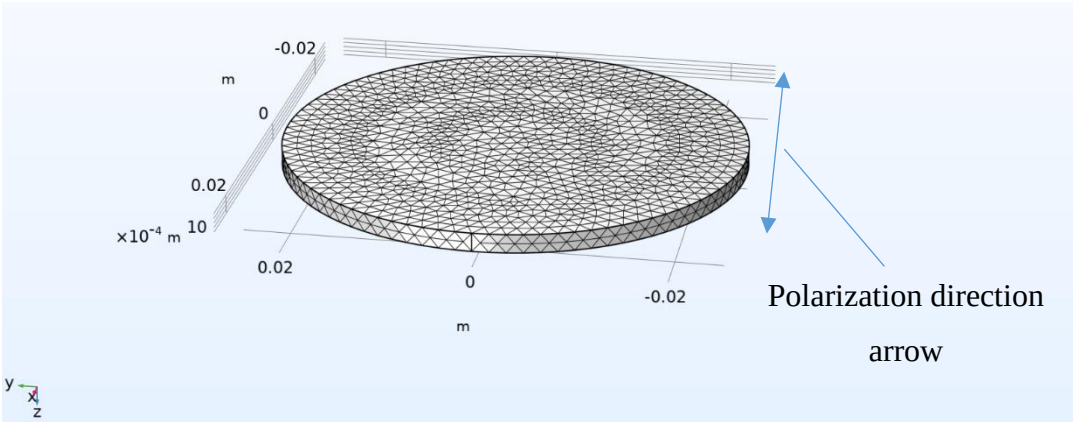

Figure 2.11 Disc-type piezoceramic mesh structure and the polarization direction

In Figure 2.12, the variation of the terminal voltage of the disc-type piezoceramic with respect to the frequency band can be seen. According to the results in the

figure, it can be said that ceramics have a constant voltage response in the FEM analyse up to 1000 Hz.

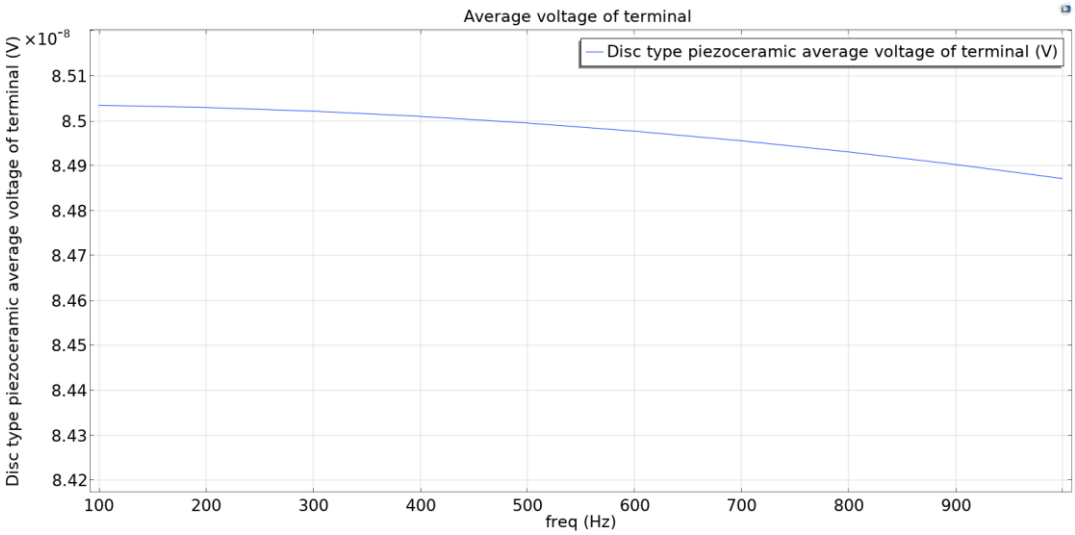

Figure 2.12 Disc-type piezoceramic average voltage of terminal

Secondly, there is also the rod-type piezoceramic part in Figure 2.13. It contains the same polarization direction as the piezoceramic disc. The lower and upper circular surfaces of the cylindrical section were determined as the terminal and ground electrode areas. Since the ceramic contains more piezo material per unit surface area than others, it results in a relatively more efficient sensor for this type of application. In Figure 2.14, the voltage values produced by the ceramic are given, where 1 Pa pressure is applied to all surfaces up to 1000 Hz.

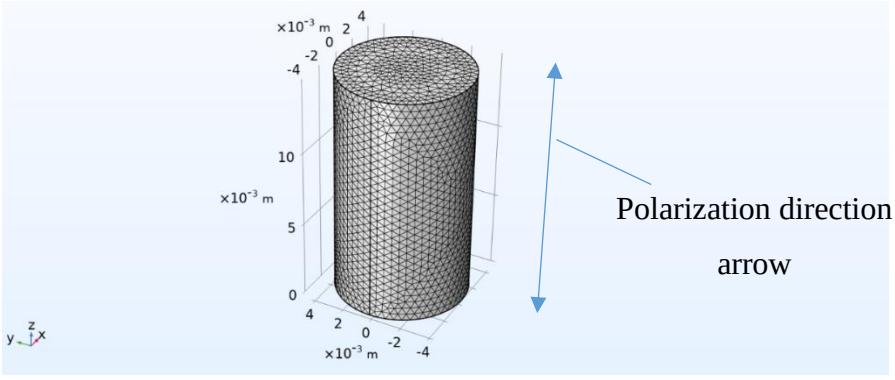

Figure 2.13 Rod-type piezoceramic mesh structure and the polarization direction

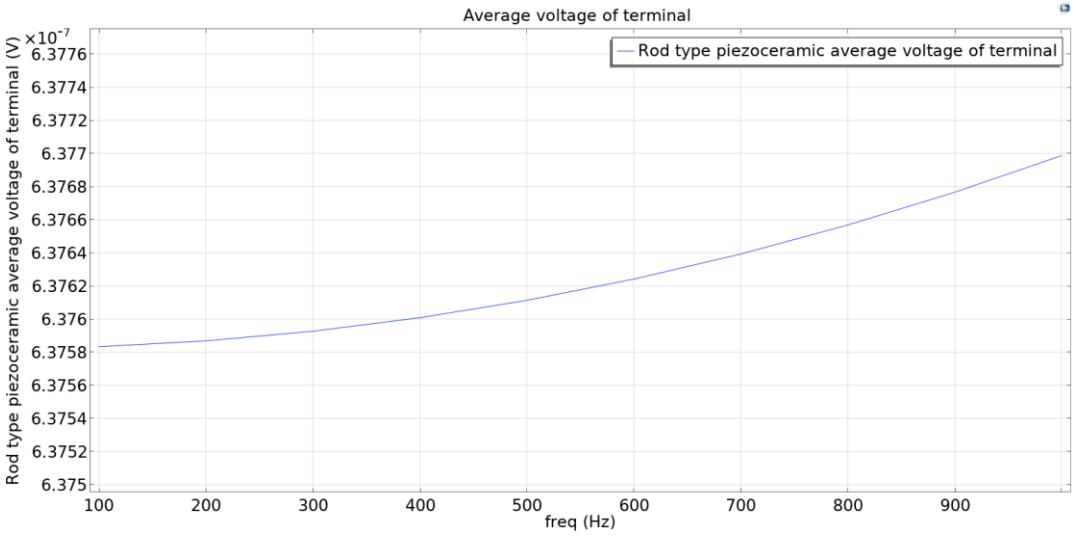

Figure 2.14 Rod-type piezoceramic average voltage of terminal

In Figure 2.15 Tube-type piezoceramic mesh structure and the polarization direction can be seen. The way the tube-type piezoceramic works is different from the previous two ceramics. Since the mode shape is in the form of "breathing" at the first vibration frequency, being radially polarized makes ceramic more efficient. Coordinate transformation is required in order to define the polarization direction in cylindrical coordinates in the piezoceramic module in the COMSOL 6.0 finite element program. Conversion from orthogonal coordinate to cylindrical coordinate is described inTable 2.2.

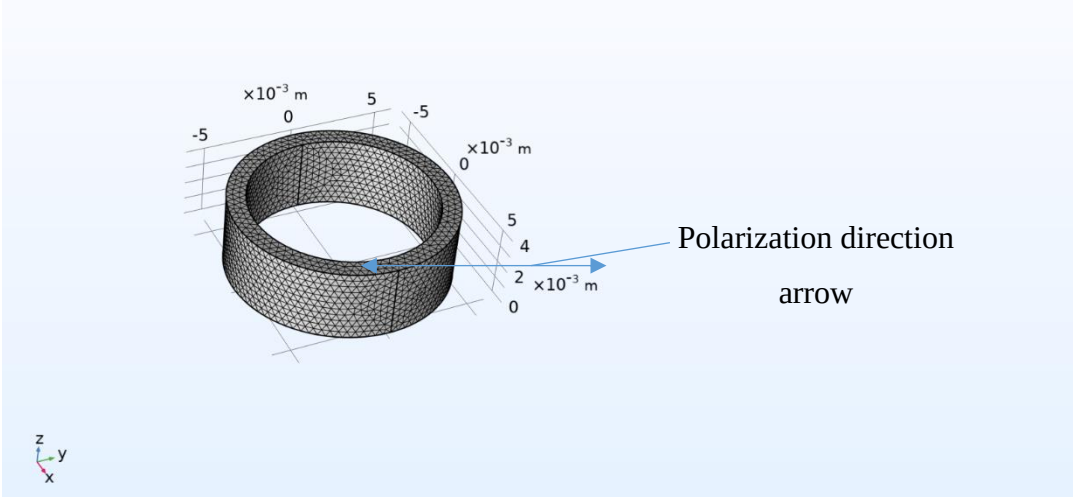

Figure 2.15 Tube-type piezoceramic mesh structure and the polarization direction

Table 2.2 Conversion formula from orthogonal coordinate to cylindrical coordinate

	x	y	z
x1	$-sin(ATAN2(Y,X))$	$cos(atan2(Y,X))$	0
x2	0	0	1
x3	$cos(atan2(Y,X))$	$sin(atan2(Y,X))$	0

In Figure 2.16, the voltage values produced by the tube ceramic are given for the case where 1 Pa pressure is applied to all surfaces up to 1000 Hz.

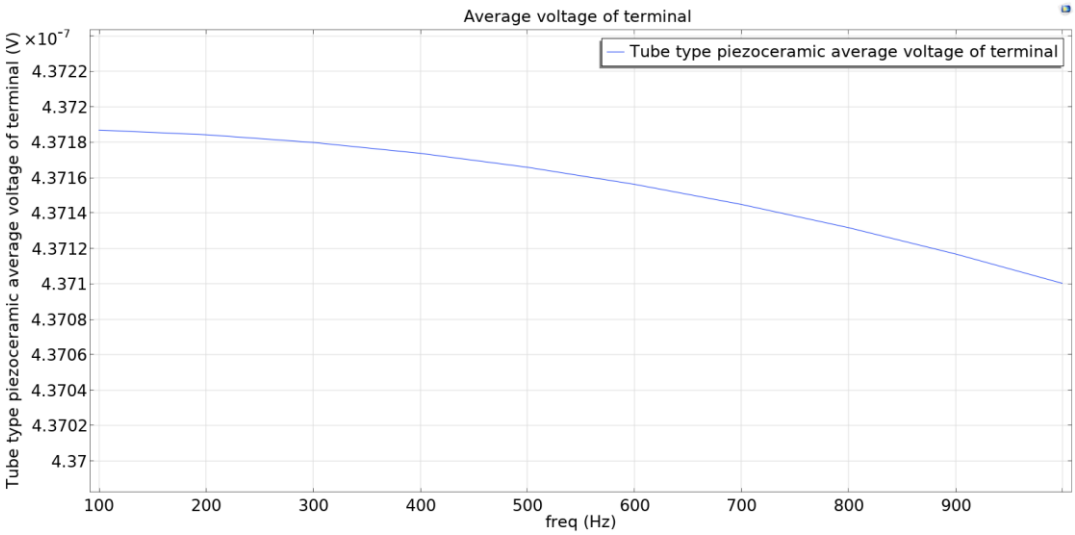

Figure 2.16 Tube-type piezoceramic average voltage of terminal

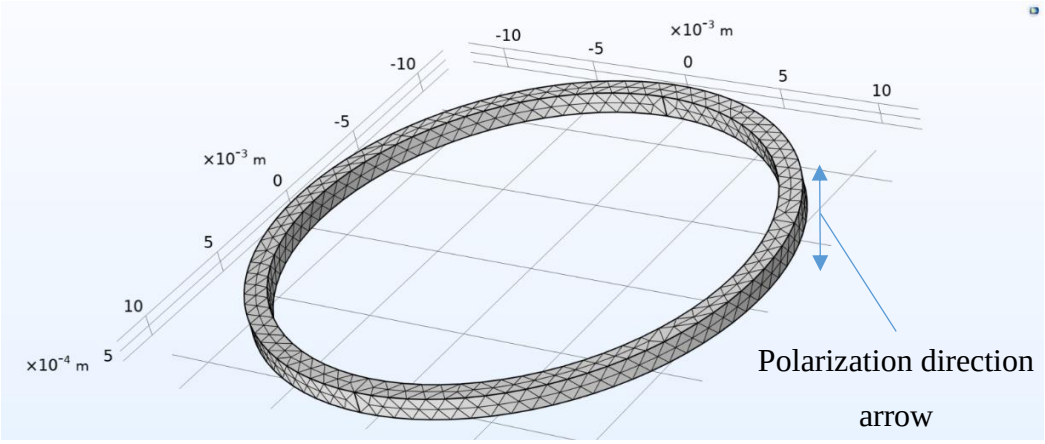

Figure 2.17 Ring-type piezoceramic mesh structure and the polarization direction

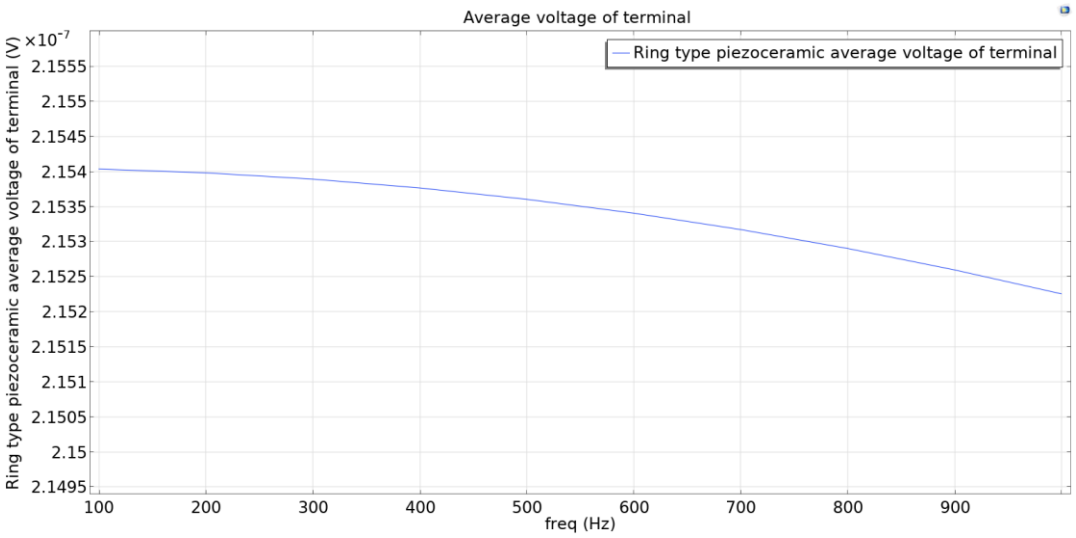

Figure 2.18 Ring-type piezoceramic, the average voltage at the terminal

In Figure 2.17, the ring type of piezoceramic mesh structure and polarization direction, and in Figure 2.18, the voltage values produced by tube ceramic are given. The voltage values are for the case that 1 Pa pressure is applied to all surfaces up to 1000 Hz

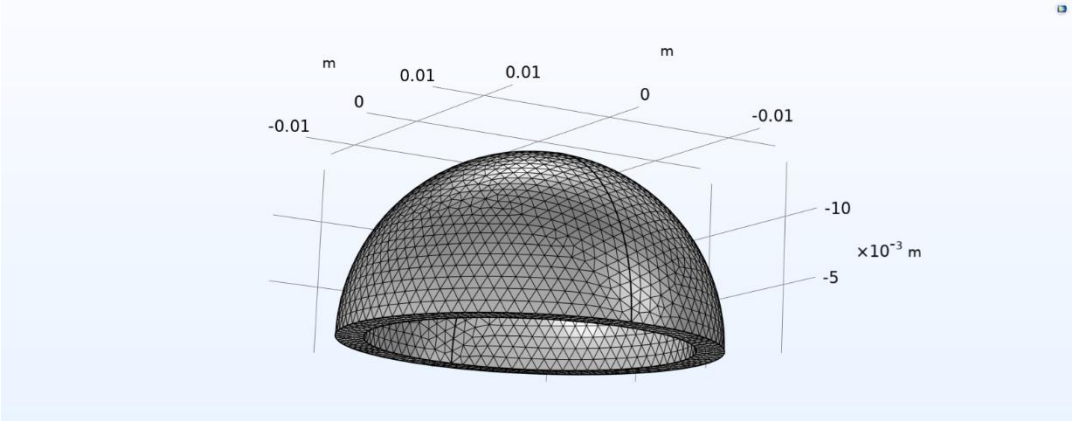

Figure 2.19 Hemisphere-type piezoceramic mesh structure and the polarization direction

The hemispherical piezoceramic is the final product to be evaluated among the piezoceramics available on the market. Hemispherical piezoceramics are spherically polarized. The inner surface of the sphere is produced as "ground" and the outer surface as "terminal". Just as the polarization direction of cylindrically polarized tube ceramics should be defined in accordance with cylindrical

coordinates, the polarization direction of hemisphere piezoceramic should be defined by spherical coordinates transformation. The conversion formula from orthogonal coordinate to spherical coordinate can be seen in Table 2.3.

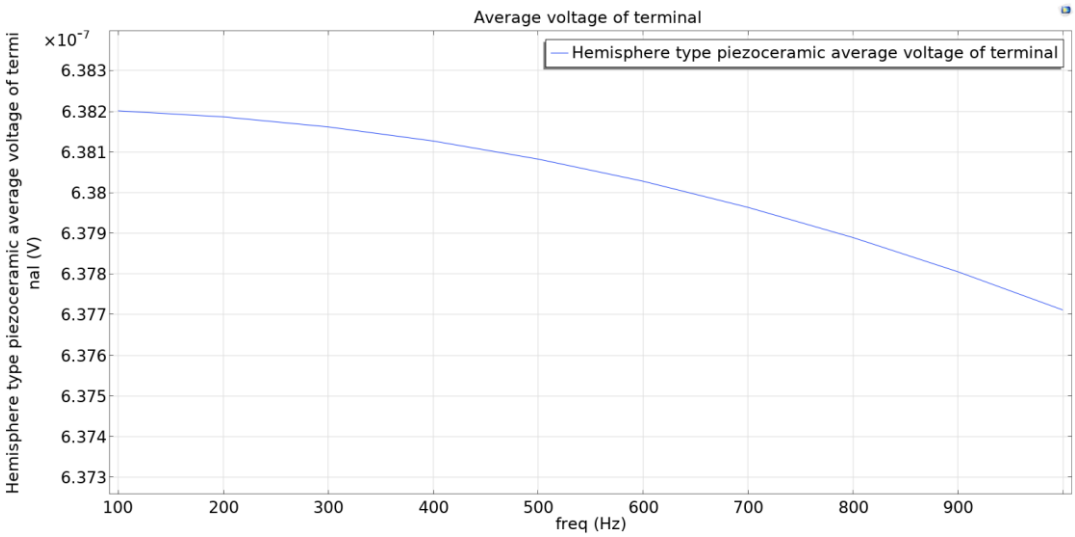

Figure 2.20 Hemisphere-type piezoceramic, the average voltage at the terminal

Table 2.3 Conversion formulas from orthogonal coordinate to spherical coordinate

	x1	x2	x3
x	$\cos\left(atan2(Y,X)\right) * \cos\left(\text{acos}\left(\frac{Z}{sqrt(X^2+Y^2+Z^2)}\right)\right)$	$-\sin\left(ATAN2(Y,X)\right)$	$cos\left(atan2(Y,X)\right) * sin\left(acos\left(Z/sqrt(X^2+Y^2+Z^2)\right)\right)$
y	$sin\left(atan2(Y,X)\right) * cos\left(acos\left(Z/sqrt(X^2+Y^2+Z^2)\right)\right)$	$cos\left(atan2(Y,X)\right)$	$sin\left(atan2(Y,X)\right) * sin\left(acos\left(Z/sqrt(X^2+Y^2+Z^2)\right)\right)$
z	$-sin\left(ATAN2(Y,X)\right)$	0	$cos\left(acos\left(Z/sqrt(X^2+Y^2+Z^2)\right)\right)$

Table 2.4 Mesh element numbers and piezoceramics average voltage of terminal(V) 5 types of piezo ceramics

	Mesh elements		Piezoceramics' average voltage at the terminal (V)
Disc	Tetrahedra	11194	0.085
	Triangles	4056	
	Edge Elements	182	
	Vertex Elements	4	
Rod	Tetrahedra	99017	0.6225
	Triangles	4588	
	Edge Elements	162	
	Vertex Elements	4	
Tube	Tetrahedra	28866	0.4
	Triangles	4752	
	Edge Elements	372	
	Vertex Elements	4	
Hemisphere	Tetrahedra	37147	0.6375
	Triangles	6162	
	Edge Elements	254	
	Vertex Elements	6	
Ring	Tetrahedra	2060	0.2
	Triangles	1376	
	Edge Elements	348	
	Vertex Elements	8	

In Table 3, the information on the mesh structure used in the finite element analysis and the voltage outputs of the analysis are presented. This information is not the data obtained because of vascular occlusion within the scope of the study, but the comparison data for the selection of piezoceramics, which are the sensing parts of the sensor.

Increasing the number of ceramics used contributes to the sensing capacity of the sensor in different ways. It is appropriate to have as many ceramics in the sensor as possible, but still, the number of ceramics is limited due to the structure of the

signals (the dimension of the effect of the acoustic signal formed) and the dimensions of the measurement area.

According to Table 2.4, three types of ceramics (tube, hemisphere, and rod) have been tested against RVS and directivity.

Due to its geometric advantage, tube ceramics can be used with one of the other two piezoceramic variants. In other words, both hemisphere and rod piezoceramics can be used concentrically with tube piezoceramics. The following pairs of these three piezoceramic types have been evaluated for final design:

- Tube-rod combinations
- Tube-hemisphere combinations

The electrical outputs of the hemisphere and rod piezoceramics were measured to be close to each other. One difference is that the rod piezoelectric ceramic occupies less space than the hemisphere ceramic, which also means that compared to the tube-rod pair, the tube-hemisphere couple will be less in numbers owing to the necessity to keep the size of the sensor structure around 100 mm (as explained in Chapter 2.3).

2.3.2 Number of ceramics

An alternative design with 8-rod tube piezoceramic pairs can be seen in Figure 2.21. In Figure 2.22, there are 3 alternative designs that have been trailed before the final design, which are (a) 9 pairs tube-hemisphere combination design, (b) 9 pairs tube-rod combination design, and (c) 5 pairs tube-rod combination design.

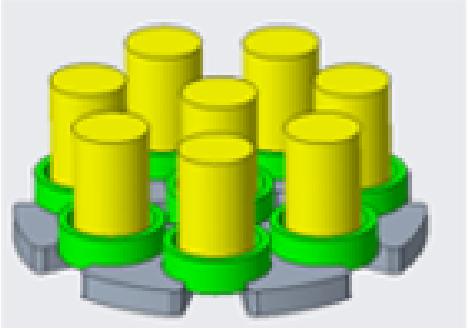

Figure 2.21 8 rod-tube piezoceramic pairs Design Alternative 1

Four alternative designs were evaluated according to the geometric constraints:

- The largest artery diameter is around 10 mm [53] [54] [55].
- The distance from the arteries to the skin is between 10 mm and 60 mm [53] [54] [55].
- The occlusion effects extend to a maximum of 100 mm [31] [32].

Apart from the piezoceramics, a shell structure will also be created to ensure and maintain the correct positioning of the ceramics while forming their outer region which also acts as a protection against environmental noise. All these additional layers bring along an increase in the sensor size.

Table 2.5 Design alternatives

Design Alternative 1		**Design Alternative 2**		**Design Alternative 3**		**Design Alternative 4**	
Type of ceramics	**No. of ceramics**	**Type of ceramics**	**No. of ceramics**	**Type of ceramics**	**No. of ceramics**	**Type of ceramics**	**No. of ceramics**
Rod	8	Hemisphere	9	Rod	9	Rod	5
Tube	8	Tube	9	Tube	9	Tube	5
Dimensions of sensing element	Ø 40 mm	Dimensions of sensing element	85 x 85 mm	Dimensions of sensing element	45 x 45 mm	Dimensions of sensing element	45 x 45 mm

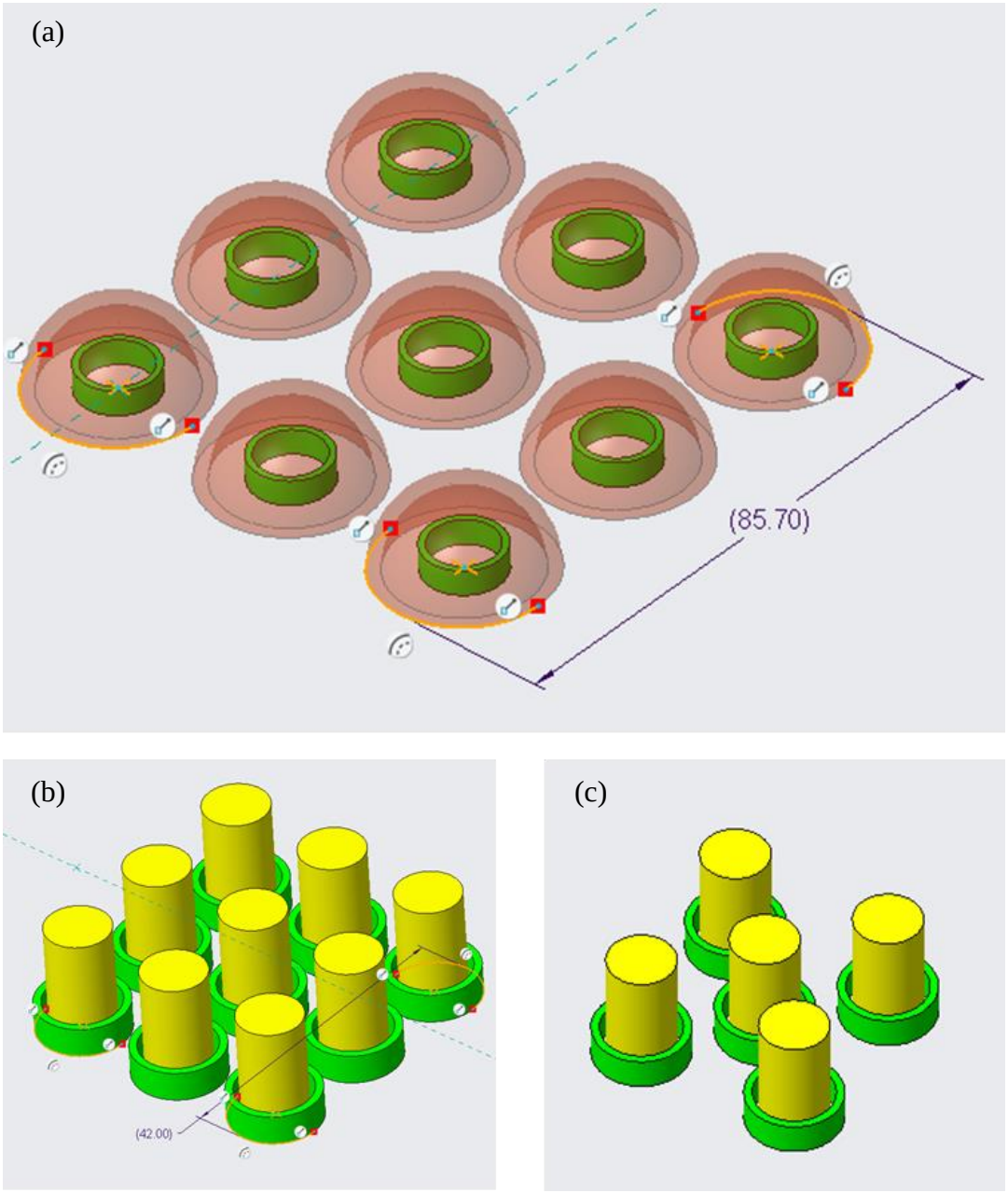

Figure 2.22 (a) 9 pairs tube-hemisphere combination Design Alternative 2 (b) 9 pairs tube-rod combination Design Alternative 3 (c) 5 pairs tube-rod combination Design Alternative 4

All outputs have been evaluated together, and the ceramics that will be used within the sensor have been decided as 1x rod type and 1x tube type piezoceramic, as a

pair. As a design decision, 8x PZT pairs,i.e Design Alternative 1, was used considering the sensor dimensions and sensitivity requirements of the application.

2.3.3 Sensor Structure & Production

Once it was decided that 8x rod type and 8x tube type piezoceramic pairs would be used in the sensor design, two issues remained unresolved for the sensor to be assembled:

- How to electrically connect the piezoceramics: in parallel or series. This also impacts the RVS value and polar pattern of the sensor.
- Requirements of the sensor mechanical structure.

2.3.3.1 Design of Sensor Structure

The features of the mechanical structure of the sensor are:

- It should hold the piezoceramics in the correct position, i.e., they would be placed axisymmetrically and the dimensions of all ceramics on the axis perpendicular to the measurement surface should be the same.
- The inner medium of the sensor must be able to receive signals from the measurement surface effectively, i.e. with minimum propagation/reflection losses.
- It must provide isolation against acoustic signals coming from a direction other than the measuring surface of the sensor, i.e. directional as required,
- It must physically protect the piezoceramics and its solders against impacts.

The next step subsequent to the definition of the types, numbers, and position orientations of the piezoceramics, i.e. the sensing elements of the sensor, is the determination of the mechanical structure in accordance with the criteria above. In Chapter 2.3.1 and Chapter 2.3.2, it was decided to use Design Alternative 1 among four different conceptual designs. In Figure 2.23, Design Alternative 1 is seen together with the positioning apparatus designed.

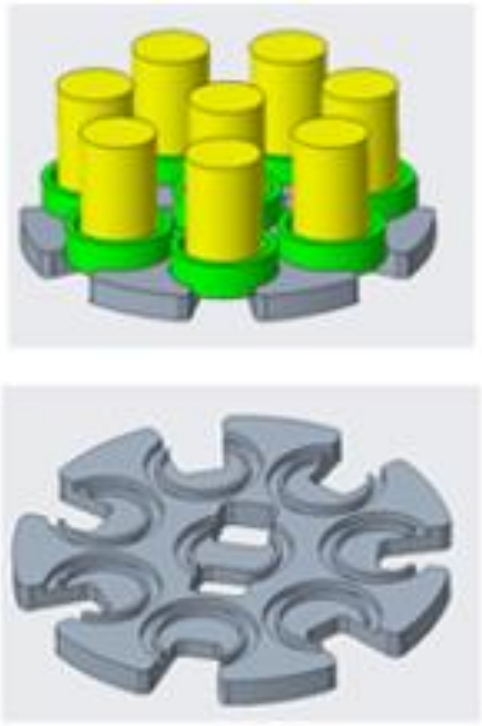

Figure 2.23 Ceramics with an apparatus for production (Design Alternative 1)

The sensor is designed to consist of 3 main structures:

- Shell Structure,
- Polyurethane Filling Material, and
- Piezoceramic Pairs.

Piezoceramics should be placed in the sensor structure as given in Figure 2.23 (Design Alternative 1). According to this, a shell structure is designed as given in Figure 2.24. It has a pool where the piezoceramics are located, an air duct surrounding the pool, and a hole at the bottom of this pool, which acts as an electrical outlet for the cables that have been soldered to the electrodes of the piezoceramics.

It was evaluated that filling in the pool with a proper filler material helps transmit the signal to the piezoceramics. In this way, in case of vascular occlusion, the acoustic signal that the sensor will receive through touching the skin will be maximized in the area where the artery is located.

In Chapter 2.2 and Chapter 2.2.2, Sensor types were emphasized, and it was stated that the design of the sensor would be an “Impedance Matching Type Sensor” considering the terms of the requirements and dynamics of the application. According to this decision, the acoustic impedance of the skin tissue and the filling material should be selected as close to each other as possible in order to maximize the power of the acoustic signal transmitted from the skin tissue to the piezoceramics. This material will be filled in the pool of the shell structure, covering the piezoceramics and filling in all the remaining volume. The positioning of piezoceramics can be seen in Figure 2.25 and the filling material placed in the pool can be seen in Figure 2.26.

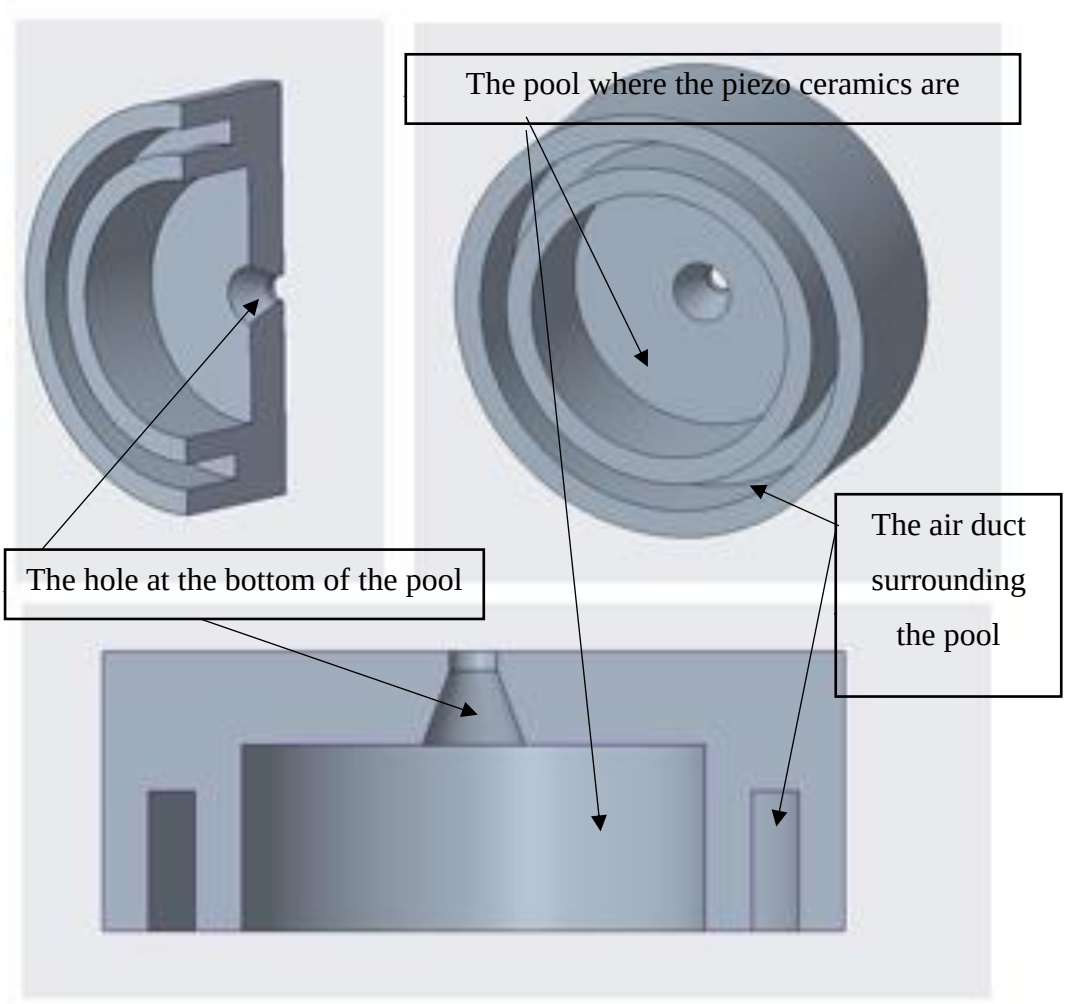

Figure 2.24 The shell structure in which the ceramics are placed

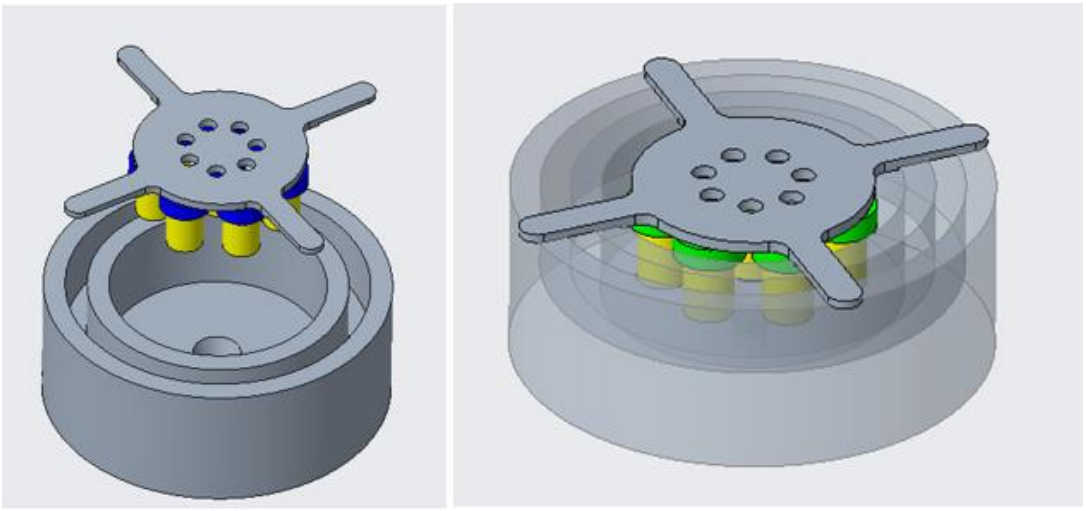

Figure 2.25 Positioning of piezo ceramics

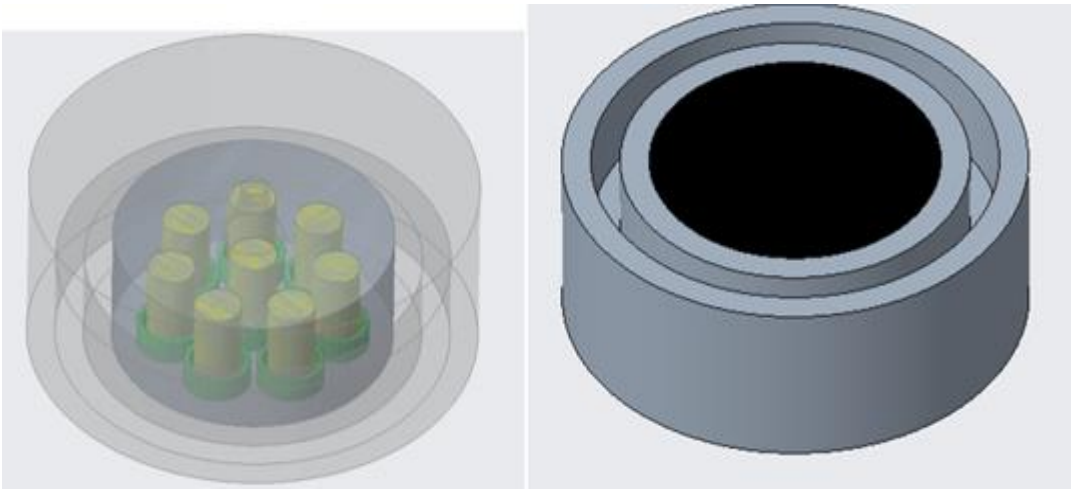

Figure 2.26 Sensor

In “Acoustic Impedance Matching Type” sensors, isolation can be achieved by making a mismatch on the acoustic impedances at the angles where the signal is not desired to be received to create a directivity on the sensor.

The acoustic impedance of the shell structure material (VisiJet ABS Like material[70]) and the acoustic impedance of the air [64] that will fill the air channel placed around the pool of shell structure are quite different from the acoustic

impedance of the skin tissue structure [64] and polyurethane filling material [71], where the signal is desired to be transferred from. According to this structure, only

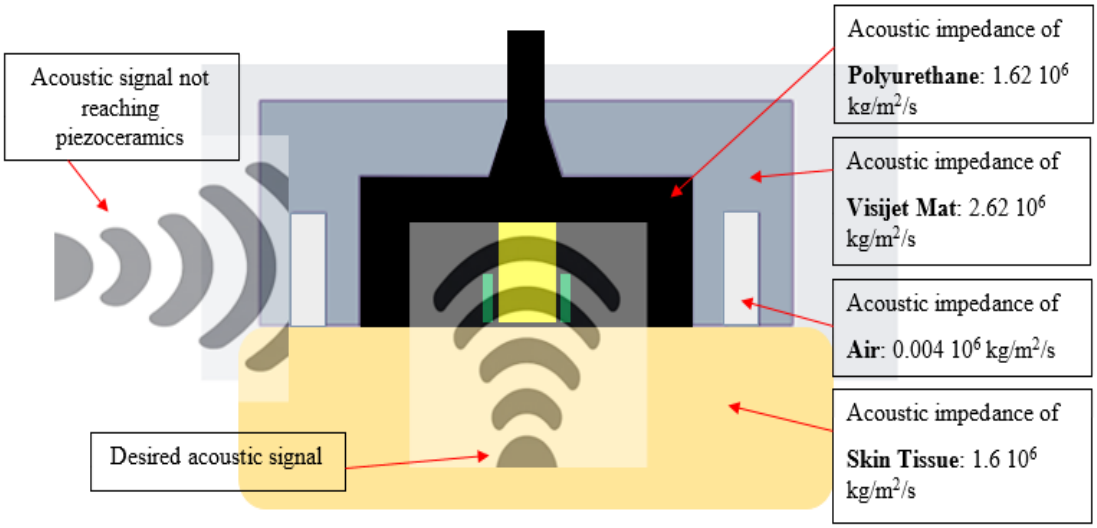

the desired acoustic signals are expected to be efficiently transferred into the Polyurethane Filling Material which is the only medium that touches the skin.

Figure 2.27 Impedance matching and mismatching mechanism of the sensor

As visually explained in Figure 2.27, the acoustic signal from the skin tissue is transferred to the piezoceramics shown in yellow and green. However, the acoustic signal from the side of the sensor cannot be efficiently transferred to piezoceramics due to the differences between the impedances of the shell structure material (VisiJet ABS Like material[70]), air[64] and polyurethane filling material layers[71].

Acoustic impedance is the product of the density and the speed of sound; and specifies the ratio of acoustic pressure to particle velocity. By definition, acoustic impedance is directly proportional to density. The speed of sound depends on elasticity and density, and elasticity increases as it increases and density decreases. [72-74]

The properties of VisiJet ABS Like material and polyurethane filling material layers that were chosen for the application owing to their acoustic impedances are given in Appendix A.

2.3.3.2 Finite Element Analysis of the Sensor Structure

Another decision to be made after determining the types and number of piezoceramics is to decide the electrical connection of the piezoceramics; either in parallel or series.

The decision to use serial or parallel affects the sensing capacity of the sensor in two different ways:

- In parallel connection: RVS does not change, and directivity varies with respect to frequency. In our case, the main lobe occurs, i.e. directivity increases at the main lobe (at $\theta = 0°$)
- In series connection: RVS increases, and directivity varies with respect to frequency. In our case, directivity is slightly affected.

Parallel circuit connection preference is related to the SNR value described in chapter 2.1 design parameters. The electrical potential difference on the piezoceramics induced by the acoustic pressure is shared across ceramics, and therefore does not increase in parallel connection. This can be interpreted similarly to connecting multiple batteries in parallel. The fact that the voltage stays the same, means that the RVS values would remain the same. On the other hand, with the use of multiple piezoceramics of the sensor, the DI value, i.e., the directivity, increases compared to a single piezoceramic. If the piezoceramics to be connected in parallel have an SNR value above the detection threshold for the incoming acoustic signal, the parallel connection may be preferred to increase the directivity of the sensor [75].

Piezoceramics can be operated in a series connection. In this case, the voltage generated by the acoustic pressure increases cumulatively throughout the circuit. Therefore, the output voltage value obtained per unit pressure is expected to increase; so does the RVS. However, every piezoceramic, especially when used in passive mode, has a phase noise. The serial connection increases the broadband

noise on the circuit, in which case, the SNR value may not necessarily increase since the noise floor might be expected to raise to a higher value [76-80].

In series connection of the piezoceramics, the voltages induced by the acoustic signal accumulate over each ceramic, and the resultant voltage output is then input to the preamplifier or the signal processing circuitry in the electronic unit. Since the voltages on each ceramic are added on top of each other, the sensitivity of the sensor towards the angle of incidence (direction of the source) is reduced. As such, the directivity increase is observed to be less in systems with series connections compared to systems with parallel connections [76-80].

The method of serially-connected piezoceramics is uncommon in applications due to their fewer advantages over the parallel connection. Especially in cases where weak signals induced by turbulence due to arterial occlusion are a matter of concern, any risk of an increase in environmental or electronic noise should be eliminated or mitigated.

In cases where the signal cannot be recovered using a sensor with parallel-connected sensing elements, another option might be to process the outputs of each piezoceramic, separately. The signal to be measured is deterministic, as opposed to the noise originating from the sensor data acquisition system, which is randomly distributed. When the outputs of different piezoceramics are evaluated cumulatively through signal processing software, the increase in the deterministic signal becomes higher than the random noise. This operation is called “Array gain” and it provides an increase in the SNR [81], which is directly proportional to the number of array elements used.

Dey et al. [76] positioned the piezoceramics in an acoustic sensor mechanically in series but connected electrically in parallel.

RVS and DI values of the existing structure with parallel circuit connection were analyzed using a finite element model through the COMSOL 6.0 Multiphysics commercial analysis tool.

There are two important goals of finite element analysis. First, to get the RVS values of the sensor and second DI values of the sensor, together with the 3D radiation pattern in polar coordinates.

The RVS and DI values and their calculations are explained in Chapter 2.1.2 and Chapter 2.1.3. It is not necessary to know the behavior of the sensor during vascular occlusion application to be able to calculate or analyze the RVS and DI values. To be more precise, let us assume a reference case, where the sensor will be used to capture the reference acoustic signals. To calculate the RVS and DI values, an RMS pressure of 1 Pa on the surface of the sensor was taken as a reference, rather than the real pressure values in the application. For this reason, a finite element model was created with a pressure of 1 Pa-RMS with a water domain in front of the solid model of the sensor structure.

The FEM analysis was set up with the COMSOL Multiphysics 6.0 as follows. A three-layer water domain, Figure 2.29, is positioned in front of the solid model of the sensor, Figure 2.28. The simulation is based on a lossless environment where the pressure of 1 Pa RMS defined at the three-layer water domain reaches the front surface of the sensor with the same magnitude. As explained in Chapter 2.1, the RVS and DI values of the sensor are calculated with reference to the 1 Pa RMS pressure on the front surface of the sensor. Analyses were carried out in the 50 Hz-1000 Hz frequency band. In the graphs below, the images and results obtained at

350 Hz are given. This frequency is one of the most dominant frequencies [31-32] according to previous research made.

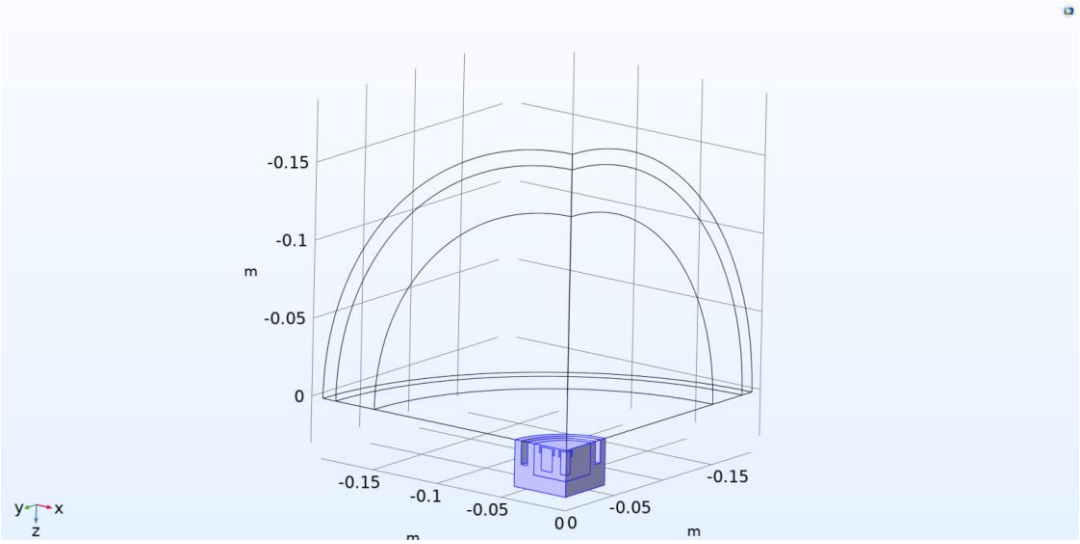

Figure 2.28 Solid domain

In Figure 2.28 and Figure 2.29, Solid Domain and Water Domain can be observed. FEM analysis requires serious computational power since the analysis of such a sensor structure has to incorporate a complex geometry, different material types, and a high mesh density. To save time and space, analyses were made using the axis of symmetry. The displays are given in a quadrant for convenience.

The water domain, which is defined on the front surface of the sensor to receive the signal, has been defined in 3 layers. The layers are as follows:

PML: A Perfectly Matched Layer applies a complex coordinate scaling to a layer of virtual domains surrounding the physical region of interest. When appropriately tuned, this layer absorbs all outgoing wave energy in frequency-domain problems, without any impedance mismatch causing spurious reflections at the boundary.

BPF: Background Pressure Field node to model a background/incident pressure wave to study the scattered pressure field *p*s, which is defined as the difference between the total acoustic pressure *p*t and the background pressure field *p*b:

IWD: Inner Water Domain.

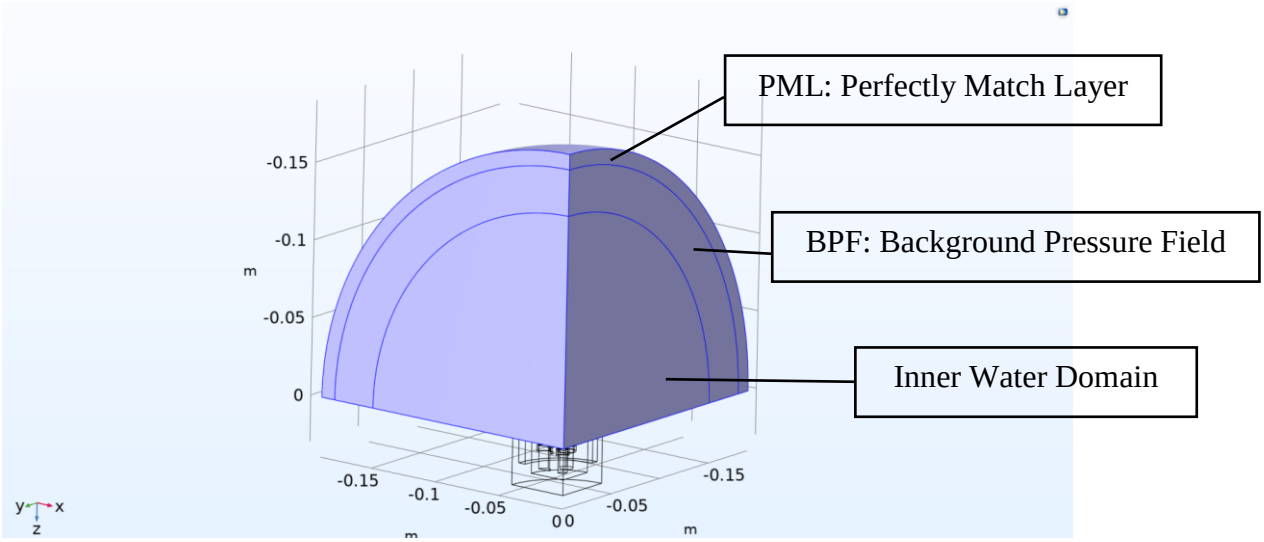

Figure 2.29 Water domain.

The PML domain, defined as the outermost layer, is used to avoid or minimize the possible reflections in the Finite Element Model. For this reason, it is defined outside the layer in which the acoustic source is also defined (BPF: Background Pressure Field). Thanks to the PML domain in FEM analysis models, it is ensured that the sensor is modeled in an infinite volume of water and therefore is not exposed to any acoustic reflection. For a properly functioning PML, the difference in sound pressure level between its inner and outer surfaces should be at least 40 dB [82]. The PML used in the model is illustrated in Figure 2.30. The difference between the inner and outer surface pressures is around 80 dB in the model of this study.

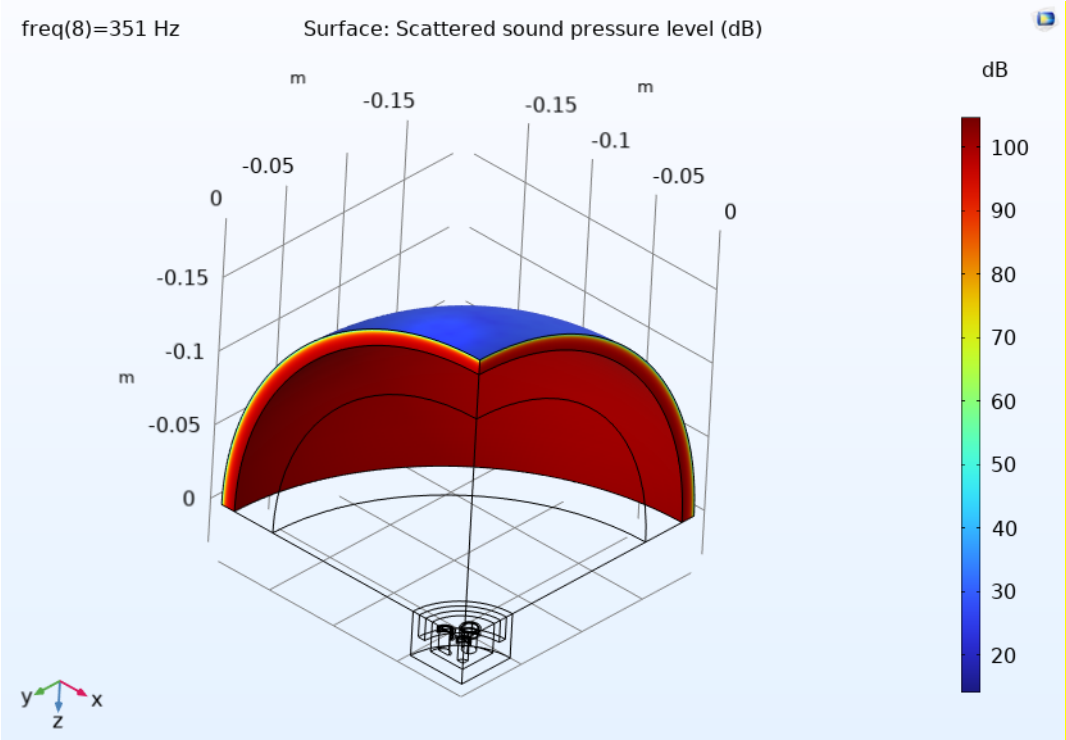

Figure 2.30 PML was created to reduce the effects of reflection and other losses.

Under the PML is the BPF. In BPF, the acoustic signal that will be transmitted to the reception surface of the sensor is defined. In this FEM model, the acoustic signal is defined to propagate in the form of a plane wave:

$$p_b = p_0 e^{-i(k\,.x)} = p_0 e^{-ik_i(\frac{x\,.e_k}{|e_k|})} \qquad \text{Eqn. 2. 5}$$

Where

- P_0 →Wave amplitude,
- k → Wave vector (amplitude $ks = \omega/c$)
- E_k → Awave direction vector
- x → Location on the boundary.

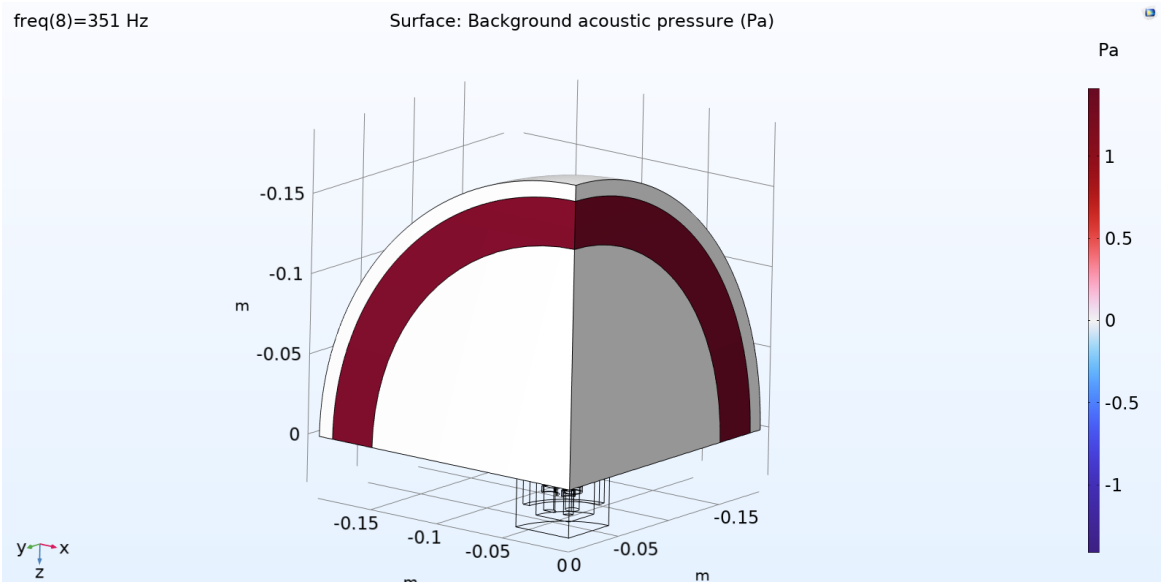

Figure 2.31 Background Pressure Field section where the acoustic pressure is defined in the pressure acoustic section in front of the sensor.

Figure 2.31 shows the BPF domain defined between the PML and Inner Water Domain. In Figure 2.32, the defined acoustic signal at 1 Pa RMS at 350 Hz is seen in the BPF domain. The direction of the acoustic signal is the +z axis.

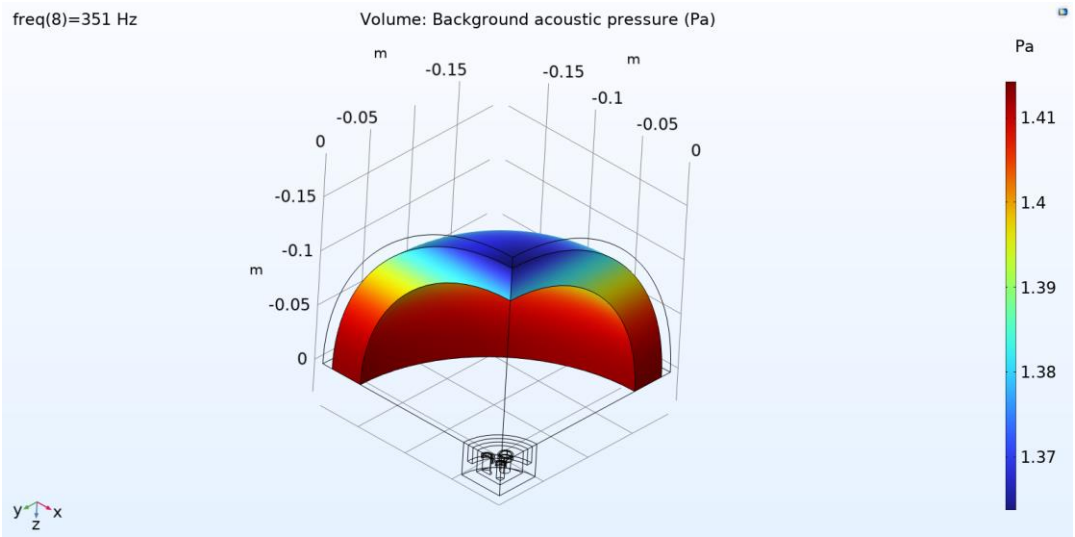

Figure 2.32 Acoustic pressure at 350 Hz in the Background Pressure Field domain.

The distribution of the acoustic pressure induced on the sensor surface is given in Figure 2.33. The sensor receives the acoustic signal at this surface. In Figure 2.34, terminal surfaces (+ electrodes) defined on piezoceramics are observed. The electrical potential difference, i.e., voltage, induced by the acoustic pressure is gathered from this surface.

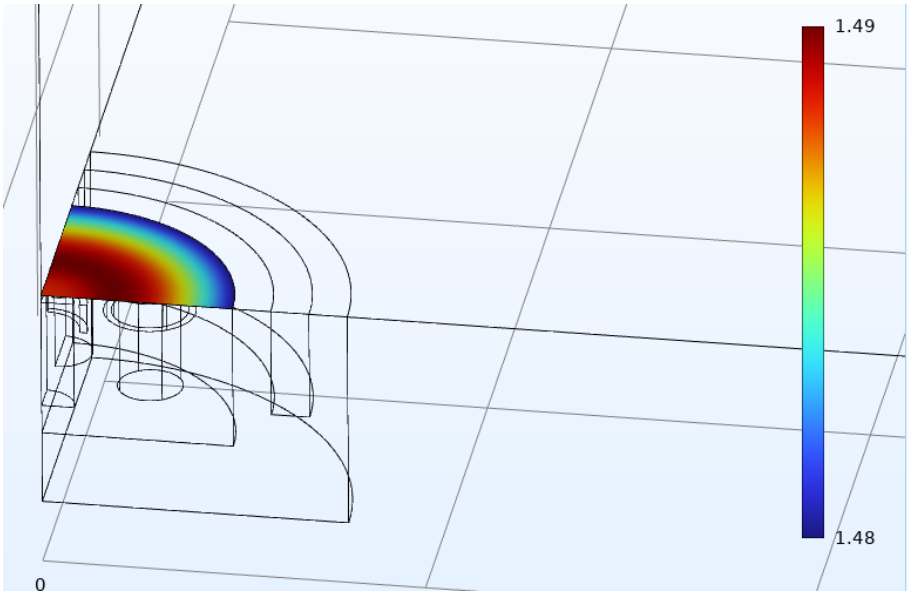

Figure 2.33 Acoustic pressure on the sensor originating from the Background Pressure Field at 350 Hz.

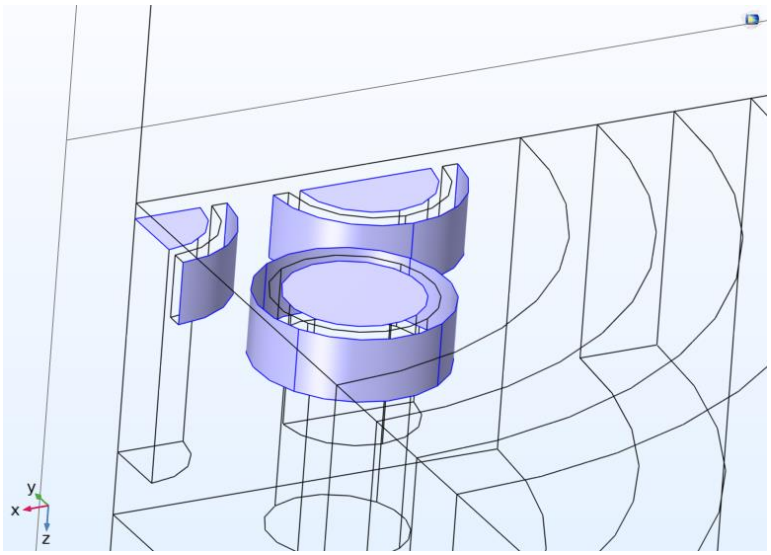

Figure 2.34 Electrodes defined on piezoceramics

As stated in 2.3, in addition to the three different materials used in the sensor, another one was used in the FEM analysis, adding up to a total of four different materials used, as given in Figure 2.35 Materials.

Related to material properties are gathered from COMSOL library[82]

- Lead Zirconate Titanate (PZT-5A1)
- 3M Polyurethane A/B [71]
- VisiJet ABS Like material [70],
- Water, liquid.

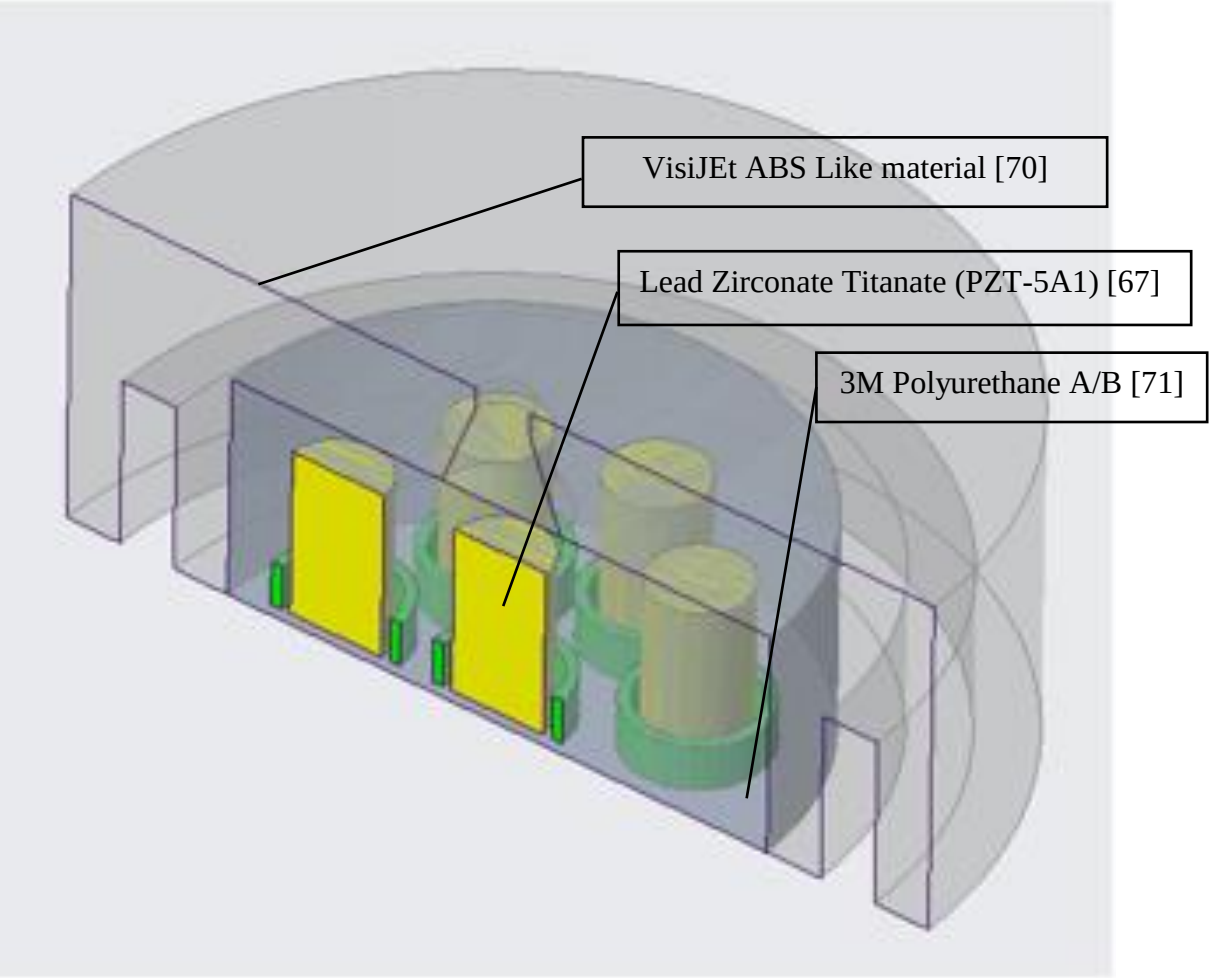

Figure 2.35 Materials

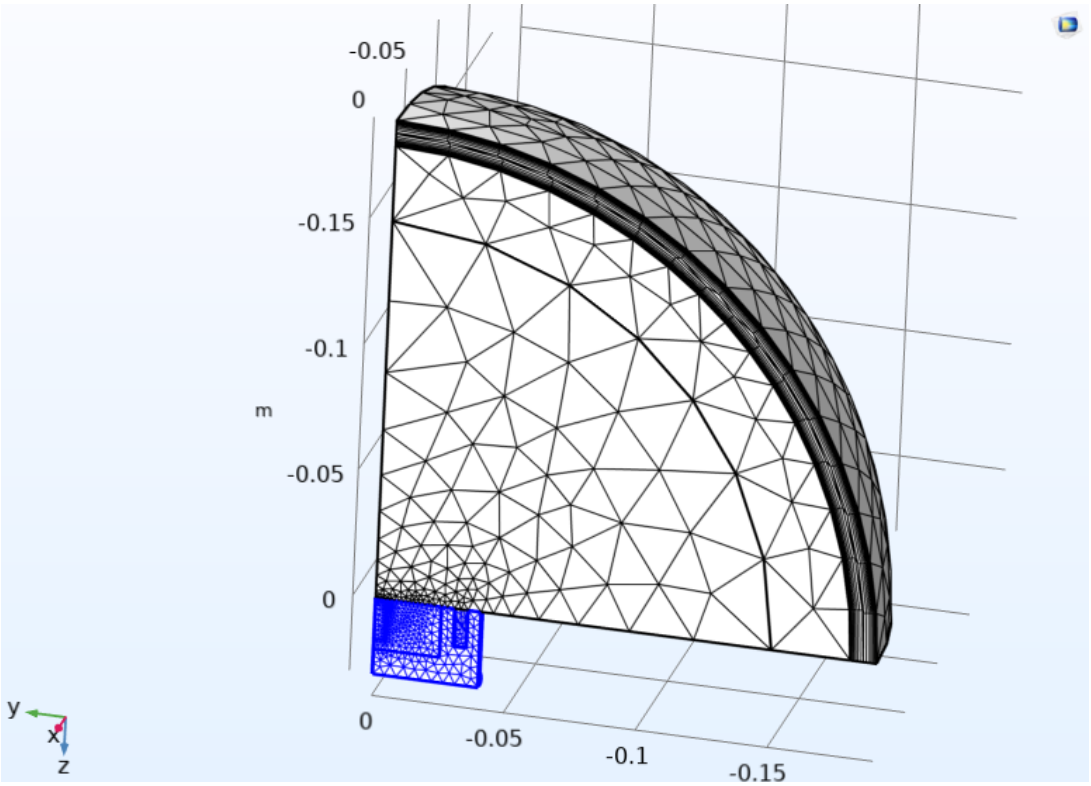

Figure 2.36 Mesh region 1- Sensor

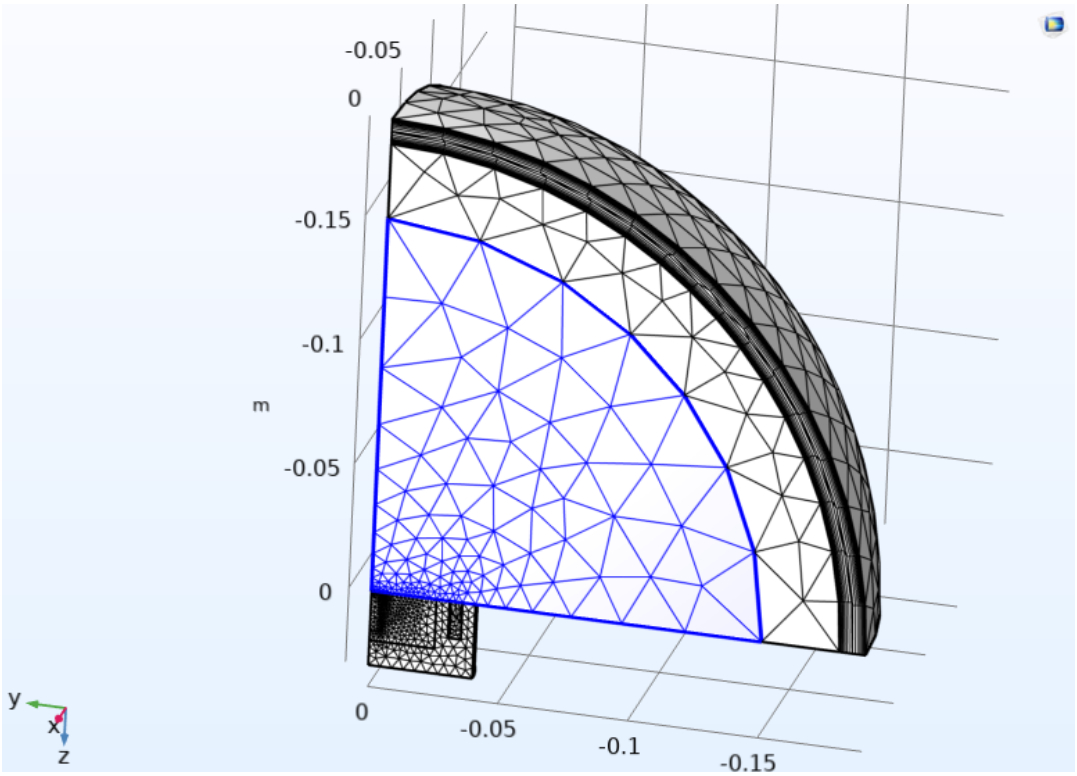

Figure 2.37 Mesh region 2 - Inner Water Domain

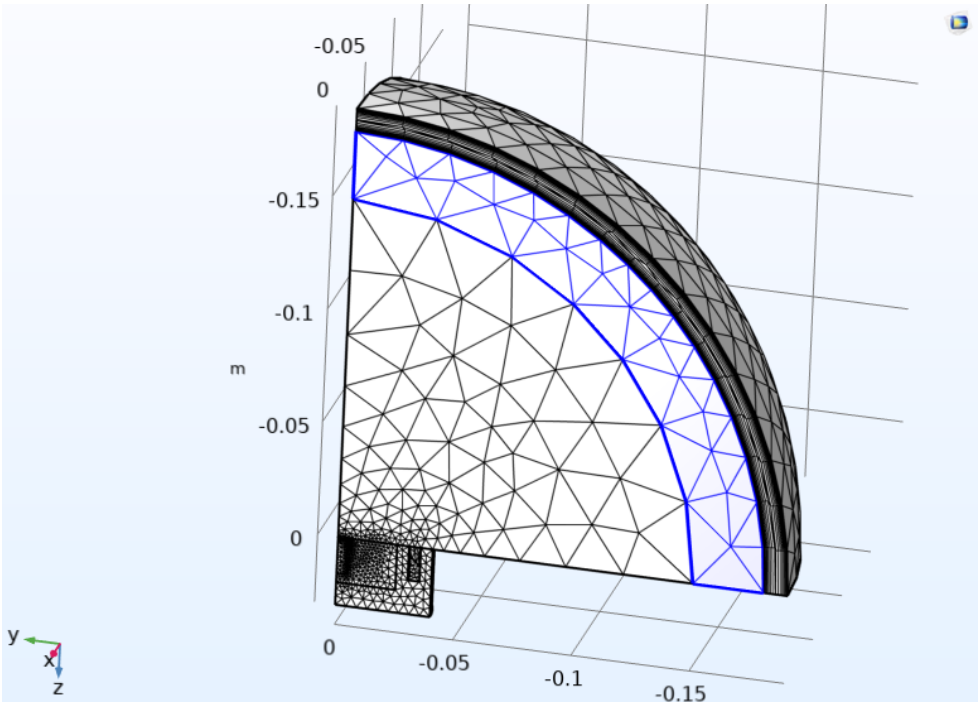

Figure 2.38 Mesh Region 3 - Background Pressure Field

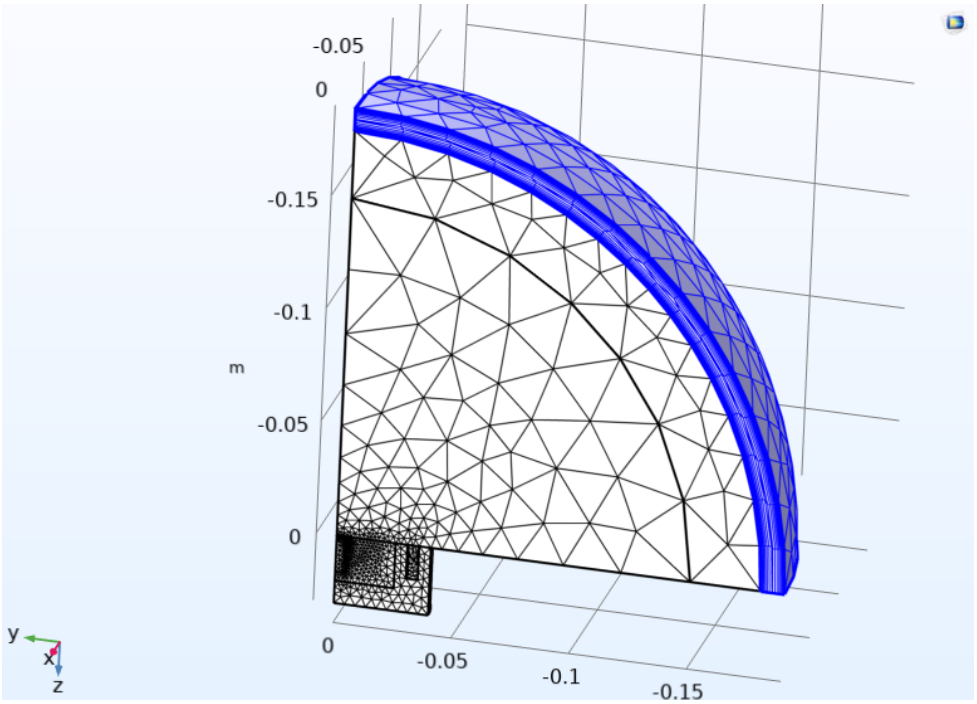

Figure 2.39 Mesh region 4 - Perfectly Matched Layer

Four different types of mesh structures were created in the FEM model. Details of the mesh structures are given in Table 2.6:

Table 2.6 Mesh details

	Mesh region 1	Mesh region 2	Mesh region 3	Mesh region 4
Domain Name	Sensor	Inner Water Domain	Background Pressure Field	Perfectly Matched Layer
Element Number	69311	6828	1346	7018
Element type	Tetrahedra	Tetrahedra	Tetrahedra	Tetrahedra & Prisms
Mesh/Volume Ratio	7.74E-04	4.36E-06	0.0077	0.0214
Mesh Criteria	Extremely Fine	Maximum Element Size: 1500[m/s]/fmax/6	Maximum Element Size: 1500[m/s]/fmax/6	Boundary Matching Element

In Figure 2.36, Figure 2.37, Figure 2.38, and Figure 2.39, Mesh region 1- Sensor, Mesh region 2 - Inner Water Domain, Mesh Region 3 - Background Pressure Field, and Mesh region 4 - Perfectly Matched Layer are given, respectively.

The setup was created in the COMSOL software using its Pressure Acoustic, Electrostatic and Solid Mechanic modules to obtain through simulation the Voltage value output, to an input of the 1 Pa RMS acoustic pressure.

According to this structure, the mesh structure of the intra-sensor unit, which is the most acoustically-sensitive part, was defined to be “Extremely Fine” and the mesh type was selected as Tetrahedra. The mesh type and flatness used in the Water Domain parts were determined according to the highest frequency. According to the information suggested in the Comsol Acoustic Module [82], the mesh criteria given in the pressure acoustic module are as follows:

$$\text{Mesh maximum Element Size} = \left(\frac{1500\left[\frac{\text{m}}{\text{s}}\right] \text{x6}}{\text{fmax}}\right) \qquad \text{Eqn. 2.6}$$

Accordingly, the mesh size to sample the highest frequency is determined and applied to the entire domain.

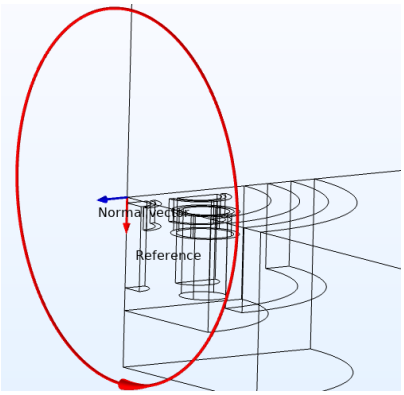

Figure 2.40 RVS and DI parameter vector

RVS (Mentioned in Chapter 2.1.2) and DI (Mentioned in Chapter 2.1.3) values were extracted according to the FEM analyses. The reception of the sensor may vary due to the direction of the acoustic pressure. Indicates that the calculated

direction is important for extracting the DI values. When specifying a DI value, the reference direction from which the calculation is made must be given. The direction in which the DI values are calculated within the scope of this study is given in Figure 2.40. The red circle is the reference to the polar pattern plot. On the other hand, RVS values are extracted at the front surface of the Sensor.

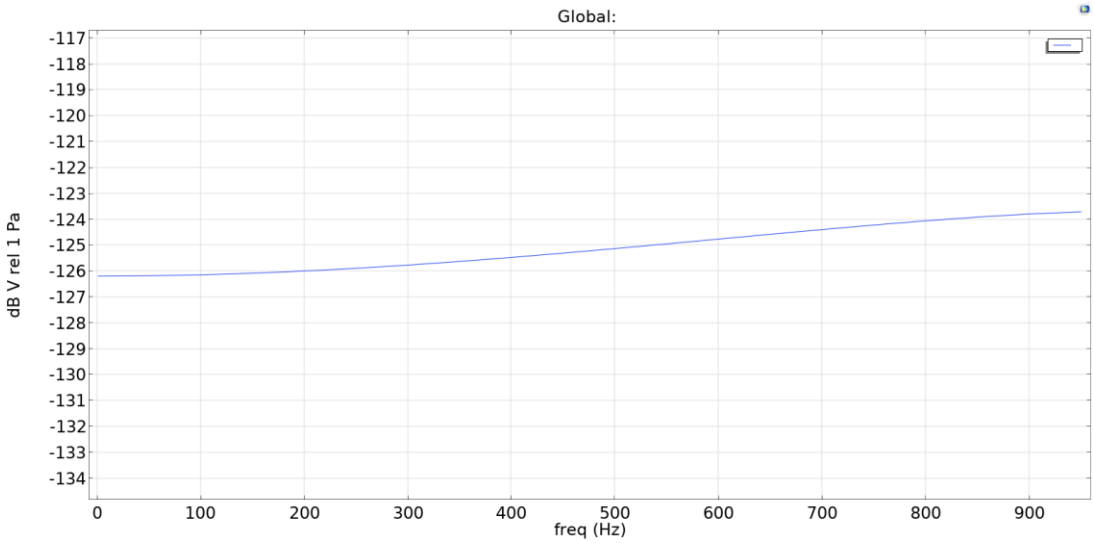

Figure 2.41 RVS graph of Sensor

In Figure 2.41 according to the formulas in Eqn 2.3 and Eqn 2.4, the RVS value in dBV vs freq" graphs are given. The RVS value is within ±5 dBV in the range of 0-1000 Hz. At frequencies around 350 Hz which are more important in the case of vascular occlusion, the RVS value is around -126 dBV (in Eqn 2.3 and Eqn 2.4, Vref is chosen as 1 V and Pressure on Sensor (Pref) is chosen as 1 Pa RMS). Another important parameter is the Directivity Index (DI). DI value calculated according to Eqn 2.4. Recall:

- D (θ, ϕ): Directivity index of a given direction
- Lp (θ, ϕ): The received sound pressure level for a given direction
- Lp_{avg} (θ, ϕ): The received sound pressure level, averaged over all angles
- (θ, ϕ) : A direction indicator where
    - θ: latitude referenced to the sensor centerline,

- ϕ: longitude from the horizontal sensor plane.

In the analysis, 1 Pa RMS signal was applied from the BPF domain separately from every angle according to Eqn 2.4 (The θ and ϕ parameters are used to specify the direction and angle of the incoming wave.). The sound pressure level received is calculated at each angle and likewise, the average of the sound pressure levels received over all angles is also calculated. The ratio of these two values gives us the Directivity Factor (DF). The DI value is the decibel representation of the DF.

Figure 2.42 gives the DI value of 1x Rod type and 1x Tube type pair. 1x Rod type and 1x Tube type piezoceramics are connected in parallel. On the other hand, In Figure 2.43, the DI value of 8x Rod type and 8x Tube type pairs connected in parallel is given.

The sensor directivity is increased by the use of 8x PZT ceramics couple. There is a directionality of nearly 135 degrees on the 5-dB SNR line using a single couple of ceramics. This value has decreased to 70° while using 8 couple of PZT ceramics, which means an increase in the directivity. With this enhancement, it is aimed to receive the small signals simply by adjusting, i.e. increasing the directivity of the sensor.

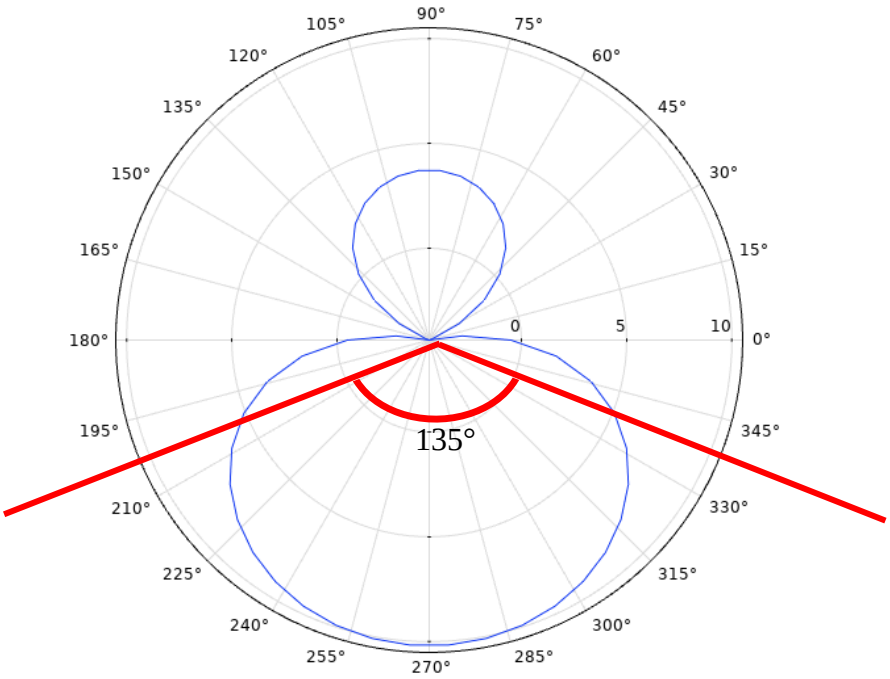

Figure 2.42 DI value of 1x rod type and 1x tube type pair

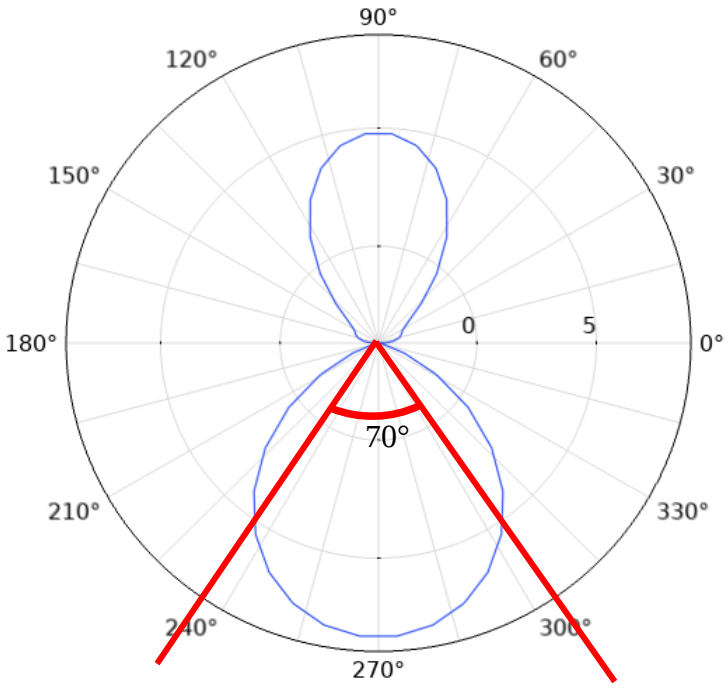

Figure 2.43 DI value of 8x rod type and 8x tube type pairs

According to the values given in Figure 2.41, Figure 2.42, and Figure 2.43, the sensitivity value of 126 dBV ±3 dBV with parallel connection is sufficient according to the minimum readable voltage value given in Figure 2.5. In light of this information, the improvement in the DI value was deemed beneficial for the application.
Therefore, as a design parameter, the parallel connection was used as an outcome of the FEM analysis.

2.3.3.3 Sensor structure production

After the design of the sensor structure and the type of electrical connections to use were determined, the prototype production phase started. There are two important points to remark on in sensor production. First, while the piezoceramics are placed in the pool in the sensor housing, they must be suspended in the polyurethane filling material without touching any part of the shell structure. This is to isolate the shell structure from mechanical vibrations. Otherwise, these vibrations would possibly create unwanted noise, with vast impacts on the overall sensor characteristics.

The second important point is that the cables coming from the sensor terminals and ground electrodes should reach the sensor cable intact. The decision to connect piezoceramics in parallel was made in Chapter 2.3.3.2. Accordingly, the cables coming from the upper and lower circular areas in the rod-type ceramics and from the inner and outer cylindrical surfaces in tube ceramics will be paired and the area will be filled with polyurethane filling material.

Figure 2.44 Ceramics with a production apparatus

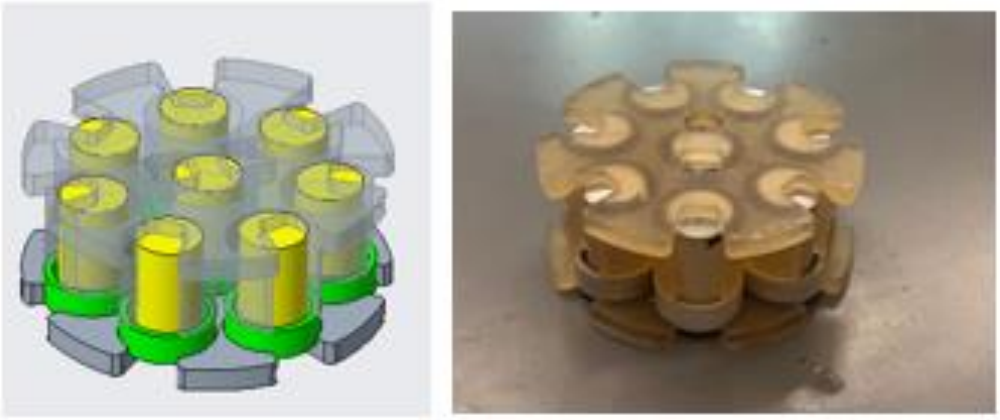

Figure 2.45 Second production apparatus for aligning rod-type ceramics

As seen in Figure 2.44, a production apparatus is used to position the piezoceramics correctly. With this apparatus, the ceramics were positioned as intended within the sensor, then soldered. The ceramics were tested against the signals they received and proper reception was confirmed. Immediately after, a second production apparatus in the Figure 2.45 was used to check the planarity of the rod ceramics.

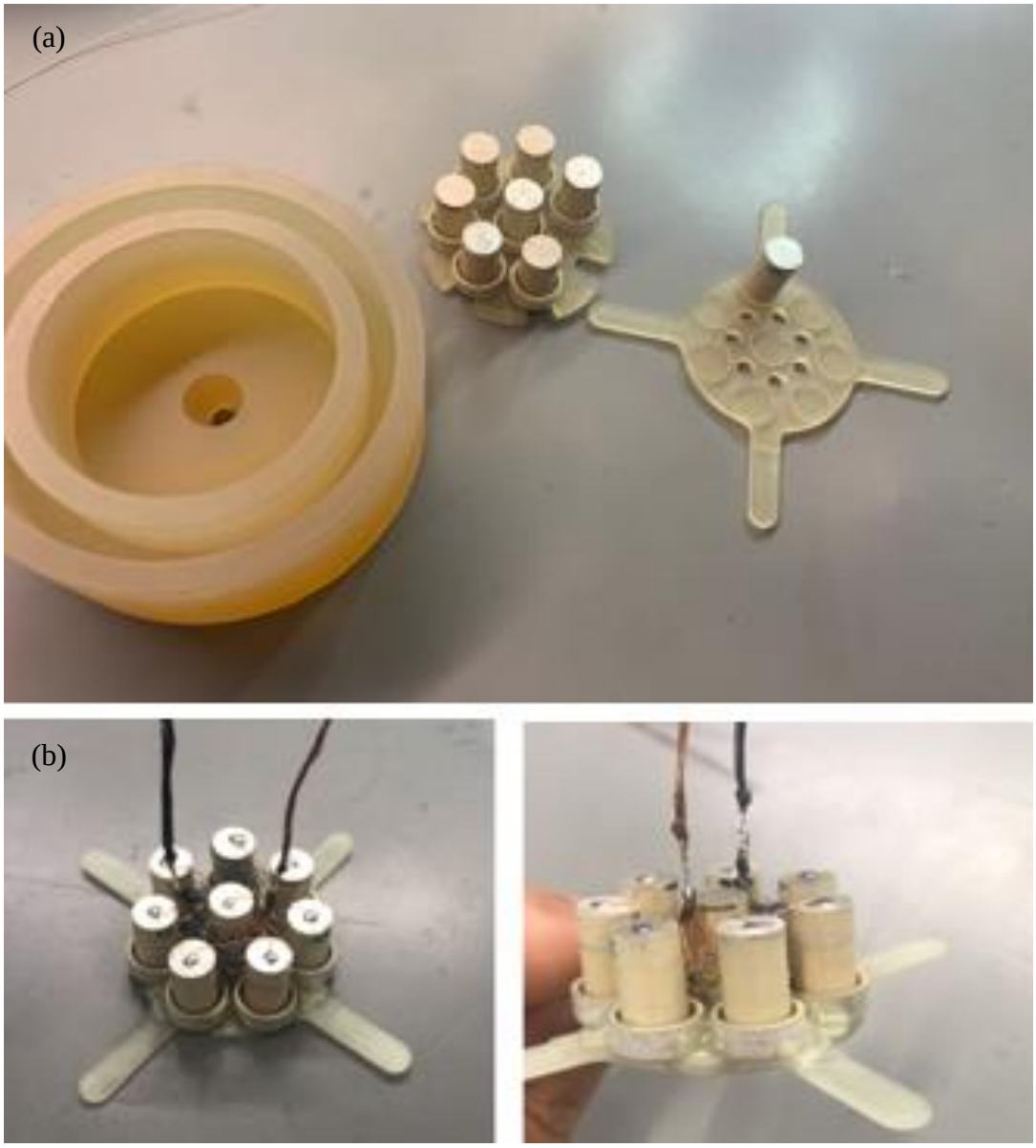

Figure 2.46 (a) The manufactured shell piece and soldered piezoceramics, (b) Third production apparatus

Figure 2.46 (a) shows the shell structure, the design process, and details of which are described in Chapter 2.3.3.1. In addition, the image of the CAD model created after the design of the part is available in Figure 2.24. The shell structure powder

was produced with the sintering method in 3D systems brand FabPro 1000 3D model three-dimensional printer [83].

A third production apparatus was designed and produced in this 3D printer to position the piezoceramics in the sensor (both in the vertical and horizontal axes) and for use during the casting process of the polyurethane filling material. It can be seen in Figure 2.46 (b).

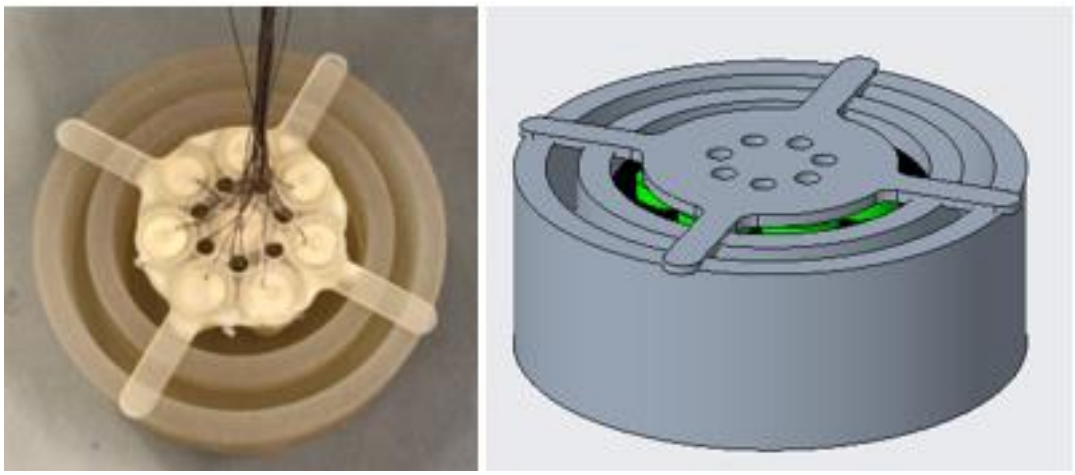

Figure 2.47 Positioning of ceramics before the first step of polyurethane filling

Figure 2.47 shows the shell structure and piezoceramics positioned using the third production apparatus after soldering and preparation for the casting process of polyurethane filling material.

Polyurethane filling material is a two-component material that is a commercial-off-the-shelf product from 3M. The photo of the material (two-component liquid material) as supplied is shown in Figure 2.48.

The casting process of the Polyurethane filling material has been made in two stages. First, the polyurethane filling material will be poured to the point where it can hold the tube ceramics in the pool of the shell structure, as seen in Figure 2.49. This operation is called "initial casting". After casting one, the polyurethane filling material is left out to cure for 24 hours. The completed version of "casting one" is shown in Figure 2.49 with both their CAD drawings and the photographs of the prototypes.

After initial casting, a final casting is done. This process is referred to as “final casting”. In the Casting Two process, the shell structure deletion is filled with polyurethane filling material. As a result of this process, the piezoceramics are placed axisymmetrically at a distance of 0.5 mm from the surface. The cables connected in parallel from the piezoceramics come out from the back side of the sensor in a two-core structure (+ and -).

Figure 2.48 3M Brand Polyurethene

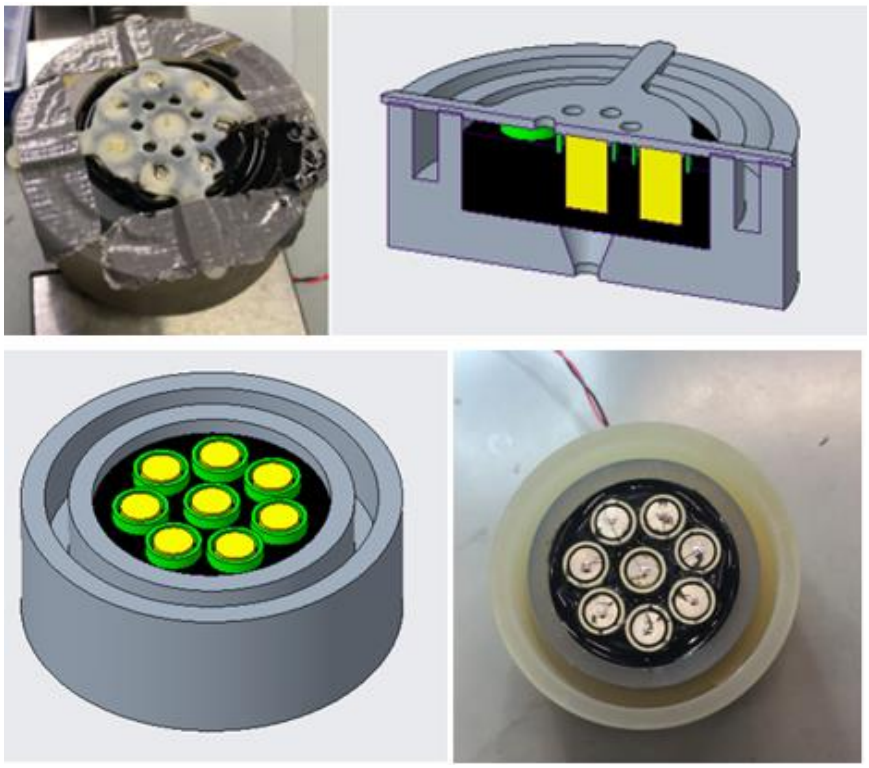

Figure 2.49 The sensor structure after the process of “casting one”

Polyurethane filling material casting has two points for consideration. The first is to ensure that no air bubbles remain in the filling material during casting (or to ensure that they come out during the curation period), and the second is to keep the structure stationary on a flat surface during this period.

After the casting two processes, the sensor structure is completed. In Figure 2.50, the completed sensor structure is given.

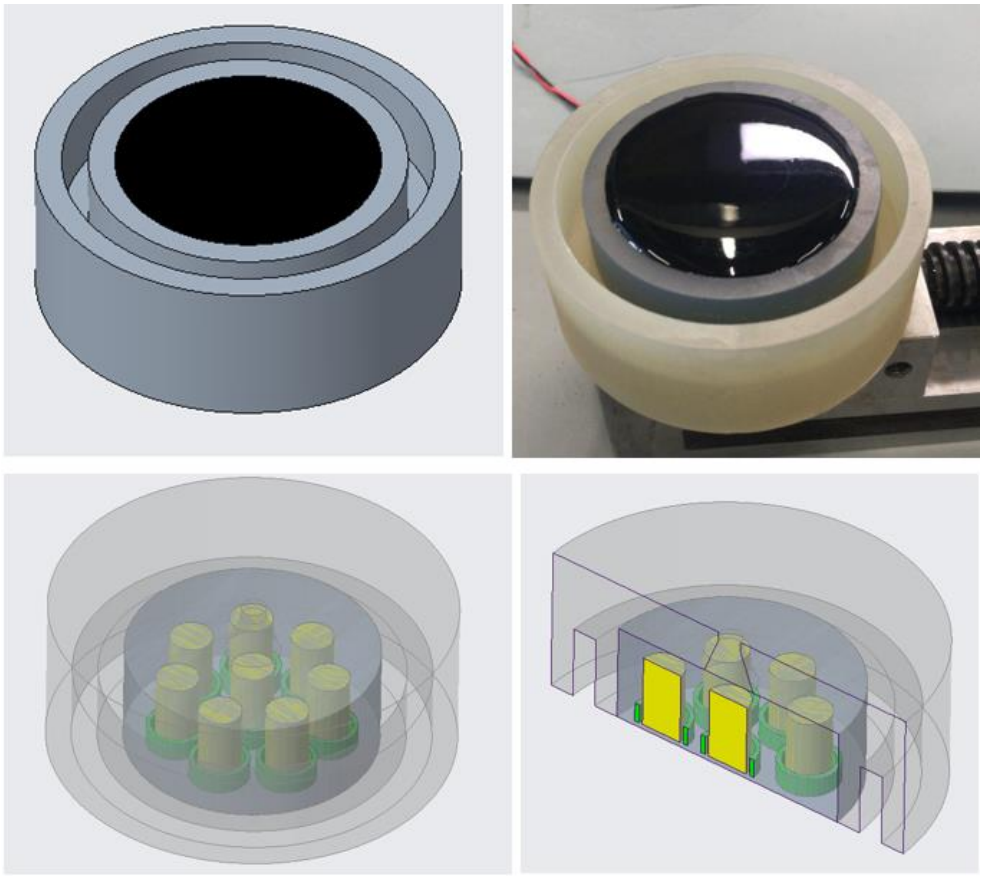

Figure 2.50 Sensor

2.3.3.4 Sensor data acquisition system

Acquisition, monitoring, and evaluation of the analog signals generated by the sensor are important and have to be handled with care and diligence. A low-noise data acquisition system should be used to reduce the input noise and reach the desired SNR values mentioned in Chapter 2.1 Design parameters.

From the RVS values calculated in Chapter 2.3.3.2and the intra-arterial pressure values [31-32] found in the literature, it can be predic ted that the power of the acoustic signal will be between -125 dBV and -115 dBV. Accordingly, the electronic noise floor of the data acquisition system is preferred to be less than -125 dBV to avoid the loss of the signal.

The data acquisition systems available in the market have relatively higher noise levels (generally, sound analyzers are used for such applications), especially at low frequencies. For example, the noise floor level of the Rohde-Schwarz UPV Audio Analyzer, which is one of the most known and preferred devices in the market, operating in the DC to 250 kHz band, is -130 dBV in the 0-10000 Hz band [84].

In this study, an electronic card designed for a high-end sonar system will be used. The electronic card can be seen in Figure 2.51 and the noise floor of the electronic card and sensor together can be seen in Figure 2.5. The noise floor of this circuitry is around -130 dB.

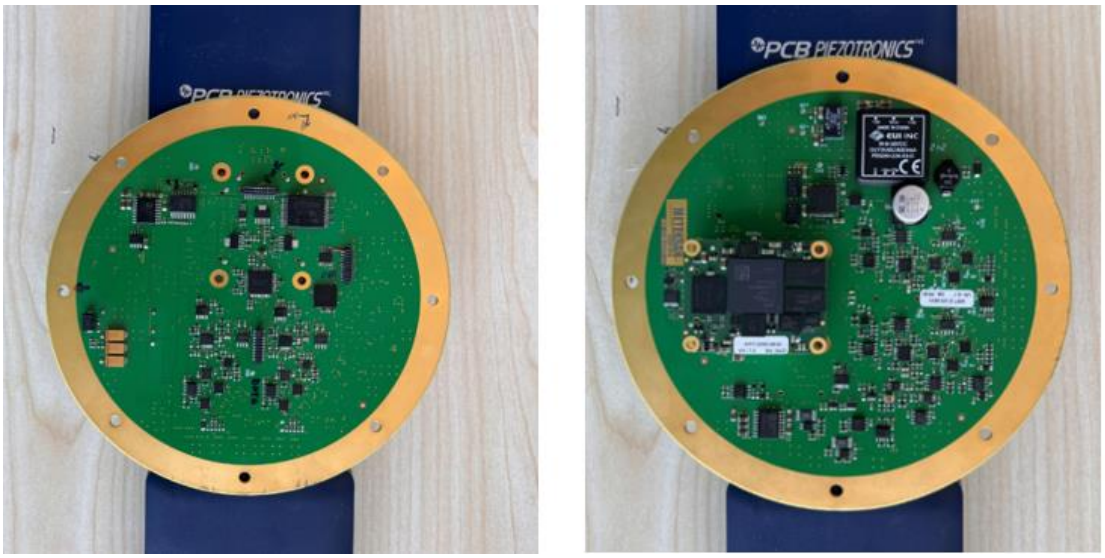

Figure 2.51 Signal processing electronic card – Low Noise

In the testing environment, a measurement was made while the EMI/EMC shielded case was in use to mitigate the effects of the electromagnetic field in the environment.

Figure 2.52 EMI&EMC shielded electronic card

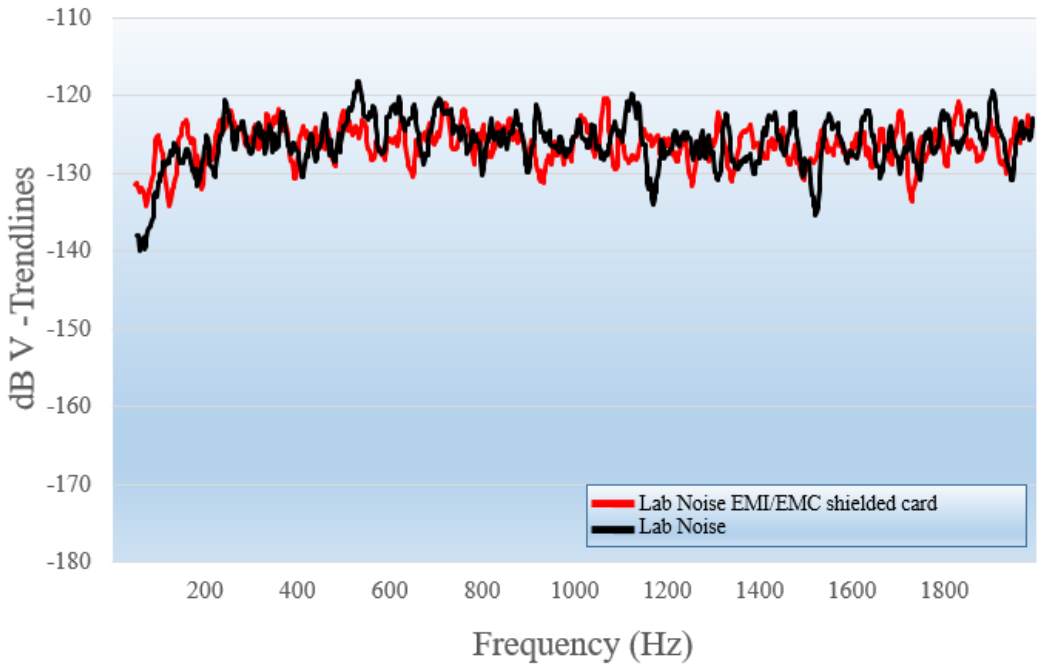

Figure 2.53 Lab noise electronic card EMI/EMC shielded or not

Figure 2.52 shows the signal-processing electronic card and its EMI/EMC shielded case. To investigate the effects of the EMI/EMC shielding, two recordings were made in a lab environment dominated by acoustic noise; one with the shielding case, and the other without. The frequency spectrum of the data recorded in these two is presented together in Figure 2.53. According to the records taken, it is

observed that for this particular environment and the electronic board used, the effects of the EMI/EMC shielding case were insignificant and it is claimed that even the electronic board without the EMI/EMC protection was observed not to have been interfered by the electromagnetic noise present within the lab environment.

The logic of the operation of the data acquisition system is as follows. The piezoceramics convert the acoustic pressure applied on themselves into electrical voltages. These analog voltages are then transmitted to the front-end electronic circuit. The analog voltages, i.e. signals, are digitalized and become ready for processing.

In the time domain, the continuous data from the sensor is sampled at 31.250 Hz. FFT conversion is provided with 8125 points of 31250 sample data taken in 1 second. According to these numbers, the refresh of FFT graphs is approximately 4 times for a second. Thus, 8 times FFT is created in a sample recording performed in 2 seconds, and the average of these data is taken. Accordingly, the FFT resolution is 0.25 Hz.

CHAPTER 3

EXPERIMENTAL STUDIES

3.1 Experimental setup

A test setup has been created to characterize the performance of the contact-type acoustic sensor. This sensor, designed for the non-invasive detection of arterial occlusions, needs to be tested and approved in a test setup similar to its application or operational environment.

The first step was to create a setup in which the arterial occlusion can be simulated. For this, a tissue model with an acoustic impedance similar to the skin tissue was designed and produced. This tissue model was aimed to have a tubular cavity similar to the structure of the vascular artery and therefore needed to contain some parts to simulate vascular occlusion. In Chapter 2.3, it was mentioned that a material whose acoustic impedance is close to the acoustic impedance of the skin tissue is preferred in the design of the sensor structure. Therefore, it was also decided to make use of the same material for the skin tissue [71]. In Figure 2.48, the material from 3M that was used in both the sensor structure and the tissue todel is given.

In order to create a tissue todel from the polyurethane material [71], the disposable mold shown in Figure 3.1 (a) was produced. Inside this mold, there is a tubular cavity protrusion with a diameter of 10 mm.

In Figure 3.1 (b), the hollow-shaped occlusion samples representing different rates of occlusion in the form of different hole diameters are given. These parts are designed to fit into the tubular cavity of the tissue todel. The tissue model prototype disposable mold (on the left side of the picture) is also given in the same figure.

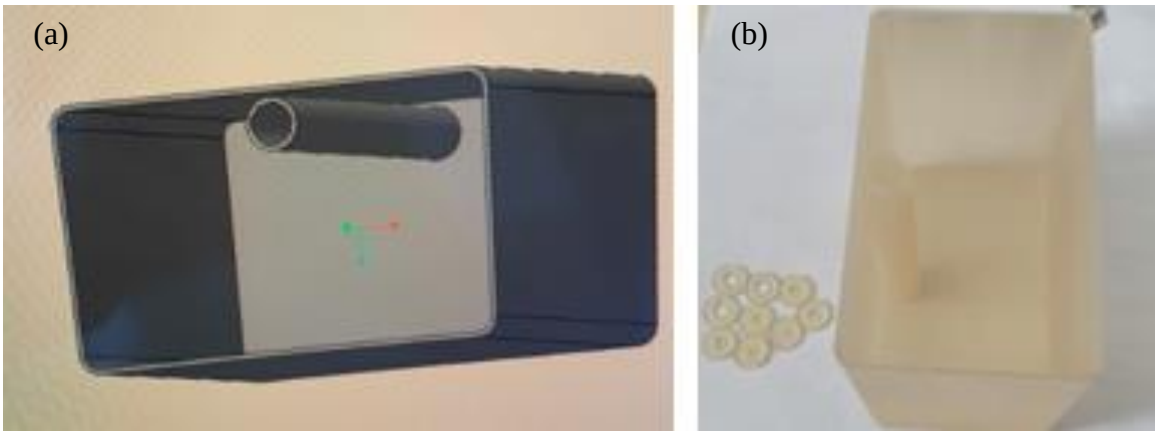

Figure 3.1 (a) Tissue model prototype disposable mold and (b) the hollow-shaped occlusion Samples

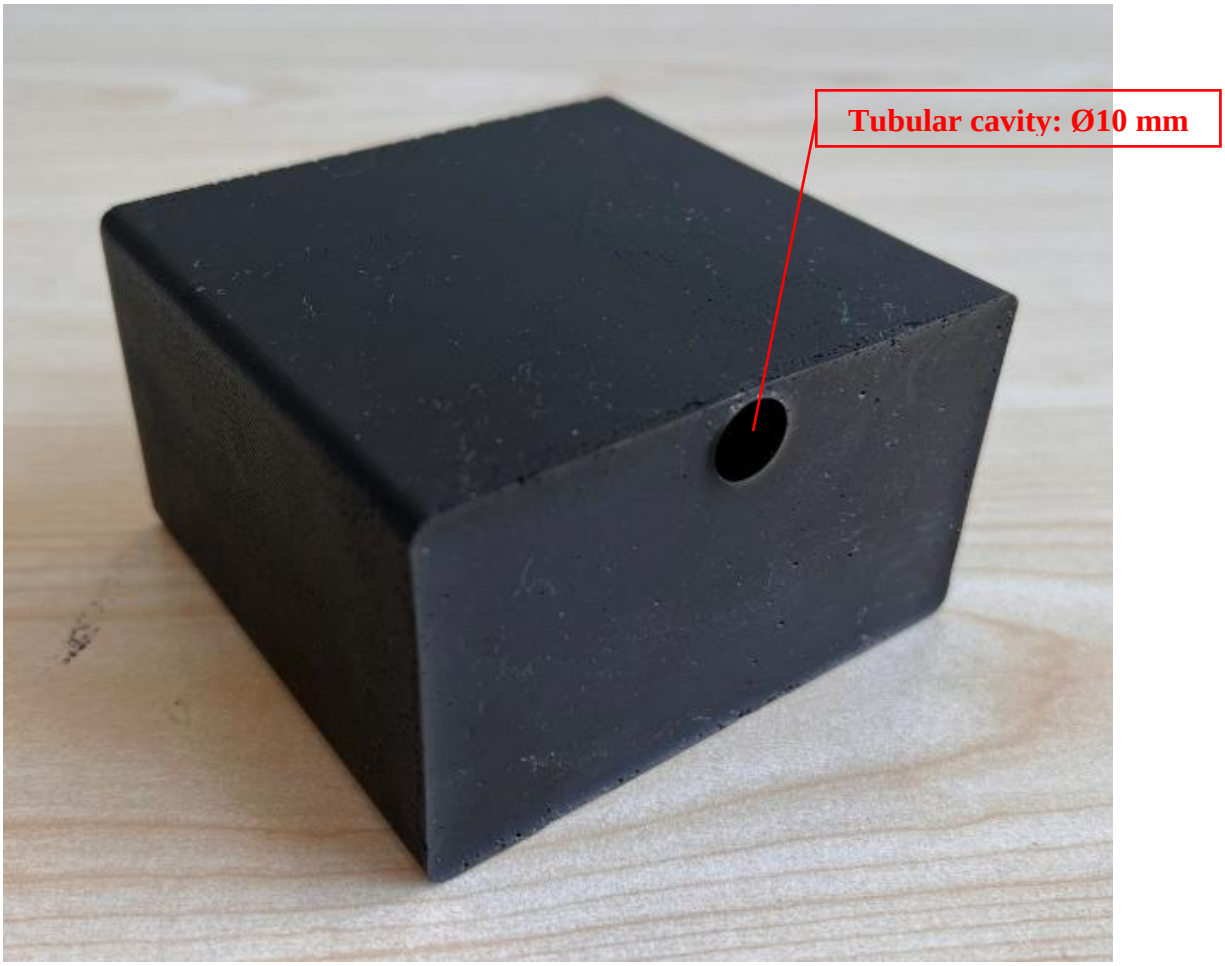

Figure 3.2 Tissue model

Among the arteries in the human body, the largest diameter is in the aorta, femoral, brachial, and common carotid arteries. The arteries with the most occlusion problems are the branches of the aorta and the carotid artery. The carotid artery is close to the skin surface, contains a high flow rate, and develops stenosis together with cardiovascular diseases. This led the researchers investigate the acoustic non-invasive diagnosis methods of the artery [54-56]. For these reasons, a space was created in the tissue model to simulate the carotid artery. The carotid artery varies between 4.66 mm and 12 mm [85]. In light of this information, an average value for the tubular cavity width was taken as 10 mm.

The parts named “occlusion samples” seen in Figure 3.3 form artificial stenosis into the tubular cavity in the tissue model. Occlusion sample parts are designed to simulate 99%, 90%, and 70% stenosis rates. Their inner diameters are 1.35 mm, 3.11 mm, and 5.39 mm, and their outer diameter is tubular cavity diameter. i.e. 10mm. the diameters can be seen in Figure 3.4.

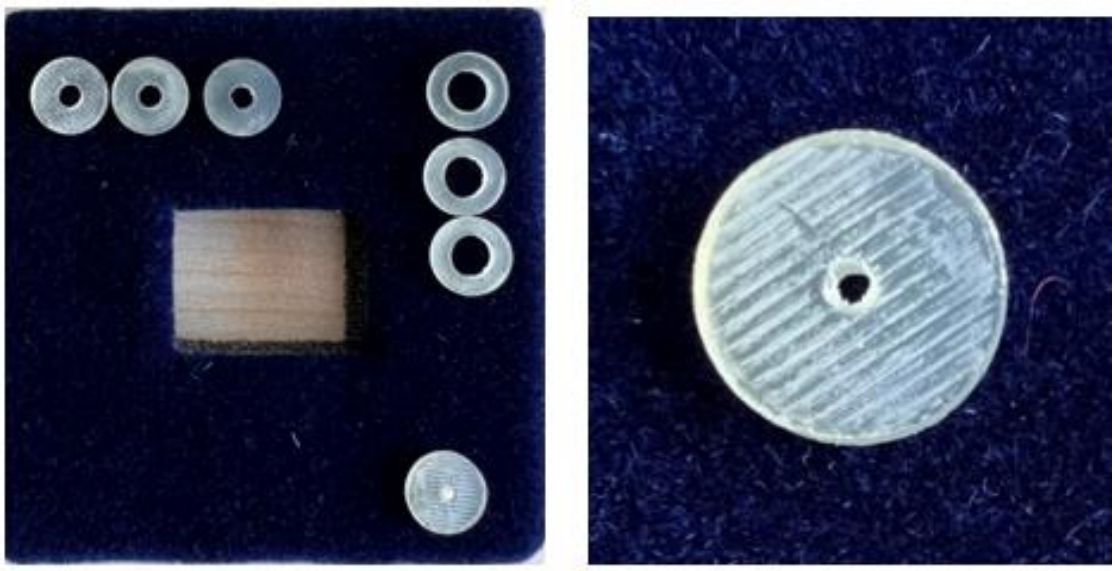

Figure 3.3 99%, 90%, And 70% pieces named as “occlusion sample”

Figure 3.4 99%, 90%, and 70% occlusion sample diameter

Table 3.1 Diameters according to the severity of occlusions

S (%)	d (mm)	D (mm)
98.2	1.35	10
90.3	3.11	10
70.9	5.39	10

Table 3.1 shows the rates of the severity of the stenosis calculated according to the measured inner diameters of the hollow-shaped parts to simulate the occlusions. These parts are shown in Figure 3.5 on which with the sensor prototype is placed in the tissue model. Experiments were carried out according to this position of the sensor shown in Figure 3.5.

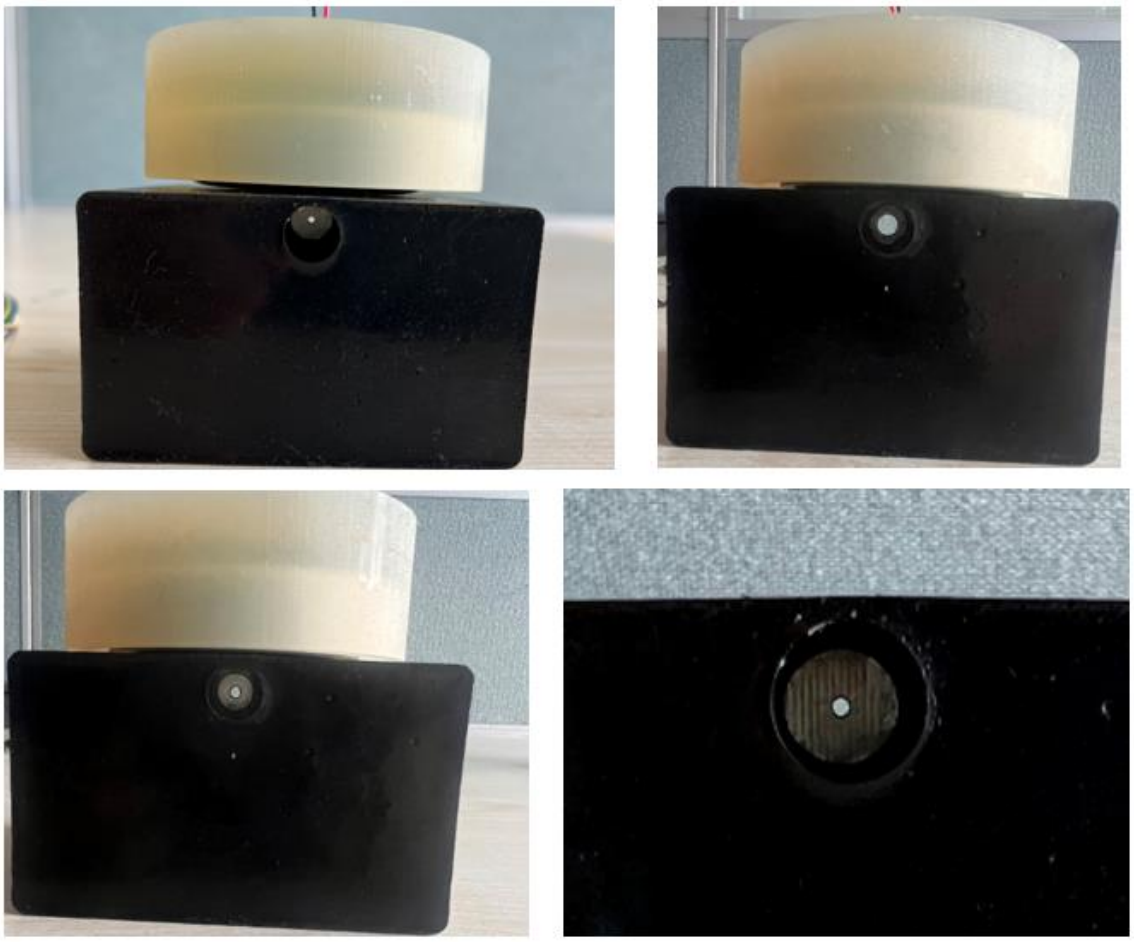

Figure 3.5 Tissue model and sensor

One cable with two cores coming out from the back side of the sensor is terminated with a connector and connected to the card. In other words, from the back of the sensor, a twisted pair of cables comes from the positive and negative electrodes of the piezoceramics. This cable enters the analog input of the electronic card with a commercial-type Molex connector[86]. This is where the time domain data is converted to the frequency domain and further analysis is conducted using the FFT data. Figure 3.6 (a) shows the cable from the sensor carrying the analog signals produced by the piezoceramics.

Another cable is placed between the electronic card and the computer. With the help of this cable, the data is transmitted to the user interface software (a software was used as the user interface to display the data on a personal computer). This cable also supplies

the electronic board from a power source of 24V and 0.3 Amps. It can be seen in Figure 3.6 (b).

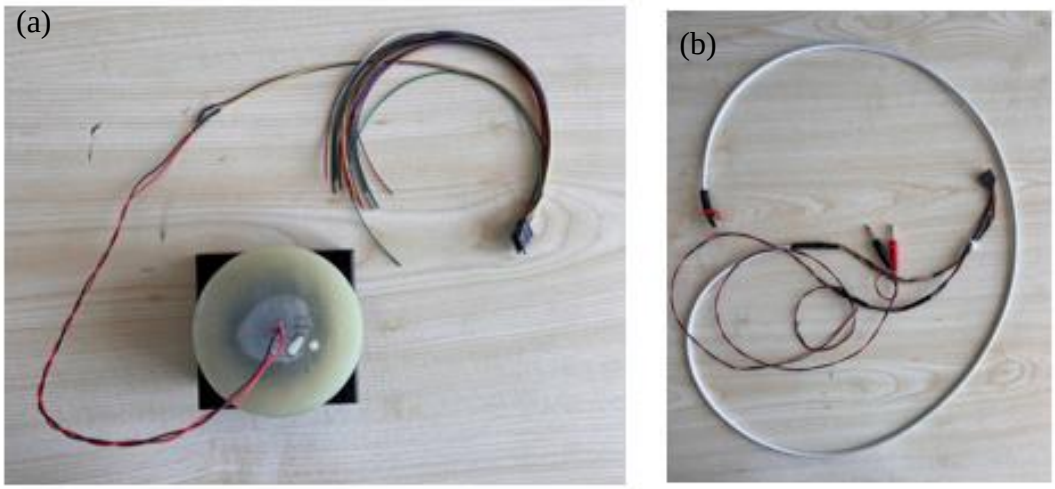

Figure 3.6 - Sensor cables (a) cable between the sensor and electronic card (b) cable between electronic card and computer

During the acoustic tests, a hydraulic hose was fed into the tissue model and another one was used for the discharge. In Figure 3.7 (a), the hydraulic pipes entering and exiting the tissue model can be seen, and inFigure 3.7 (b), the valve positioned at the discharge pipe outlet that was used to adjust the flow rate is given.

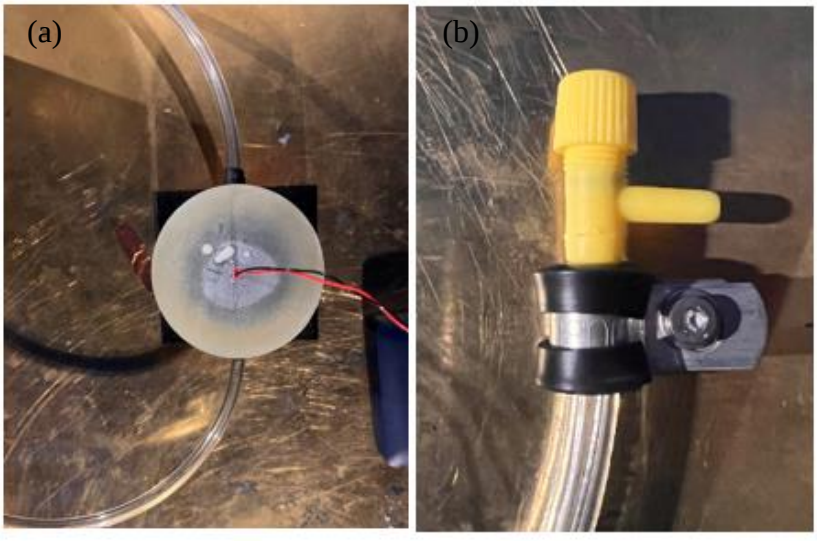

Figure 3.7 (a) Hoses (b) Valve

The flow rate of the water supplied to the tissue model is adjusted with two parameters. First, the injector seen in Figure 3.8 pumps water from the inlet hose seen in Figure 3.7 (a) into the tissue model. The flow rate was simply adjusted by allowing a certain volume of water from the injector into the tissue model at a given period of time. For example, the flow rate created for 20 mL/sn was made possible by manually pushing the injector from the 50 ml level to the 10 ml level in two seconds, i.e. 40 ml in 2 secs.

The second parameter used to adjust the flow rate is the yellow valve in Figure 3.7

Figure 3.7 (b). The outlet hose of the Tissue model is opened to the atmosphere. Maintaining a continuous but steady flow into the atmosphere for 2 seconds is a challenge, as it is difficult to control the movement of the injector head in Figure 3.7. Using the valve, the resistance of the flow can be adjusted, making it easier to deliver the water to the inlet hose at the desired rate. This system has also been useful in raising the pressure inside.

In order to reveal the effects of static pressure, the inlet hose was given a loop path one meter above the tissue model and then connected to it, as seen in Figure 3.10. In the experiments, first, the whole hydraulic system from the injector to the valve was filled with water, then the water was injected.

Figure 3.8 The injector used to pump water

In Figure 3.9, the experimental setup can be seen. This setup includes the tissue model, the hydraulic pipes carrying the water that passes through the entire system, the sensor, the injector, the electronic card, the power unit, and the computer where the data is evaluated. In Figure 3.9 a zoomed-in image can be seen containing the tissue model and the sensor.

Figure 3.9 Experimental setup, the tissue model and the sensor

To be able to detect vascular occlusion by non-invasive acoustic methods, acoustic signals of very small amplitudes must be captured. As described in Chapter 2, measuring signals of low amplitudes require minimal noise environment to maximize the SNR value. It is almost impossible for a sensor to distinguish the acoustic signals related to vascular occlusion from environmental noise in a noisy environment.

As part of this study, all experiments have been carried out in an acoustically isolated room with minimum environmental noise. Before starting the experiments, the following conditions were carefully recorded with the prototype sensor :

- The minimum noise level in the acoustic chamber when all devices are removed.
    - During the recording, no devices other than the sensor were kept in the room.
- The maximum noise level in the acoustic chamber when all devices are operational

- Such as air conditioning, fan noises of electronic devices, and vibrations from the table where the sensor is located.

- The recordings of the tissue model experiment setup with a 20 mL/sn flow without any stenosis.

The minimum noise measurement can be seen in Figure 3.10. The experimental setup set up in the acoustic room is as shown.

The measurements were taken using the acoustic contact sensor prototype show some scattered data. This is due to turbulence characteristics and the digitization processes capacity of the electronic card specified in Chapter 2.3.3.4. Figure 3.11 shows the records of a water-pumping test measurement (red color-scattered data) at a flow rate of 20 mL/sninto the tissue model without stenosis. In order to prevent this scattering due to both data processing and turbulence effects, a 10-data moving average of the FFT graphs is taken. Actual test data in Figure 3.11 is shown in red, where the moving average derived from the actual test data is given in black.

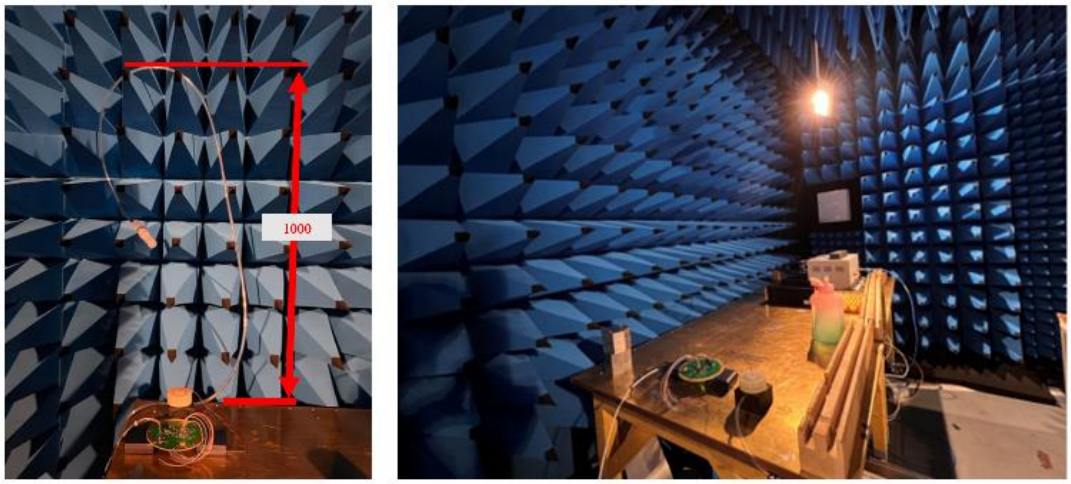

Figure 3.10 Low background noise acoustic room

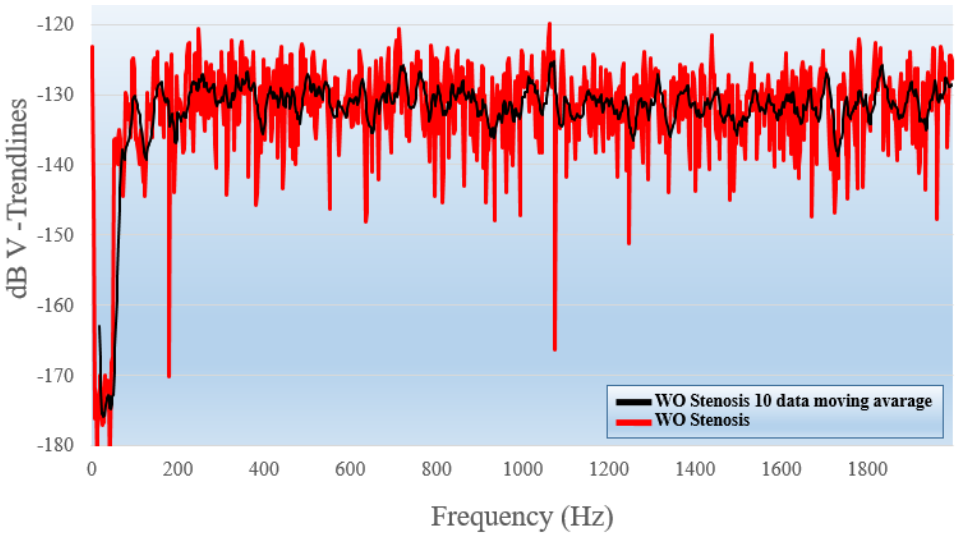

Figure 3.11 The data of without stenosis and 10 data without stenosis moving average recordings

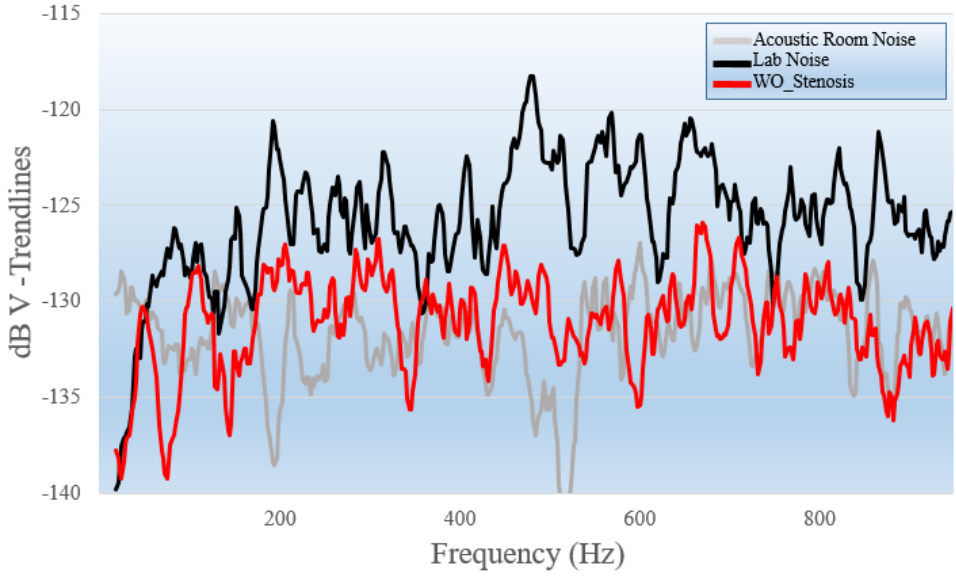

Figure 3.12 Acoustic room, lab noise and without stenosis situation data measurement

Similar to the method in Figure 3.11, the recorded and processed test data are shown in Figure 3.12. According to Figure 3.12, the acoustic background noise in the chamber is at a significantly lower level compared to the laboratory environment.

After the data is digitized on the electronic card, it is sent to a control interface on the computer.

3.1.1 Experiment plans

According to the relevant studies in the literature [3, 14, 32, 66, 85] and as mentioned in Chapter 3.1, the artery with the highest flow rate is the carotid in the neck region. In this artery, the blood flows relatively faster compared to the others and the occlusion rates are found to be higher [51-54]. The peak flow rate through a normal carotid artery is around 20 mL/sn(diameter: 6.4 mm, Reynolds number 3840 [51] (recall: The carotid artery varies between 4.66 mm and 12 mm [85], mentioned as around 6.4 mm [14, 32] before)). In the experiments for sensor characterization, tests were carried out at this flow rate, and using half of this flow rate, two cases where different Reynolds numbers apply were tested at three different occlusion levels.

Table 3.2 Test plan for acoustic contact sensor

Test No	Severity of stenosis	Reynolds number	Q (flowrate) mL/sn
99-2	98.2	1270	10
99-3	98.2	2540	20
90-2	90.3	1270	10
90-3	90.3	2540	20
70-2	70.9	1270	10
70-3	70.9	2540	20

The purpose of these experiments is to confirm the characteristics of the sensor with all its parameters and to confirm its suitability for the targeted application of atherosclerosis. In these measurements, attention was paid to the accuracy of the

flow rate and the whole experimental setup. Before and after the experiment, all parts of the setup were checked then the recordings were taken.

CHAPTER 4

RESULTS & DISCUSSION

All results are presented by applying 10-point moving average to the experimental data as mentioned in Chapter 3. The frequency band, which was narrowed to 50-2000 Hz using analog filters, is then limited to 50-1000 Hz using a digital filter. Since the frequency band is limited to 1000 Hz as in most of the studies in the literature, the same band (50 Hz-1000 Hz) was used in this study, as well.

According to the experiment plan in Table 3.2, the names are given according to the "Test No" in the graphics presenting the test results. To give an example, the Reynolds number is 2540 and the flowrate is 20 mL/snfor the experiment with the number "Test No: 99-3". According to the cross-sectional area calculation by the diameter of the occlusion samples, the occlusion severities in the experiment environment were also added to Table 3.2. This information has been given in Table 3.1 before.

All test scenarios in Table 3.2 are compared with the condition named “without stenosis”. Without stenosis condition is as follows: It is the test condition created without placing any occlusion samples into the tubular cavity in the tissue model, where the flow rate is at 20 mL/sn. The “without stenosis” condition has been referred to as “WO stenosis” in the graphs.

4.1 Experimental test results.

First, the test condition Test No 99-3 is given. According to this condition, the flow noise with 2540 Reynolds Number or 20 mL/snflowrate for a diameter of 10 mm was compared with the WO stenosis test data. The stenosis severity of the occlusion sample used in Test No 99-3 is 98.2.

In Figure 4.1, Results of Test No 99-3 and WO Stenosis conditions are given.

According to Figure 2.41, it can be said that the RVS value of the sensor does not change between 50 Hz and 1000 Hz with respect to the frequency. According to this information, the RVS is not the root cause of the increase and decrease in signal strength.

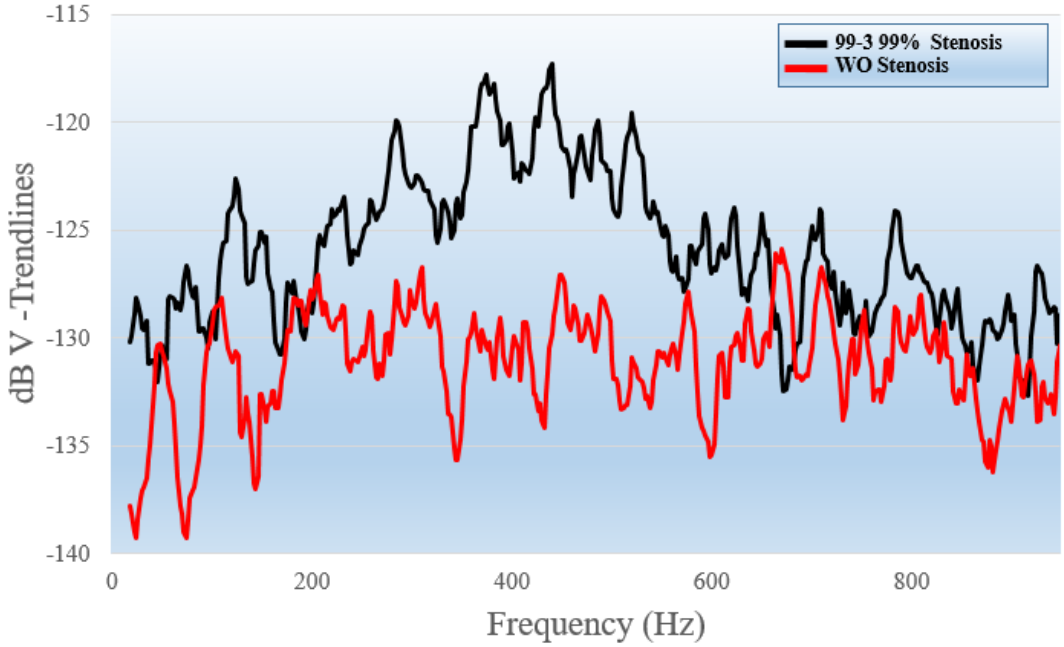

Figure 4.1 Test No 99-3 and WO stenosis

In Figure 4.1, the test strength of the data in Test No 99-3 is significantly higher than the WO stenosis data. It can also be said that there is a clear difference between 0 Hz and 600 Hz, which is similar to what is mentioned in the literature. In addition, the difference between the two cases can be observed up to 1000 Hz, albeit less in 600-1000 Hz compared to 50 Hz-600 Hz.

The difference in power between the data in the 50 Hz-200 Hz band is less than the difference in the band 200 Hz-400 Hz. According to the theoretical and experimental calculations of the acoustic signals originating from intra-arterial turbulence given in the sources in the literature, it is expected that the situation to be the similar or higher for the signals lower than 200 Hz. This difference is considered to exist due to the response of the analog filters at around 50 Hz.

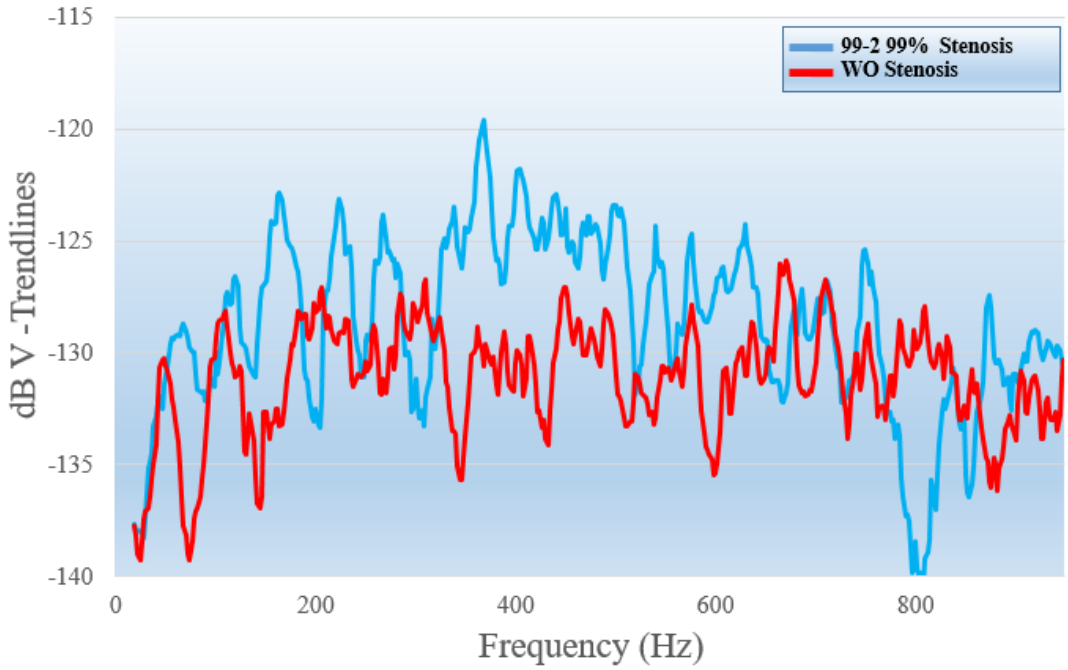

Figure 4.2 Test No 99-2 and WO stenosis

Second, the test condition in Test No 99-2 is given. According to this condition, the data of flow with Re = 1270 or 10 mL/snflowrate for a diameter of 10 mm was compared with the WO stenosis test data. The stenosis severity of the occlusion sample used in Test No 99-2 is 98.2.

In Figure 4.2, Data of Test No 99-2 and WO Stenosis condition are given.

It can be seen in Figure 4.2 that the data in Test No 99-2 is also noticeably higher than the WO stenosis data. It is still easy to see the distinction between 0 Hz and 600 Hz, which is noted in the literature. Additionally, up to 1000 Hz can be used to detect the difference between the two scenarios. When compared to Test No. 99-3, Test No. 99-2's test data amplitudes are lower. But it's still very recognisable.

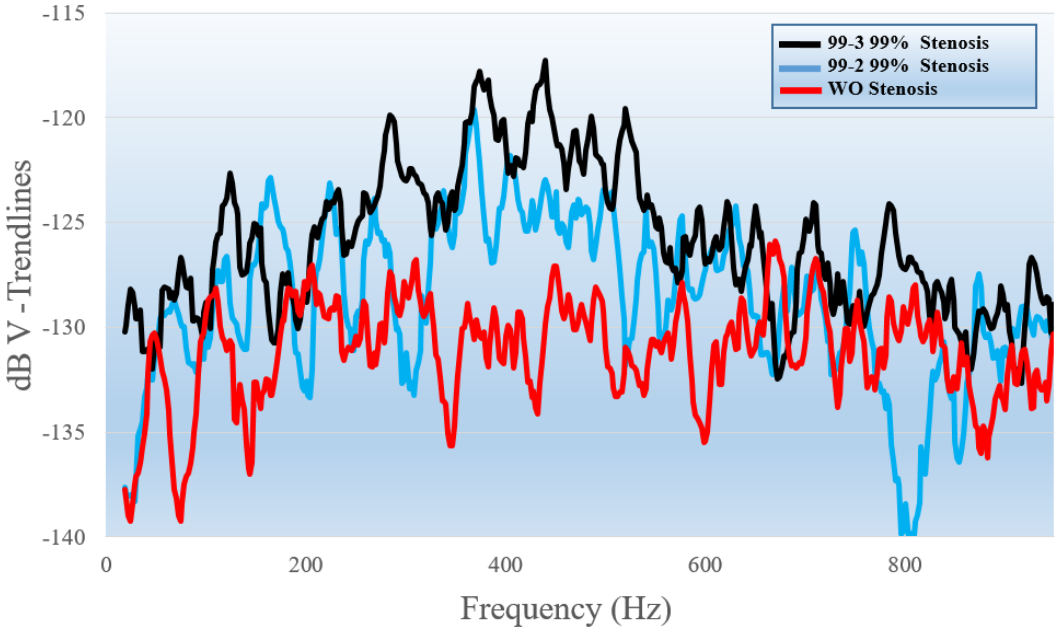

Figure 4.3 Test No 99-3, Test No 99-2, and WO stenosis

A comparison of Test No 99-3, Test No 99-2, and WO stenosis test data can be seen in Figure 4.3. The data in Test No 99-3 and Test No 99-2 yield similar characteristics. In particular, the increase in the signal strength of the data in Test No 99-3 and Test No 99-2 between 200 Hz and 600 Hz is evident, while the WO stenosis condition gives almost a constant value.

Third, Test Condition 90-3 is provided. The flow noise with Re = 2540 or 20 mL/snflowrate for a diameter of 10 mm was compared with the results of the WO stenosis test under these circumstances. The occlusion sample utilized in Test No. 90-3 has a stenosis severity of 90.3.

In Figure 4.4 Test No 90-3 and WO stenosis, Data of Test No 90-3 and WO Stenosis condition are given. Test No 90-3 is clearly higher than Wo Stenosis condition. Although it has less amplitude than the results of Test No 99-3 and Test No 99-2, it has an amplitude of around -120 dBV. The increase in the signal strength between 200 Hz and 600 Hz is similar to the increase in the other bands.

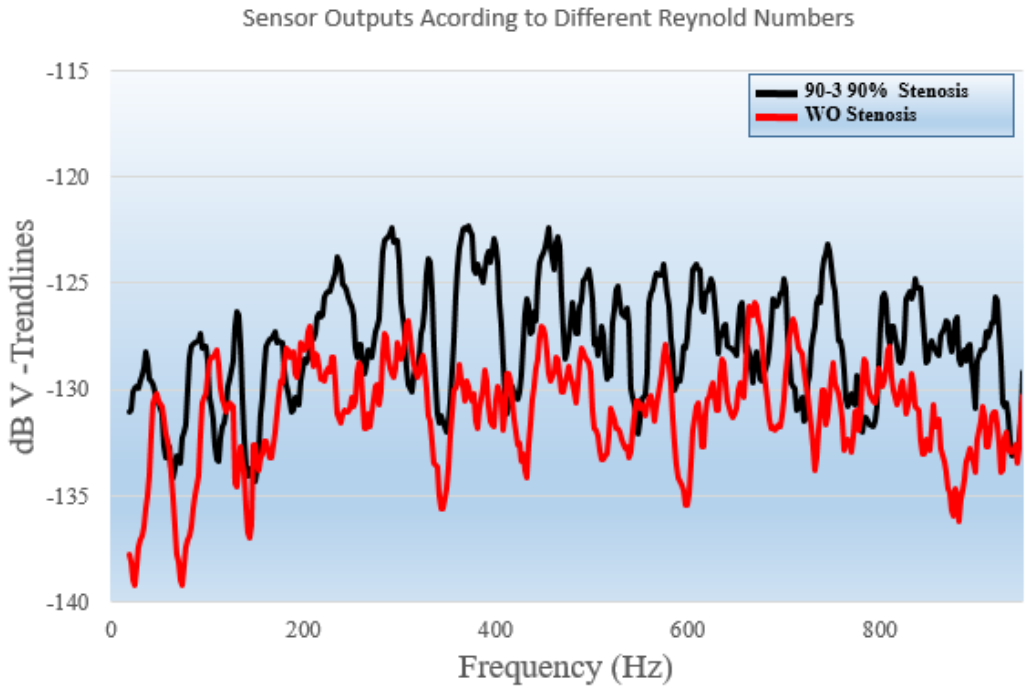

Figure 4.4 Test No 90-3 and WO stenosis

Fourth, Test Condition 90-2 is done. The flow noise with Re = 1270 Reynolds or 10 mL/snflow rate for a diameter of 10 mm was compared with the results of the WO stenosis test that under scenarios. The occlusion sample used in Test No. 90-2 has a stenosis severity of 90.3.

In Figure 4.5, Data of Test No 90-2 and WO Stenosis condition are given.

These test results show that the signal's strength decreases, especially at low frequencies. There are amplitude reductions as compared to earlier tests, particularly Test No. 99-3 and Test No. 99-2. At various frequencies between 200 Hz and 400 Hz, it resembles Test No. 90-3 in terms of features, but the amplitudes are typically smaller.

A comparison of Test No 90-3, Test No 90-2, and WO stenosis data can be seen in Figure 4.6.

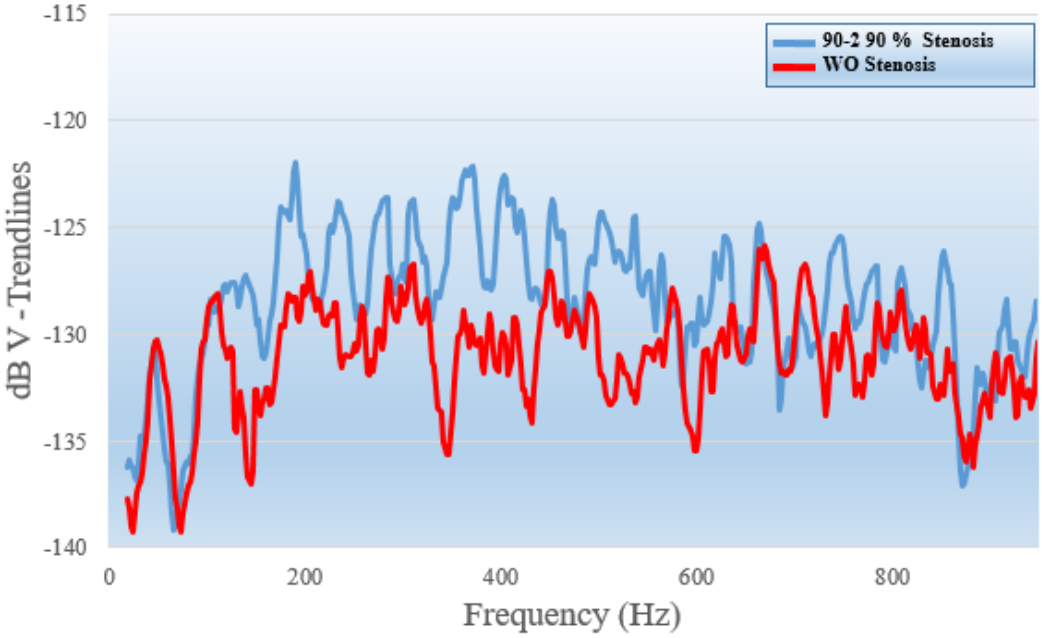

Figure 4.5 Test No 90-2 and WO stenosis

Fifth, the test condition Test No 70-3 is given. According to this condition, the flow noise with 2540 Reynolds Number or 20 mL/snflowrates for a diameter of 10 mm was compared with the WO stenosis test data. The stenosis severity of the Occlusion Sample used in Test No 70-3 is 70.9.

In Figure 4.7 Data of Test No 70-3 and WO Stenosis condition are given.

Test No 70-3 is noticeably higher than the WO Stenosis condition for the frequency band between 300 Hz and 1000 Hz. No distinguishable test data was found according to the reference WO Stenosis condition below 300 Hz. The amplitudes of Test No 70-3 and WO Stenosis signals between 300 Hz and 600 Hz are higher than those between 600 Hz and 1000 Hz.

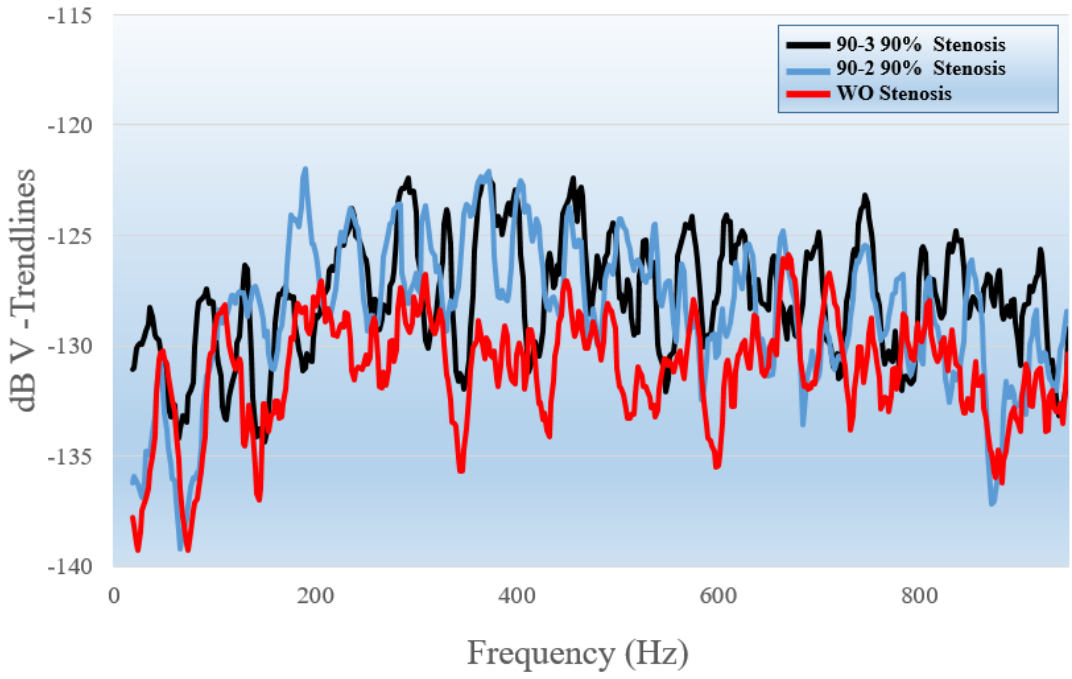

Figure 4.6 Test No 90-3, Test No 90-2, and WO Stenosis

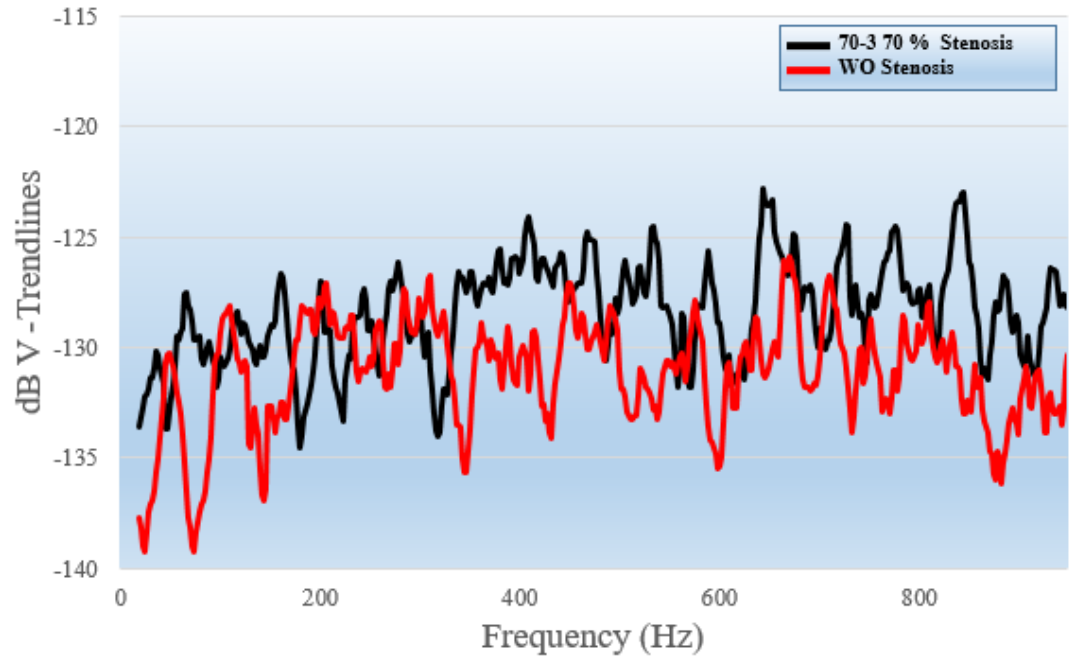

Figure 4.7 Test No 70-3 and WO Stenosis

Sixth, the test condition Test No 70-3 is given. According to this condition, the flow noise with 1270 Reynolds Number or 10 mL/snflowrates for a diameter of 10 mm

was compared with the WO Stenosis test data. The stenosis severity of the Occlusion Sample used in Test No 70-2 is 70.9.

In Figure 4.8, Data of Test No 70-2 and WO Stenosis condition are given. In addition, a comparison of Test No. 70-3, Test No. 70-2, and WO Stenosis data can be seen in Figure 4.9.

The data obtained in 70% occlusion tests, i.e., Test No. 70-3 and Test No. 70-2, can be distinguished from WO Stenosis data around 300 Hz. As in Test no 70-3, no distinguishable test data was found according to the reference WO Stenosis condition below 300 Hz.

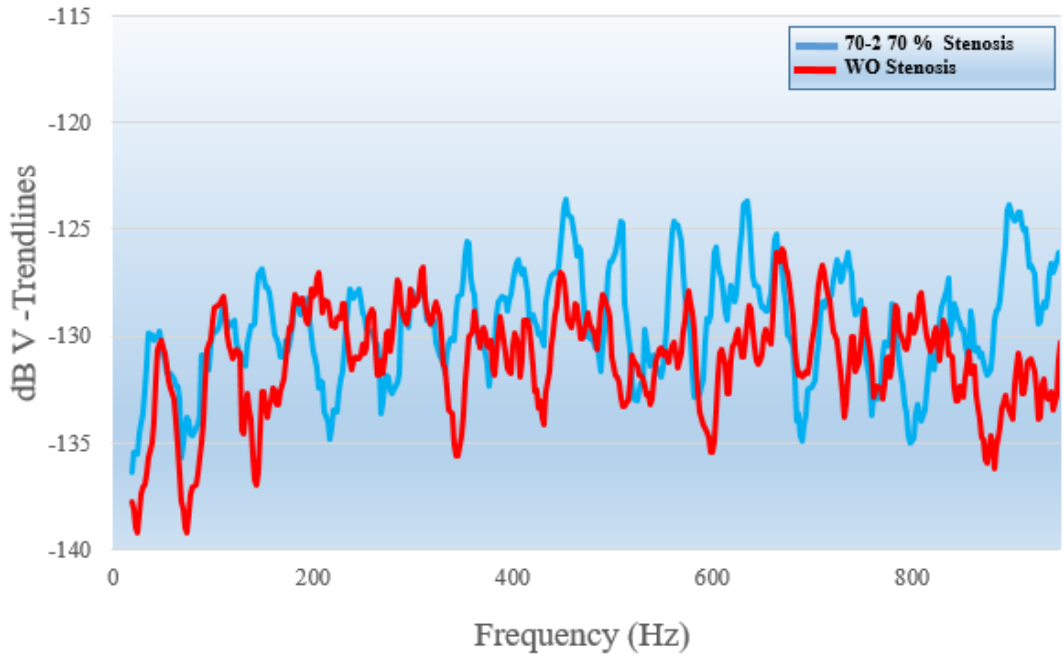

Figure 4.8 Test No 70-2 and WO stenosis

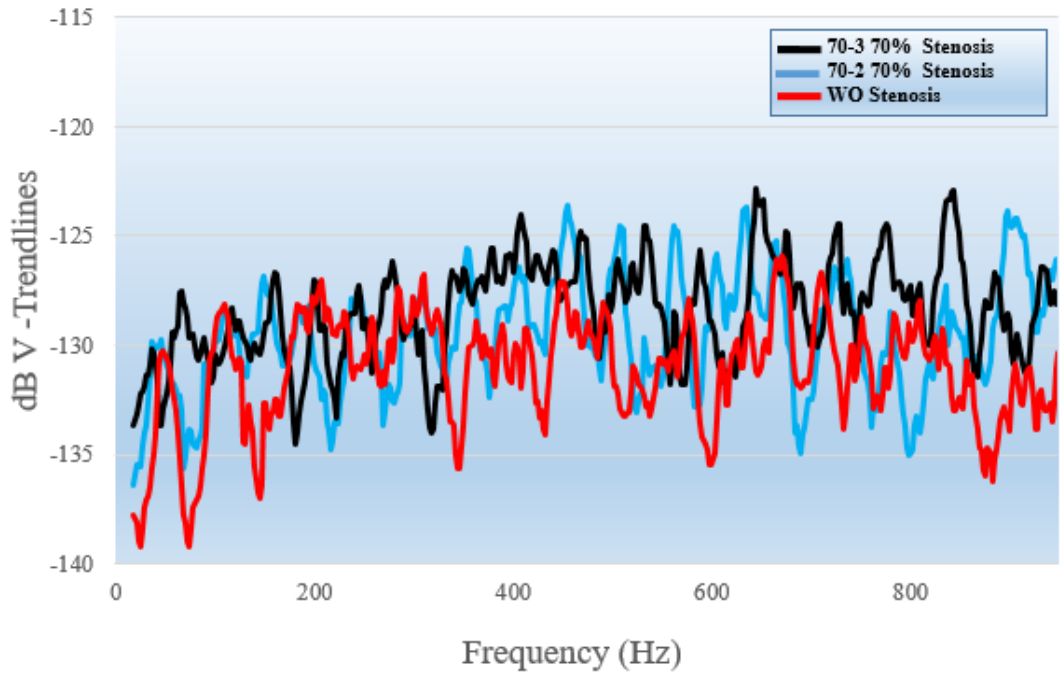

Figure 4.9 Test No 70-3, Test No 70-2, and WO Stenosis

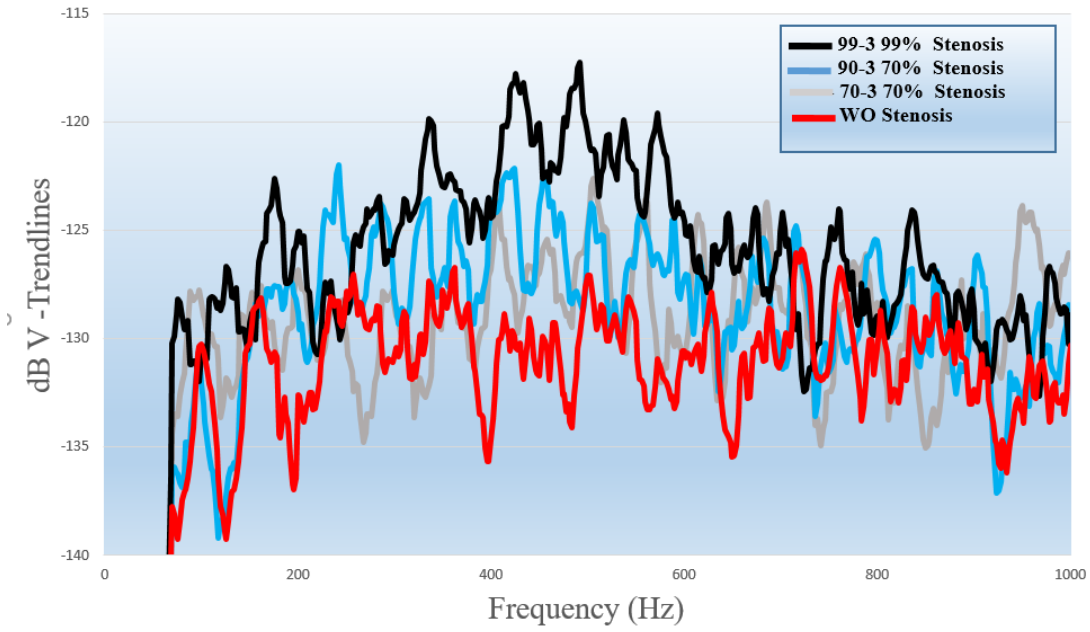

Figure 4.10 Test No 99-3 Test No 90-3, Test No 70-3, and WO Stenosis

In Figure 4.10, the stenosis data of Test No. 99-3, Test No. 90-3, Test No. 70-3, and WO are compared. Accordingly, it can be said that the three test data are noticeably separated from each other and from the WO stenosis test data.

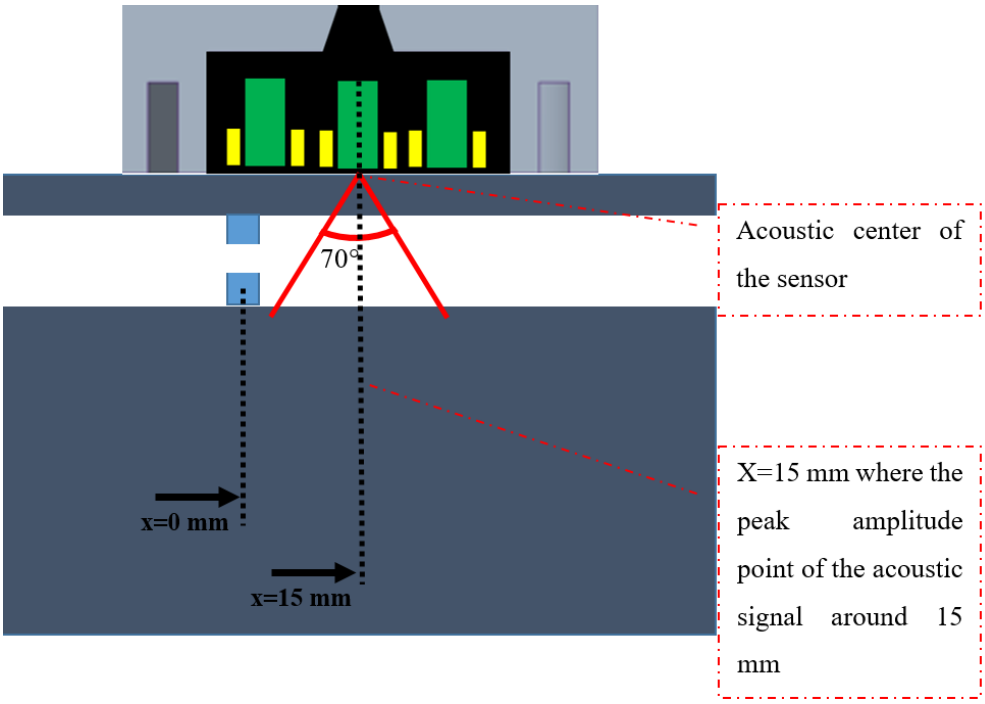

Figure 4.11 The orientation of the test setup where the sensor is centered at x=15mm

Another consideration during the testing phase is the length of the occlusion zone where the flow reaches the steady state. Also mentioned in the literature review section of Chapter 1, Borisyuk et al. [28] described the change in stenosis-induced flow regime in 5 main sections. The 5th region is the part where the flow returns to the steady state flow. It can be seen in Figure 1.1.

Salman, Sert and Yazicioglu et al. [31], Salman and Yazicioglu et al. [32] and et al. [52], Padmanabhan et al. [37], and Schwartz et al. [43] showed in the graphs of the experimental and theoretical models they created that this length is around 100 mm. Figure 1.3, Figure 2.1, Figure 2.2, and Figure 2.3 are from these studies. In light of this information, the amplitude of the acoustic signal peaks around 15 mm after the occlusion sample downstream, and the lowest occurs at around 100 mm. Tests were carried out by bringing the acoustic center of the sensor to these two points on the

tissue model: First, the acoustic center of the sensor is 15 mm away, and second, the acoustic center of the sensor is 100 mm away from the occlusion sample downstream. The orientation of the test setup where the sensor is 15 mm away from the occlusion sample downstream can be seen in Figure 4.11, whereas the orientation for the 100 mm case is in Figure 4.12 These two tests were performed using the same occlusion sample, which yields 90.3% of stenosis severity. In Figure 4.11 and Figure 4.12, the 3-dB beam pattern previously given in Figure 2.43 is shown with red solid lines.

In Figure 4.13, the data that belongs to the test case of 90% stenosis where x=15 mm and x=100 mm can be seen. The difference between these two test data is obvious and can be easily detected. Accordingly, it can be said that the acoustic signal received between 50 Hz and 1000 Hz completely disappears when x=100 mm.

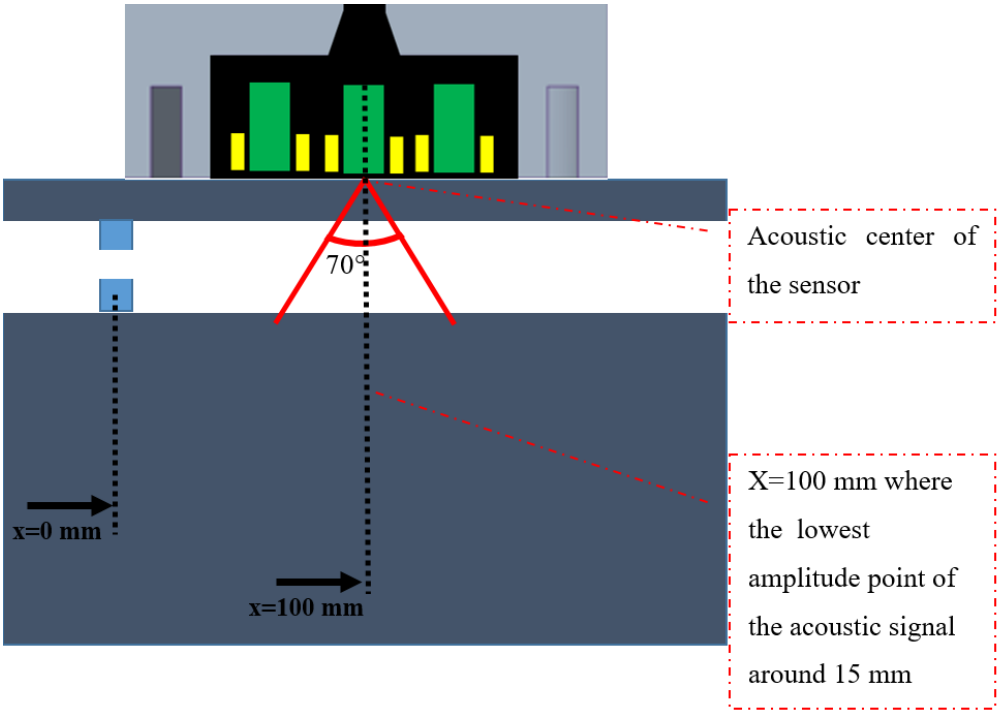

Figure 4.12 The orientation of the test setup where the sensor is at x=100

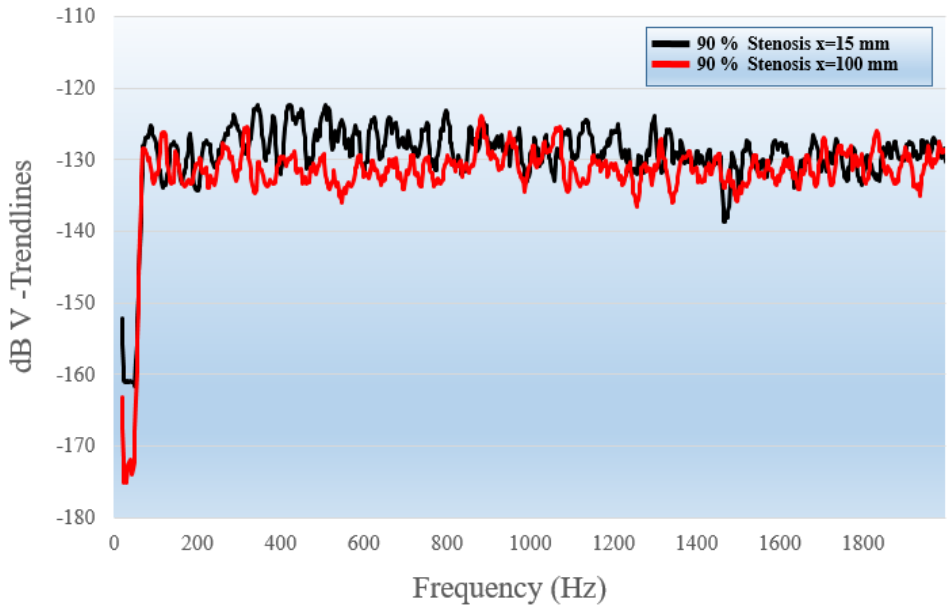

Figure 4.13 Test data of 90% stenosis x=15 mm vs 90% stenosis x=100mm

Based on the measurements taken within the scope of this thesis, which is the non-invasive determination of vascular occlusion by acoustic means, it can be said that the results obtained are found to be in agreement with the information in the literature. The turbulence caused by vascular occlusion creates an important signal for acoustic measurements, especially at low frequencies between 50 Hz to 1000 Hz. The data also stand out as the blood flow rate and occlusion amount increase. On the other hand, it is also possible to say that around 300 Hz is the dominant frequency to detect the acoustic signal due to the turbulence-induced flow regime.

Table 4.1. Three stenosis severity points at 350 Hz from Figure 1.3 [32]

Stenosis Severity	Frequency	SPL (dB)	Pressure (Pa)
90%	350 Hz	15	5.62
70%	350 Hz	0	1
50%	350 Hz	-5	0.56

Salman, Sert and Yazicioglu et al. [31], Salman and Yazicioglu et al. [32] and et al. [52], Padmanabhan et al. [37], and Schwartz et al. [43] state some pressure values as the input for acoustic contact-type sensor design. Regarding the pressure at the

artery wall (and Figure 4.14), the peak pressure is 5.6 Pa (15 dB ref 1 Pa). On the other hand, the lowest pressure value is 0.562 Pa (-5 dB ref 1 Pa).

As mentioned in Chapter 2.1, the analog signal from the sensor is digitized and converted to dB scale referencing 1V. This value returns the sensitivity value in dBV. The formula of analog to digital conversion can be seen in Eqn. 4.4. From Figure 4.4, it can be seen that the value of the graph at 350 Hz is -118 dBV. According to Eqn 2.4, -118 dBV is equal to an analog voltage with an amplitude of $1.3x10^{-6}$ V (1.3 µV) at 350 Hz.

In Figure 2.41, it can be seen that the RVS value at 350 Hz is -126.4 dB V ref 1 Pa. By using the RVS formula given in Eqn 2.3, it can be calculated that the pressure value around 350 Hz is 2.62 Pa. Figure 4.14 shows the schematic representation of this calculation.

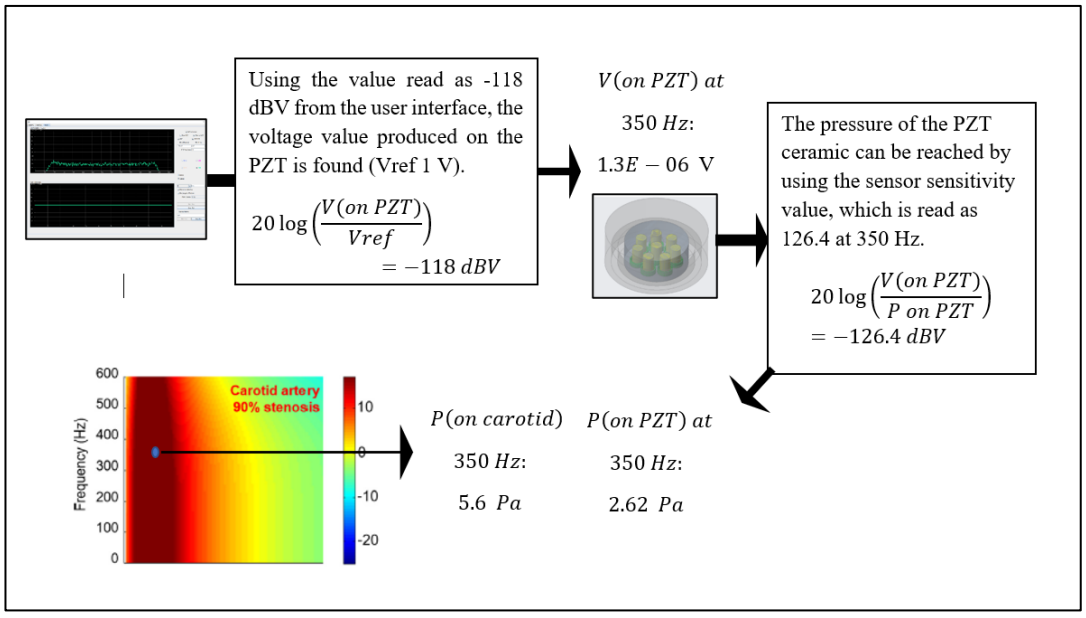

Figure 4.14 - Schematic representation pressure calculation at 350 Hz [3]

In Figure 4.14, the intravascular pressure was calculated as 5.6 Pa at the arterial wall at 350 Hz in the studies conducted in the literature. According to the measurements and results, the pressure calculated in the experimental setup (to which PZT ceramics are exposed) is 2.62 Pa, on the sensor surface.

It can be said that these two pressure values are compatible with each other. It is expected that the pressure value, which is 5.6 Pa at the arterial wall, is measured as 2.62 Pa on the sensor contact surface. The main reason for the difference is the losses due to the impedance mismatch between the arterial wall, skin tissue, and sensor contact surface as well as the propagation losses within different media.

To sum up, the sixth-order polynomial trendlines of three measurements in different stenosis severity (99%, 90%, and, 70%), made with a flow rate of 20 mL/sn, are shown in Figure 4.15. Accordingly, it can be said that the amount of occlusion has a significant effect on the acoustic signal because, in Figure 4.15, the acoustic measurement data are ordered in a distinguishable way from top to bottom according to the arterial occlusion rates.

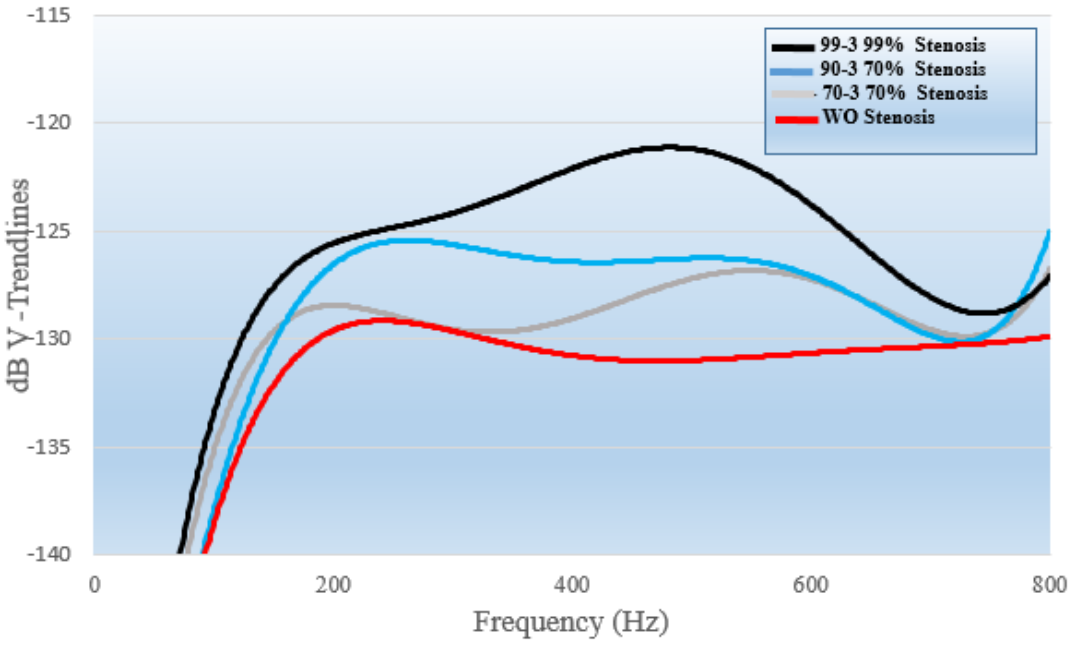

Figure 4.15 Sixth-order polynomial trendline of Test No 99-3, Test No 90-3, Test No 70-3, and WO Stenosis data.

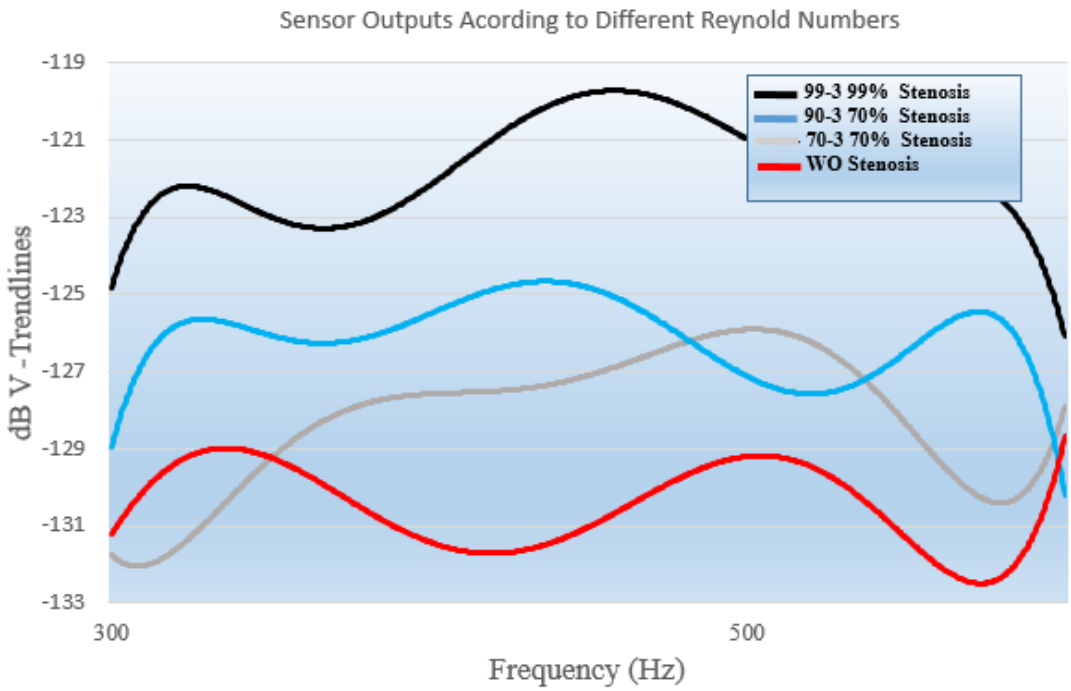

Figure 4.16 Sixth-order polynomial trendline of Test No 99-3, Test No 90-3, Test No 70-3, and WO Stenosis data between 300 Hz and 600 Hz.

In Figure 4.15, the sixth-order polynomial trendline of Test No 99-3, Test No 90-3, Test No 70-3, and WO Stenosis data is calculated across the entire frequency band. The same data was calculated between 300 Hz and 600 Hz in Figure 4.16. According to WO Stenosis data in Figure 4.16, Test No 70-3 data has an average SNR of 3 dB, Test No 90-3 data has an average SNR of 5 dB and Test No 70-3 data has an average SNR of 8 dB.

CHAPTER 5

CONCLUSION

The detection of vascular occlusions using a non-invasive methods can be considered as a crucial development in medical technology. It is very clear that using acoustic methods in diagnosis is one of the viable alternatives for this purpose with state of the art technology.

Having stated this, despite the advanced techniques in measurements, signal processing, and post-processing, there are still some serious physical challenges to overcome. Although it has been studied for many years, the determination of vascular occlusions by acoustic methods is yet to be implemented.

Even if there is no definitive diagnosis, it is still useful to be able to create a preliminary diagnosis that would possibly give an idea to the medical doctors and the patients in high-risk groups. Considering the adverse effects of the current diagnostic methods, another possible scenario is that related organ failure is triggered by other health issues since the patient having a vascular occlusion may also have other systematic health problems. To give an example of this situation, kidney failure is a very common condition among patients with arterial occlusions. When diagnosing with angiography, which is currently the most popular method, patients are given an "opaque substance". This substance can be excreted by the kidneys with difficulty. Considering now that a potential vascular occlusion patient may also have kidney problems, we can understand how important the non-invasive methods are and can become in the near future.

The most important step for non-invasive methods is the development of the required sensor. This study was carried out to show whether acoustic methods can be utilized within the concept of non-invasive diagnosis.

5.1 Goals Accomplished

In Figure 4.1 to Figure 4.14 the experiments given are the outputs of a set of experiments that have been carried out a number of times.

Within the scope of this study:

- A sensor design with “RVS” and “Polar Pattern (Beampattern)” values in sensing the associated frequencies has been made.
- The conceptual design of the sensor has been verified, and the sensor has been successfully produced.
- The arteries and skin tissue are modeled and these models have been physically produced and used in the measurements.
- Tests were performed to check the design with regard to the conditions of the intravascular flow.
- The outcomes of these experiments turned out to be in line with the literature.
- It is safe to claim that, in parallel with the previous studies in the literature, vascular occlusion (carotid arteries) conditions with occlusion levels above 70% can be detected without the need for advanced signal processing.
- It is clearly stated that low noise conditions in both the environment and measurement tools, as well as the frequencies at which the measurements are made, are of vital importance in detecting occlusions.

The designed sensor and its mechanical structure, together with the front-end electronics and signal processing algorithms, which as a whole focuses on non-invasive sensing of the obstruction levels in the artery, is considered as a potential candidate for the similar designs of such systems.

5.2 Future Work

This study is a proof of concept of a prototype and its approach, which may eventually turn into a medical product in the near future.

- Performance can be improved by developments in sensor elements parameters.
- Textured ceramics might be beneficial for higher sensitivity values.
- Single crystal ceramics might be considered to increase RVS, beam pattern, and frequency band.
- Customized ceramics with larger diameters can be employed, especially for low frequencies.
- Advanced signal processing algorithms would increase the detection performance of the system. There are multiple ways to achieve better detection rates available in the literature and these can be applied to improve performance.
- An application-specific electronic board can be designed and used. Limiting the operational frequency band in accordance with the field trials would reduce the noise, improving the SNR, and thus the detection performance. These are also available in the market ad in the literature. Occlusion samples of different thicknesses should be evaluated. The noise from the occlusion is considered to be strongly dependent on the thickness of the occlusion. Therefore, the flow noise levels (i.e., signals of interest) would increase, improving the detection performance.
- The shape and location of the holes on the occlusion samples could be varied. It can be expected this to have an effect on the level or frequency of the signals created by the occlusion.
- The type of material used for occlusion samples might also have an effect on the signals and noises created by the occlusion, e.g. when a viscoelastic material such as rubber/silicon is used instead of the relatively stiff 3D-

printer material used in this study. This might also constitute a better representation of the cholesterol/lipid structure inside the arteries.

- The addition of an active element to the sensor could be evaluated. This would enable a similar use to the ultrasound sensors but in acoustic frequencies.
- Using a higher or a fewer number of elements in the sensor could be investigated. The number of ceramics and their positions will be effective on the DI and RVS, therefore the detection performance of the system.

REFERENCES

[1]-A. Maton, Human Biology and Health, Prentice Hall, 1997.

[2]- W. Rosamond, K. Flegal, G. Friday, K. Furie, A. Go, K. Greenlund, N. Haase, M. Ho, V. Howard, B. Kissela, S. Kittner, D. Lloyd-Jones, M. McDermott, J. Meigs, C. Moy, G. Nichol, C. J. O'Donnell, V. Roger, J. Rumsfeld, P. Sorlie, J. Steinberger, T. Thom, S. Wasserthiel-Smoller and Y. Hong, "Heart disease and stroke statistics - 2007 update: a report from the American Heart Association Statistics Committee and Stroke Statistics Subcommittee," Circulation, vol. 115, no. 5, pp. e69-e171, 2007.

[3]- N. W. Shammas, "Epidemiology, classification, and modifiable risk factors of peripheral arterial disease," Vascular Health and Risk Management, vol. 3, no. 2, pp. 229-234, 2007.

[4]- V. L. Feigin, "Stroke epidemiology in the developing world," Lancet, vol. 365, no. 9478, pp. 2160-2161, 2005.

[5]- National Heart, Lung, and Blood Institute. 2006. Disease and condition index.

[6]-Krupp MA. 1982. Current Medical Diagnosis and Treatment. Los Altos, CA: Lange Med. Publ.

[7]-Johnson MR. 1985. Special diagnostic tests and procedures. Phys. Ther.65(12):1856–65

[8]- Shammas NW . Epidemiology, classification, and modifiable risk factors of peripheral arterial disease. Vasc Health Risk Manag 2007;3:229–34 .

[9]-D. L. Bruns, "A general theory of the causes of murmurs in the cardiovascular system," The American Journal of Medicine, vol. 27, no. 3, pp. 360-374, 1959.

[10]-R. S. Lees and C. F. Dewey, "Phonoangiography: a new noninvasive diagnostic method for studying arterial disease," Proceedings of the National Academy of Sciences of the United States of America, vol. 67, no. 2, pp. 935-942, 1970.

[11]-Bakewell, H. P., G. F. Carey, J. J. Libuha, H. H. Schloemer, and W. A. Von Winkle, Wall Pressure Correlations in Turbulent Pipe Flow, U.S. Navy Underwater Sound Laboratory Report 559-1-052-00-00 (1962).

[12]- H. T. Banks, S. Hu, Z. R. Kenz, C. Kruse, S. Shaw, J. Whiteman, M. P. Brewin, S. E. Greenwald and M. J. Birch, "Model validation for a noninvasive arterial stenosis detection problem," Mathematical Biosciences and Engineering: MBE, vol. 11, no. 3, p. 427, 2014.

[13]-Azimpour F, Caldwell E, Tawfik P, Duval S, Wilson RF. Audible coronary artery stenosis. Am J Med 2016;129:515–21 e3. DOI: 10.1016/j.amjmed. 2016.01.015.

[14] Winther S, Nissen L, Schmidt SE, Westra JS, Rasmussen LD, Knudsen LL, et al. Diagnostic performance of an acoustic-based system for coronary artery disease risk stratification. Heart 2018;104:928 LP-935. DOI: 10.1136/ heartjnl- 2017- 311944.

[15]Levitt K, Guo H, Wijeysundera HC, et al. Predictors of normal coronary arteries at coronary angiography. Am Heart J 2013;166:694–700.

[16]-Nielsen LH, Nørgaard BL, Tilsted HH, et al. The Western Denmark cardiac computed tomography registry: a review and validation study. Clin Epidemiol 2015;7:53–64.

[17]-Patel MR, Peterson ED, Dai D, et al. Low diagnostic yield of elective coronary angiography. N Engl J Med 2010;362:886–95.

[18]A. Lowe, W. Harrison, E. El-Aklouk, P. Ruygrok and A. Al-Jumaily, "Non-invasive model-based estimation of aortic pulse pressure using suprasystolic brachial pressure waveforms," Journal of Biomechanics, vol. 42, no. 13, pp. 2111-2115, 2009.

[19]A. Campo, P. Segers, H. Heuten, I. Goovaerts, G. Ennekens, C. Vrints, R. Baets and J. Dirckx, "Non-invasive technique for assessment of vascular wall stiffness using laser Doppler vibrometry," Measurement Science and Technology, vol. 25, no. 6, p. 065701, 2014.

[20]Laurent S, Boutouyrie P, Asmar R, Gautier I, Laloux B, Guize L, Ducimetiere P and Benetos A 2001 Aortic stiffness is an independent predictor of all-cause and cardiovascular mortality in hypertensive patients Hypertension 37 1236–41

[21] Mattace-Raso F U S et al 2006 Arterial stiffness and risk of coronary heart disease and stroke: the Rotterdam study Circulation 113 657–63

[22] Chirinos J A, Segers P, De Buyzere M L, Kronmal R A, Raja M W, De Bacquer D, Claessens T, Gillebert T C, St John-Sutton M and Rietzschel E R 2010 Left ventricular mass: allometric scaling, normative values, effect of obesity, and prognostic performance Hypertension 56 91–98

[23]A. Campo and J. Dirckx, "Dual-beam laser Doppler vibrometer for measurement of pulse wave velocity in elastic vessels," in Proceedings SPIE, 2011.

[24] Wang, J.-Z., Tie, B., Welkowitz, W., Semmlow, J. L., & Kostis, J. B. (1990). Modeling sound generation in stenosed coronary arteries. IEEE Transactions on Biomedical Engineering, 37(11), 1087–1094. doi:10.1109/10.61034

[25] R, Lees and J, Kistler, "Carotid phonoangiography." in Noninvasive Diagnostic Techniques in Vascular Disease, A. Bernstein, Ed. St. Louis, MO: CV Mosby, pp. 187-194, 1978,

[26] A. Miller, R. S. Lees, J. P. Kistler, w. M. Abbott, "Spectral analysis of arterial bruits (phonoangiography): Experimental validation,"Circuiatiofl., vol. 63, no. 3, pp. 515-520,1980.

[27] J. Semmlow, W. Welkowitz, J. B. Kostis, and J. Mackenzie, "Coronary artery disease correlates between diastolic auditory characteristics and coronary artery stenoses," IEEE Trans. Biomed. Eng., vol. BME-30, pp. 136-139, Feb. 1983.

[28] Borisyuk AO . Modeling of noise generation by a vascular stenosis † . Int J Fluid Mech Res 2002;29:3–18 .

[29] Y. Yazicioglu, T. J. Royston, T. Spohnholtz, B. Martin, F. Loth and H. S. Bassiouny, "Acoustic radiation from a fluid-filled, subsurface vascular tube with internal turbulent flow due to a constriction," Journal of the Acoustical Society of America, vol. 118, no. 2, pp. 1193-1209, 2005.

[30] R. J. Tobin and I. D. Chang, "Wall pressure spectra scaling downstream of stenoses in steady tube flow," Journal of Biomechanics, vol. 9, no. 10, pp. 633-640, 1976.

[31] H. E. Salman, C. Sert and Y. Yazicioglu, "Computational analysis of high frequency fluid-structure interactions in constricted flow," Computers & Structures, vol. 122, pp. 145-154, 2013.

[32]- H. E. Salman and Y. Yazicioglu. 2019. Computational analysis for non-invasive detection of stenosis in peripheral arteries, Medical Engineering and Physics m5G; June 20, 2019;8:47

[33] John Semmlow and Ketaki Rahalkar Acoustic Detection of Coronary Artery Disease. Biomed Eng. by Fordham University on 05/21/13. For personal use only2007.PMID:17425468DOI:10.1146/annurev. bioeng.9.060906.151840

[34] Veramrien H,Vollenhoven E. 1984. The recording of heart vibrations: a problem of vibration measurement on soft tissue. Med. Biol. Eng. Comput. 22:168–78

[35] Lukkarinen S, Noponen AL, Sikio K, Angerla A. 1997. A new phonocardiographic recording system. IEEE Comput. doi:10.1109/cic.1997.647844

[36] Durand LG, Pibarot P. Digital signal processing of the phonocardiogram: Review of the most recent advancements. Crit. Rev. in Biomed. Eng. 1995; 23(3/4): 163-21 9.

[37] Padmanabhan V, Semmlow J, Welkowitz W. 1993. Accelerometer type cardiac transducer for detection of low level heart sound. IEEETrans. Biomed. Eng. 40:21–28

[38] J. Wang, B. Tie, W. Welkowit7, J. L. Semmlow, and J. B. Kostis. "Modeling sound generation in stenosed coronary arteries," IEEE Trans. Biorned. Eng., vol. 37, pp. 1087-1094, Nov. 1991.

[39]1 L. G. DUffand, J. Genest, and R. Guardu, "Modeling of the transfer functions of the herut-thorax acoustic system in dogs," IEEE Trans. Biomed. Eng., vol. 32, pp. 592-{)OI, Aug. 1985.

[40] Asada H, Cho K, Au K. 2001. Smart moles: a hybrid wireless stethoscope/ telephone system using skin-attached passive microphones for continuous health monitoring and voice communication. Prog. Rep. No.3-1, MIT Home Autom. Healthcare Consort., Phase 3, Cambridge, Mass.

[41] Murrill S, Scanlon M. 2001. Design for heart sound extraction algorithm for an acoustic based health monitoring system. Prog. Rep. Access. No. ADA409127, Army Res. Lab. Adelphi, Stress Physiol. Med. Facil., Equipm. Supplies, Maryland

[42] Kroli M. 1987. Heart sound sensor. U.S. Patent No. 4672976

[43] Schwartz R, Reeves J, Sodal I, Barnes F. 1980. Improved phonocardiogram system based on acoustic impedance matching. Am. J. Physiol. 238:604–9

[44] Berson, A. S., And H. Pipberger. Measurement of chest waI.I vibrations due to the activity of the heart. J. Appl. Physiol. 21: 370-374, 1966.

[45] Coleman, D. J., J. R. Whiteman, AND C. A. CACERES. Heart sound transducer. Proc. Int. Conf Med. Electronics, 5th, 1963, Liege, Belgium.

[46] Groom, D. Standardization in phonocardiography: the microphone pickup. Cardiology 55: 129-135, 1970.

[47] Holdack, K., A. A. Luisada, And H. Ueda. Standardization of phonocardiography. Am. J. CardioZ. 15:419,1965.

[48] Courteville A, Gharibi T, Cornu J. 1998.MMG measurement: a high sensitivity microphone based sensor for clinical use. IEEE Trans. Biomed. Eng. 45:145–50

[49] C. F. Bolton, T. Parkes, R. T. Thompson, M. R. Clarck, and C. J. Sterne, “Recording sound from human skeletal muscle: Technical and physiological aspects,” Muscle Nerve, vol. 12, pp. 126–134, 1989.

[50] M. S. Goldenberg, H. J. Yack, F. J. Cerny, and H. W. Burton, “Acoustic myography as an indicator of force sustained contractions of a small hand muscle,” J. Appl. Physiol., vol. 70, p. 87, 1991.

[51] C. Orizio, R. Perini, B. Diemont, M. Maranzana Figini, and A. Veicsteinas, “Spectral analysis of muscular sound during isometric

[52] Salman HE, Yazicioglu Y, " Experimental and numerical investigation on soft tissue dynamic response due to turbulence-induced arterial vibration' Medical & Biological Engineering & Computing, 2019. DOI: 10.1007/s11517-019-01995-y

[53] Chami HA, Keyes MJ, Vita JA, Mitchell GF, Larson MG, Fan S, et al. Brachial artery diameter, blood flow and flow-mediated dilation in sleep-disordered breathing. Vasc Med 2009;14:351–60. doi: 10.1177/1358863X09105132.

[54] Sandgren T, Sonesson B, Ahlgren ˚AR, Länne T. The diameter of the common femoral artery in healthy human: influence of sex, age, and body size. J Vasc Surg 1999;29:503–10. doi: 10.1016/S0741- 5214(99)70279- X .

[55] Krejza J, Arkuszewski M, Kasner SE, Weigele J, Ustymowicz A, Hurst RW, et al. Carotid artery diameter in men and women and the relation to body and neck size. Stroke 2006;37:1103–5. doi: 10.1161/01.STR.0 0 0 0206440.48756.f7 .

[56] Salman HE, Yazicioglu Y. Flow-induced vibration analysis of constricted artery models with surrounding soft tissue. J Acoust Soc Am 2017;142:1913–25. doi: 10.1121/1.5005622 .

[57] Low-Frequency Sound and Marine Mammals: Current Knowledge and Research Needs First Paperback Edition by National Research Council (Author), Division on Earth and Life Studies (Author), Environment and Resources Commission on Geosciences (Author), Committee on Low-Frequency Sound and Marine Mammals (Author)

[58] Kryter, K.D. 1985. The effects of noise on man, 2nd ed. Academic Press, Orlando, FL. 688 pp.

[59] Richardson, W.J., C.R. Greene, Jr., C.I. Malme, and D.H. Thomson. 1991. Effects of noise on marine mammals. OCS Study MMS 90-0093; LGL Rep. TA834-1. Rep. from LGL Ecol. Res. Assoc. Inc., Bryan, TX, for U.S. Minerals Manage. Serv., Atlantic OCS Reg., Herndon, VA. 462 pp. NTIS PB91-168914.

[60] RESON TC4032 datasheet document, Retrieved 30 September, 2022 from https://geo-matching.com/uploads/default/t/c/tc4032-product-leaflet.pdf

[61]BOOK: Computational Simulation in Architectural and Environmental Acoustics: Methods and Applications of Wave-Based Computation

[62] Padmanabhan V, Semmlow J, Welkowitz W. 1993. Accelerometer-type cardiac transducer for detection of the low-level heart sound. IEEETrans. Biomed. Eng. 40:21–28

[63]Ayyaswamy, P. S. (2012). Introduction to Biofluid Mechanics. Fluid Mechanics, 779–852. doi:10.1016/b978-0-12-382100-3.10016-2

[64]Class Notes of Szabo Retrieved 30 September, 2022 from https://web.stanford.edu/class/rad225/subdir/Class3.pdf

[65] Bodyspace: Anthropometry, Ergonomics and the Design of Work, 2nd Ed,by Stephen Pheasant, Taylor & Francis Ltd;

[66]Electro-ceramic products and material specification Retrieved 30 September, 2022 from https://www.ceramtec.com/files/ms_piezoceramic-soft-materials_en_de.pdf

[67]Morgan PZT knowledge, Retrieved 30 September, 2022 from https://studylib.net/doc/18183209/piezoelectric-ceramics---morgan-technical-ceramics

[68] Jiashi Yang “The mechanics of piezoelectric structures” Publisher: World Scientific Year: 2006 ISBN: 9812567011; 9789812567017

[69] Claudia Steinem, Andreas Janshoff “Piezoelectric Sensors” Series: Springer Series on Chemical Sensors and Biosensors Publisher: Springer, Year: 2010 ISBN: 9783642071676,3642071678

[70] VisiJEt ABS Like material datasheet, Retrieved 30 September, 2022 from http://img1.wsimg.com/blobby/go/3798cebb-6e45-454a-9970-f5371ea17364/downloads/3DSystems_Accura_ABS_White_SL7810_DATASHEET_A.pdf?ver=1649679782779

[71] 3M Polyurethane A/B datasheet, Retrieved 30 September, 2022 from https://www.3m.com/3M/en_US/p/d/b40066517/

[70-3] 21. Kinsler, E. L., Frey,A. R., Fundamentals of Acoustics, John Wiley&Sons Inc., New York, 1950.

[70-4]. Beranek, L. L., Acoustics, American Institute of Physics Inc., New York, 1986.

[70-5]. Craggs, A., Hildebrandt, J.G, "The Normal Incidence Absorption Coefficient of a Matrix of Narrovv Tubes with Constant Cross Section", J. Sound Vib., vol.105, 101107, 1986.

[75] Author(s): Arnau A. “Piezoelectric Transducers and Applications” Year: 2008 ISBN: 978-3-540-77507-2,978-3-540-77508-9

[76] Nilanjan Dey, Amira S. Ashour, Waleed S. Mohamed, Nhu Gia Nguyen Series: SpringerBriefs in Speech Technology Publisher: Springer International Publishing, Year: 2019 ISBN: 978-3-319-92224-9,978-3-319-92225-6

[77]De Silva, C. W. (2015). Sensors and actuators: Engineering system instrumentation. Boca Raton: CRC Press.

[78] Lynch, J. P., & Loh, K. J. (2006). A summary review of wireless sensors and sensor networks for structural health monitoring. Shock and Vibration Digest, 38(2), 91–130.

[79]. Livingston, F. J. (2014). Technology for improving the quality of life for patients suffering from vascular insufficiency. North Carolina State University.

[80] Newnham, R. E., Skinner, D. P., & Cross, L. E. (1978). Connectivity and piezoelectricpyroelectric composites. Materials Research Bulletin, 13(5), 525–536.

[81] Paul C. Etter, "Underwater Acoustic Modeling and Simulation" Publisher: CRC Press, Year: 2013 ISBN:1466564938,

[82] Comsol Acoustic Module User Guide, Retrieved 30 September, 2022 from https://doc.comsol.com/5.3/doc/com.comsol.help.aco/AcousticsModuleUsersGuide.pdf

[83]Fabro 1000 3D printer datasheet, Retrieved 30 September, 2022 from https://3dtechnology.ie/3d-printer/fabpro-1000/

[84] Rohde-Schwarz UPV Audio Analyzer datasheet, Retrieved 30 September, 2022 from

[85] Carotid Artery Diameter in Men and Women and the Relation to Body and Neck Size, Originally published23 Feb 2006https://doi.org/10.1161/01.STR.0000206440.48756.f7Stroke. 2006;37:1103–1105

[86]Molex connector catalogue, Retrieved 30 September, 2022 from https://www.content.molex.com/dxresources/49d6/49d61e33-b566-48fd-88bc-b3da1d33c758.pdf